8-2017

Real-time Observation of Dynamic Sarcomeric Addition in an In Vivo-like Cardiomyocyte Culture Model

Zhonghai Wang
Clemson University, zhonghaiwang@outlook.com

REAL-TIME OBSERVATION OF DYNAMIC SARCOMERIC ADDITION IN AN IN VIVO-LIKE CARDIOMYOCYTE CULTURE MODEL

A Dissertation
Presented to
the Graduate School of
Clemson University

In Partial Fulfillment
of the Requirements for the Degree
Doctor of Philosophy
Bioengineering

---

by
Zhonghai Wang
August 2017

Accepted by:
Dr. Bruce Z. Gao, Committee Chair
Dr. Thomas K. Borg
Dr. Delphine Dean
Dr. Hai Yao

ABSTRACT

Cardiac hypertrophy is the enlargement of individual cardiac muscle cell (cardiomyocyte) in both size and mass, which is achieved by addition of sarcomeres, the basic contractile unit. Cardiomyocytes elongate by adding sarcomeres in series and thicken by adding sarcomeres in parallel. Though it is generally accepted that sarcomeric addition can be initiated by increased mechanical loading, the sarcomeric addition process under various mechanical overloads on molecular level remains largely unknown. Previous research on sarcomeric addition largely rely on animal models of induced cardiac hypertrophy; those experiments provide little direct evidence for sarcomeric addition process as a response to increased mechanical loading, aside from the start and end point conditions. Studies showing the dynamic addition process of sarcomeric addition are rare, due to lack of in vivo-like cardiomyocyte culture models for mechanical assays and limited choice of live imaging techniques.

In this project, a 3D cardiomyocyte culture model that recapitulates the in vivo-like mechanical loading environment, was established in vitro on a 2D PDMS substrate. With this culture model, we, for the first time, revealed the dynamic sarcomeric addition process at intercalated discs and Z discs with custom-built passive pulse splitter-based TPEF-SHG microscope, which confirmed the long-standing hypothesis of sarcomeric addition at intercalated discs and Z discs. These findings may advance the comprehension of cardiomyocyte remodeling process on sarcomeric level during development of cardiac hypertrophy.

DEDICATION

This work is dedicated to my family—my father WANG FURUI, my mother WANG YURONG, and my two sisters WANG MEILING and WANG YANLI. Without your constant supports, I would never be able to fulfill any phase of my education. Thank you very much.

ACKNOWLEDGMENTS

I would first like to thank my advisor, Dr. Bruce Z. Gao, for his guidance, supervision, and continuous help in my graduate research. I was so ignorant when I first came to Clemson and barely knew anything about research. It was Dr. Gao who had led me through all the barriers and to the door of research. He not only showed me the professional way to perform experiments, but also instructed me the way of critical thinking, from which my future will benefit.

Working with my lovely lab mates is so fun, and they have given me a big hand in my research. Lucas Schmidt helped me fabricate the stretching device, without which my project wouldn't be possible. Ailin Wei helped me characterize the myosin synthesis, which saved me from learning western blotting. Tiffany Yu assisted me in preparing culture substrates and analyzing images; she is a fast learner and a big help. Xiaoqi Yang supplied high quality cardiomyocytes to me. Cai Yuan helped me with miscellaneous work, including immunohistochemistry, programming, microfabrication, etc. I really enjoyed the days researching with these guys. Discussing research with them were really fun and inspiring.

Finally, I would like to thank my girl-friend, Siyu Ma, for her continuous support in my research and life. From times to times, when I am stressed out by research or life problems, she is always there, listening to me and saving no efforts to help me. She accompanied me through the good days and the bad, with both laughs and tears. I enjoyed the life with her, and hope this can last forever. Love you, Siyu.

TABLE OF CONTENTS

Table of Contents (Continued)

Page

LIST OF TABLES

LIST OF FIGURES

List of Figures (Continued)

Figure Page

List of Figures (Continued)

Figure Page

List of Figures (Continued)

Figure Page

List of Figures (Continued)

Figure Page

List of Figures (Continued)

Figure Page

CHAPTER I INTRODUCTION

1.1 Scope of research

The scope of the project described herein is to develop an in vivo-like cardiomyocyte culture model and utilize it for real-time observation of sarcomeric addition process triggered with applied mechanical loads, in an effort to explore and reveal the mechanisms underlying cardiac hypertrophic responses to pathophysiological mechanical stimuli. Cardiac hypertrophy refers to the enlargement of individual cardiomyocyte in both size and mass, which can occur during both physiological and pathological mechanical stimulation and lead to either enhancement or deterioration of heart function. Physiological cardiac hypertrophy is often seen during postnatal heart development, exercise and pregnancy to meet the increased demand of blood supply; pathological cardiac hypertrophy is a frequent result of diseases such as valvular diseases, hypertension, myocardial infarction and so on, and imposes lethal outcomes of heart failure and sudden cardiac arrest on the affected population [1]. According to American Heart Association, heart failure contributes to one out of every nine deaths in the United States and sudden cardiac arrest causes nine deaths out of every ten victims that are attacked out of hospital. [2] Serious though these health issues are, there are no effective therapies for one of the major causes—cardiac hypertrophy. This is largely due to the limited understanding of cardiac hypertrophy on molecular level. Sarcomeres, as the most basic contractile units of cardiomyocytes, are reported to be actively involved in the enlargement of cardiomyocytes: cardiomyocytes elongate by adding sarcomeres in series and thicken by adding sarcomeres in parallel. However, the mechanism by which

sarcomeric addition occurs under various mechanical loads remains elusive. Revealing dynamics of the fundamental sarcomeric addition process under mechanical stimulation will serve to benefit the understanding of 1) the role of mechanical loads in and 2) the molecular-level evolution of cardiac hypertrophy. It will also shed light on possible medical strategies for alleviating and curing cardiac hypertrophy or gearing a pathological cardiac hypertrophy toward physiological cardiac hypertrophy. [1, 3]

1.2 Backgrounds

Cardiac hypertrophy is a common remodeling process seen in a heterogeneous group of myocardium diseases that are associated with mechanical and/or electrical dysfunction, or cardiomyopathy [4]. The remodeling process is outlined as three phases shown in Figure 1.1 [5]. Hypertrophy develops when the work load exceeds the normal capacity of a heart of a specific mass and heart function is decreased. The increased work load to heart mass triggers growth of the heart in compensatory hypertrophy. This phase may be accompanied by synthesis of new contractile proteins as well as by cell necrosis. Depending on hearts, the function can be restored, increased or decreased in this phase. When cell necrosis exceeds growth in the later stage of compensatory hypertrophy, the work load/mass ratio starts to increase again and the heart gradually progresses to failure. Physiological hypertrophy only exhibits the first two phases, while pathological hypertrophy is likely to progress to heart failure under chronically increased myocardial work load [3].

Cardiac hypertrophy is a direct result of interaction between heart muscle and off-balanced neurohormonal and mechanical cues. Neurohormonal cues and their induced

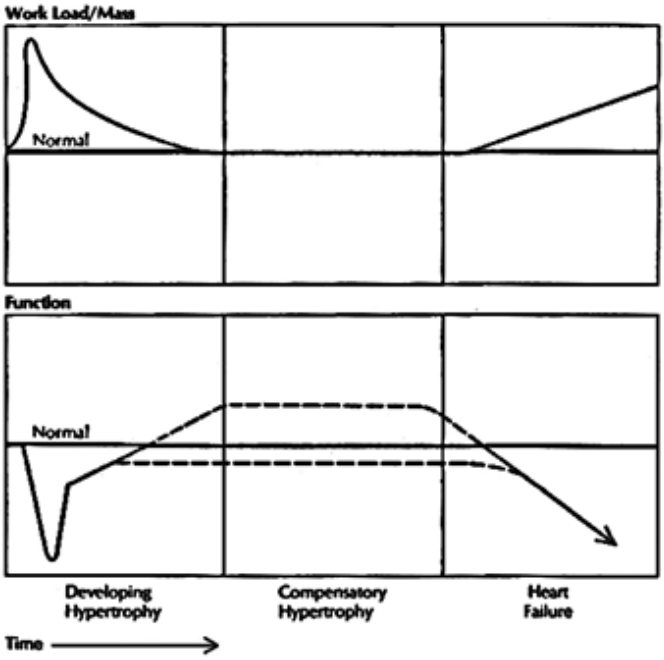

Figure 1.1 Three phases of cardiac hypertrophy. Adapted from [5] with permission from Taylor & Francis, copyright 1983.

signaling pathways have been reviewed elsewhere [6, 7], and are not included in this review as the scope of this project is cardiac structural response to increased mechanical loads. Cardiac hypertrophy comes in two typical forms with respect to left ventricle dimensions: concentric and eccentric hypertrophy as shown in Figure 1.2 [3]. Concentric hypertrophy is that heart muscle thickens without decrease of the chamber size. It is a frequent result of hypertension and aortic stenosis and is, therefore, considered an adaptive process to increased afterload or pressure overload. Experimental data has proven that wall thickening in concentric hypertrophy is proportional to the increase in afterload, which returns the systolic stress to normal. [8] Eccentric hypertrophy is defined as dilation of the left ventricle without apparent thickening of the chamber walls. The

dilation of the left ventricle is usually caused by increased volume of returned blood, a phenomenon named volume overload. The dilation of the left ventricle under volume overload can lead to pure eccentric hypertrophy [9] or a combination of concentric and eccentric hypertrophy when the chamber walls thicken in proportion to increase in radius of the left ventricle [8]. The increase in wall thickness balances the increase in pressure in concentric hypertrophy and the increase in radius in eccentric hypertrophy, thus normalizes the systolic wall stress; this is consistent with predictions from La Place's law.

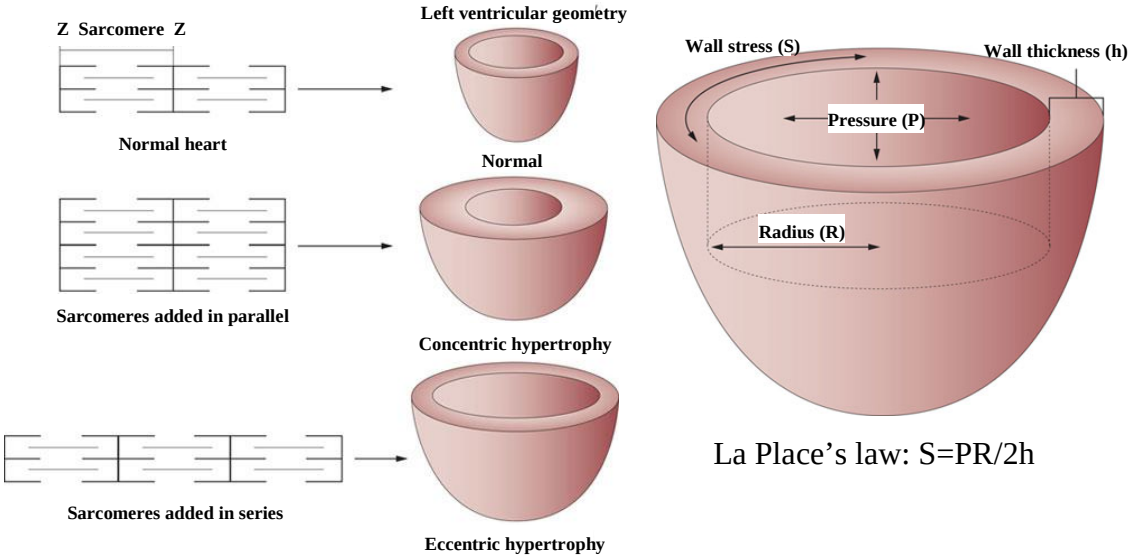

Figure 1.2 Two forms of cardiac hypertrophy and illustration of La Place's law. Adapted from [3] with permission from Nature Publishing Group, copyright 2011.

Though La Place's law predicts the thickening of heart muscle in response to increased wall stress due to alterations in afterload and/or radius, it gives no adequate explanation for the increase in radius under volume overload. Recent experimental data

and theoretical analysis now favor a strain-based growth law, which account well for both the thickening and the lengthening of heart muscle during concentric and/or eccentric hypertrophy. [10-13] Specifically, sarcomeres, the most basic contractile unit of a cardiomyocyte, are added in series to maintain the optimal sarcomeric length in response to increased fiber strain, thus elongating cardiomyocytes; sarcomeres are added in parallel to maintain the interfilament lattice spacing in response to increased cross-fiber strain, thus thickening cardiomyocytes (Figure 1.2). [10, 14, 15]

However, the process of sarcomeric addition under mechanical stimulation remains elusive. This is largely due to limitations in investigation strategies, including limited choices of high-throughput repeatable mechanical loading assays and absence of direct evaluation methods.

Early studies are unexceptionally based on animal models with disease- or researcher-induced cardiac hypertrophy. Methods for inducing cardiac hypertrophy in vivo include constrictions of blood vessels, which mimics pressure overload [16, 17], fistula of blood vessels or transventricular section, which mimics volume overload [18, 19], exercise and pregnancy, which mimics physiological hypertrophy [9, 20, 21]. Though these methods are clinical-relevant, the applied mechanical loads are not consistently controlled. Typically, It takes several days to weeks for manifestation of hypertrophy, which renders animal models low throughput for studying mechanical load-induced cardiac hypertrophy. Besides, heart samples are inaccessible for conventional microscope, which makes the assessment of hypertrophy difficult. [22]

To overcome these problems using animal models, researchers begin using primary culture of cardiomyocytes on elastic membranes for studying cardiac hypertrophic response to mechanical stimuli. Mechanical loads are directly applied to cultured cardiomyocytes by stretching the supporting membrane. Hypertrophic responses of these cardiomyocytes have been confirmed on transcriptional, translational, and post-translational level [23-28], which testifies the use of cardiomyocyte culture as an alternative to animal model for studying mechanical-load induced cardiac hypertrophy. Technical advances in last several decades have enabled alignment of cardiomyocytes on various substrates [29], which permits studying effects of directional strain on cardiac hypertrophy. Cardiomyocyte culture has become an increasing important tool for cardiac hypertrophy-related studies due to: 1) that it permits high throughput and controllable mechanical loading assays; and 2) that it is easily accessible for a variety of treatments and evaluation methods. [22]

However, a concern is whether studies base on cardiomyocyte culture are clinical-relevant. [30] Given this concern, animal models continue to be used, while other alternatives are being sought for. One alternative is to use explants of cardiac muscle from healthy animal and externally apply mechanical loads on those explants. [31] Another alternative is to use freshly isolated adult cardiomyocytes because sarcomeric structures within these cells are made in vivo and are well preserved during isolation. [32] The cardiac explants and adult cardiomyocytes offer the advantages of clinical relevancy of animal models and the advantages of mechanical-loading and evaluation accessibility of cardiomyocyte culture. However, isolating tiny heart tissues that are

suitable for conventional microscope requires much practice and application of controlled mechanical loads can be very difficult on tiny tissues or individual cardiomyocytes.

For cell cultures and cardiac explants, applied mechanical loads come in several forms, including cyclic/static stretch, uniaxial/biaxial/uniform stretch, or a combination of both. [24, 26, 28, 33, 34] Biaxial cyclic stretch is the most clinical-relevant because it is the exact form of mechanical load during heart beating. However, it is not the best option for research purposes. Cyclic stretch does not arouse stronger hypertrophic response than static stretch in in vitro studies [35], while it introduces motion artifacts and makes live observation impossible. Biaxial stretch obscures the study of effects of strain directionality on load-induced hypertrophy. Besides, more and more researchers believe the accumulated end diastolic strain accounts for both longitudinal and transverse sarcomeric addition, which can be simulated by static stretch. [10, 12, 14] Mechanical loads can be readily conveyed to groups of cells by stretching the supporting substrates , or directly applied to individual cells with carbon fibers[36], micropipette, tweezers and probes of atomic force microscope (AFM) [37]. Other methods for mechanical loading application such as hydrostatic compression and fluid shear system have never been used on cardiomyocytes; thus, they are not discussed here. [38]

The major substrate for cardiomyocyte-related mechanical assays is made of silicone despite of its constituents [23-28, 39, 40]. Polydimethylsiloxane (PDMS) is the most prevalent material for cardiomyocyte culture in load-induced sarcomeric addition studies due to its excellent biocompatibility and flexibility. Another advantage is that engineering cardiomyocyte alignment that mimics the anisotropic organization of

cardiomyocytes in native hearts could be easily achieved on PDMS substrates. Use of other rubber-like elastomers, such as polyesters, has been seen exclusively in bioreactors for cardiac tissue engineering, which involves the application of cyclic stretch [41].

Currently, knowledge on load-induced sarcomeric addition heavily relies on stationary images produced by transmission electron microscopy (TEM), and immunohistochemistry. Results based on stationary images are inconclusive and can sometimes be misleading. Time-lapse imaging for sarcomeric addition under mechanical loading is demanded for understanding the process; however, related studies using time-lapse imaging are rare. Solution for live cell imaging, such as fluorescent analog cytochemistry and fluorescent protein fusion techniques, have been successfully used for many years on primary cultures of various cells including cardiomyocytes. [42] Recently, we have built a second harmonic generation (SHG) microscope [43] in our lab, with which dynamics of myosin filaments during sarcomeric addition within mechanical-loaded single cardiomyocytes was revealed for the first time. [28]

Despite of the achievements that have been made, mechanisms underlying sarcomeric addition under cardiac hypertrophy remain elusive. Direct visualization of this process under controlled mechanical loads in heart samples or their equivalent representatives is yet to be achieved. Studies on roles of fundamental sarcomeric and cell structures, such as Z discs and intercalated discs, in sarcomeric addition demand live imaging of multiple sarcomeric components/complexes. It is challenging, but is substantially beneficial to understanding sarcomeric addition under mechanical loads if achieved. Therefore, we proposed this project, aiming at developing an in vivo-like

cardiomyocyte culture model that permits high throughput mechanical assays, and visualizing the dynamics of two sarcomeric components during sarcomeric addition under various mechanical stimuli.

1.3 Research goals and specific aims

Our long-term goal is to understand how sarcomeric addition is regulated by mechanical-loading conditions. The objective of this project is to test the hypotheses that longitudinal stretch will cause sarcomeric addition through sarcomeric protein insertion at Z-discs and that transverse stretch will cause sarcomeric addition either through longitudinal splitting of an existing myofibril (the contractile element composed of sequentially connected sarcomeres) or sarcomeric addition using an existing myofibril as a template. To test these hypotheses, we will first establish an in vivo-like cardiomyocyte culture model on deformable PDMS substrates, which recapitulates key features of the mechanical loading environment in the heart. This kind of cardiomyocyte culture will then be used in mechanical assays to induce sarcomeric addition, which will be non-invasively observed with a lab-built TPEF-SHG microscope. The specific aims are:

Aim 1: Establish a cardiomyocyte-culture model on a PDMS substrate with anisotropic cardiomyocyte organization and intercalated disc-like cell-cell interfaces.

Aligned elongated cardiomyocytes with intercalated disc-mediated cell-cell coupling are one of the most important characteristics of the mechanical loading environment in the heart. We will use several state-of-the-art techniques to align cardiomyocytes on PDMS substrates, including topographical patterning and

microcontact printing. Cell-cell coupling at the longitudinal ends of cardiomyocytes will be reinforced by electrical field stimulation. Quality of cardiomyocyte alignment and profile of cell-cell interfaces will be evaluated by immunocytochemistry. The culture model with the best alignment and intercalated disc resemblance will be used in following mechanical assays.

Aim 2: Determine whether sarcomeric addition can occur at intercalated discs in response to uniaxial static stretch

Intercalated discs are one of the most frequently altered structure in hypertrophic heart. Our published data have demonstrated that when an isolated single cardiomyocyte is under static stretch, using the SHG channel of our lab-built confocal microscope we can capture the dynamics of sarcomeric myosin filaments, which represent various modes of sarcomeric addition. We will use this confocal microscope (the SHG channel) to determine the dynamics of myosin filaments in the cardiomyocyte culture model (established in Aim 1) in response to externally applied longitudinal and transverse static stretch. The goal is to examine whether sarcomeric addition can occur at intercalated discs. In addition to that, we will also examine whether various modes of sarcomeric addition observed in an isolated cardiomyocyte occur in a cardiomyocyte culture model in which the cell under study is in contact with other cells through in vivo-like cell-cell junctions.

Aim 3: Determine the morphological changes of Z discs in response to uniaxial static stretch

In the literature, both in vitro and in vivo data have demonstrated thickening and longitudinal splitting of Z discs under increased mechanical load. Z discs undergoing these changes captured by static images have been hypothesized to be the nucleation sites for new sarcomeric addition in response to mechanical stimuli. We will use the TPEF channel of our confocal microscope to observe the dynamics of EYFP-tagged α-actinin, the major component of Z discs, in the culture model used in the previous aims. To determine the role of Z discs in sarcomeric addition, we will simultaneously use the SHG channel to observe the dynamics of the sarcomeric myosin filaments. The goal is to examine whether myosin filaments will be inserted into the broadened Z discs or attached to the split Z discs to finalize sarcomeric addition.

1.4 Significance and innovation

Understanding the sarcomeric addition process that cardiomyocytes initiate in response to increased mechanical load is critical to understanding mechanisms underlying alterations in heart function. Although the most important heart function, contraction, is determined by the contractility of each sarcomere, the process of sarcomeric addition in response to mechanical stimuli may, instead of intensifying contractility, progressively lead to decrease of heart function and even heart failure. Such an incurable consequence affects millions of people in the US alone. Of the 900,000 people diagnosed with heart failure annually, half die within 5 years of diagnosis [6], a huge concern in public health. The development of treatment for heart failure is currently hindered by the elusive mechanism underlying cardiomyocyte remodeling in response to increased mechanical load. Previous studies are almost unexceptionally based on fixed samples; results from

these studies are not only slow-coming but also inconclusive. The project proposes to use live imaging techniques on cardiomyocytes cultured in vitro for resolving these challenges. The proposed research is significant because 1) it will change the way that mechanical load-induced cardiomyocyte remodeling process—sarcomeric addition—is studied; and 2) it will generate solid knowledge on mechanical load-induced cardiomyocyte remodeling process faster when high throughput in vitro culture models and live imaging assays are combined. This will considerably contribute to the understanding of sarcomeric addition process under increased mechanical load and is expected to lead to development of new therapeutic strategies for treating mechanical loading caused heart failure.

This proposed study is innovative in two ways. First, an in vivo-like cardiomyocyte-culture model, which recapitulate the anisotropic organization of myofibrils and intercalated disc-like cell-cell junctions, will be developed on an elastic substrate , which permits application of direction-controllable mechanical loads. Only in such an in vivo-like model, appropriate mechanical load can be added to longitudinally aligned sarcomeric structure in a clinically relevant manner (e.g., in vivo-like force-exertion direction) and stimulate sarcomeric addition processes that occur in an actual heart muscle. This new and substantively different approach of visualizing sarcomeric addition processes will dramatically advance our understanding of cardiomyocyte remodeling in response to mechanical loading.

Second, new sarcomeric addition involves unraveling and weaving hundreds of sarcomeric proteins in the correct order and at the correct location during continuous

contraction; hence, dynamic observation is critical. Currently, most knowledge on sarcomeric addition is based on static images of altered sarcomeric patterns in hypertrophic cardiomyocytes, and thus may not be conclusive. For example, there are many studies showing alterations in Z discs in the hypertrophied heart, such as broadened Z discs, split Z discs and misregistered Z disc, which have been posited to be intermediate processes of new sarcomeric addition. These suppositions require confirmation from dynamic imaging, which records, instead of a static image from a fixed cell culture, a sequence of events from a live cell culture that lead to the formation of new striated structures. Application of cardiomyocytes with fluorescence-tagged sarcomeric proteins created through GFP transfection can achieve live-cell imaging and has been used to successfully reveal dynamic sarcomerogenesis. However, it is still largely unclear whether the GFP-tagged sarcomeric protein will affect sarcomerogenesis. This doubt is more significant when two sarcomeric proteins are transfected, which is essential for a complete understanding of the sarcomeric addition process. Our novel SHG microscope can visualize sarcomeric myosin filaments (not myosin molecules that have not formed sarcomeric myosin filaments) without addition of any molecular marker. It can reveal any myosin filament-related dynamic sarcomeric addition process. Combined with the visualization of a GFP-tagged sarcomeric protein (e.g., α-actinin in the Z discs) simultaneously achieved using the TPEF channel, our proposed imaging approach is expected to reveal never-before-seen dynamic sarcomeric addition processes in a cell construct.

CHAPTER II LITERATURE REVIEW

2.1 Structure of heart muscle and sarcomeres

The heart is one of the earliest organs that become functional during embryo development. It has four chambers—left/right atria and left/right ventricles; they work as a functional syncytium under orchestra of pacemaker cells at sinoatrial node (located at the wall of right atrium) through the conduction system, which rapidly delivers electrical stimulation in a well-coordinated way. During each heartbeat, sequential mechanical and electrical events take place and blood is ejected out from the heart to the circulation system. The first event is cardiac diastole when all four chambers dilate and blood fills them passively. It is followed by atria systole when atria contract and fill blood to ventricles actively. In the last phase—ventricle systole, blood is ejected into both the pulmonary and aorta by contraction of ventricles. Those three phases constitute a cardiac cycle.

The function of the heart as a blood pump relies on heart muscle, especially the heart muscle in the ventricles. The constituents of heart muscle are cardiomyocytes, whose phenotypes and ultrastructures vary from chamber to chamber [44]. Here, we will focus on describing cardiomyocytes in ventricles, because they are the cells that are enlarged during cardiac hypertrophy. In ventricular heart muscle, cardiomyocytes are usually mono- or bi-nucleated [45], branched and are end to end connected through intercalated discs with adjacent rod-shaped cardiomyocytes. This anisotropic organization of cardiomyocytes enhances the efficiency of contraction of cardiac muscle fiber. Extracellular matrix fills the interstitial space between cardiomyocytes and

provides fundamental mechanical support during each cardiac cycle. [46] The hierarchical structure of heart muscle is illustrated in Figure 2.1.

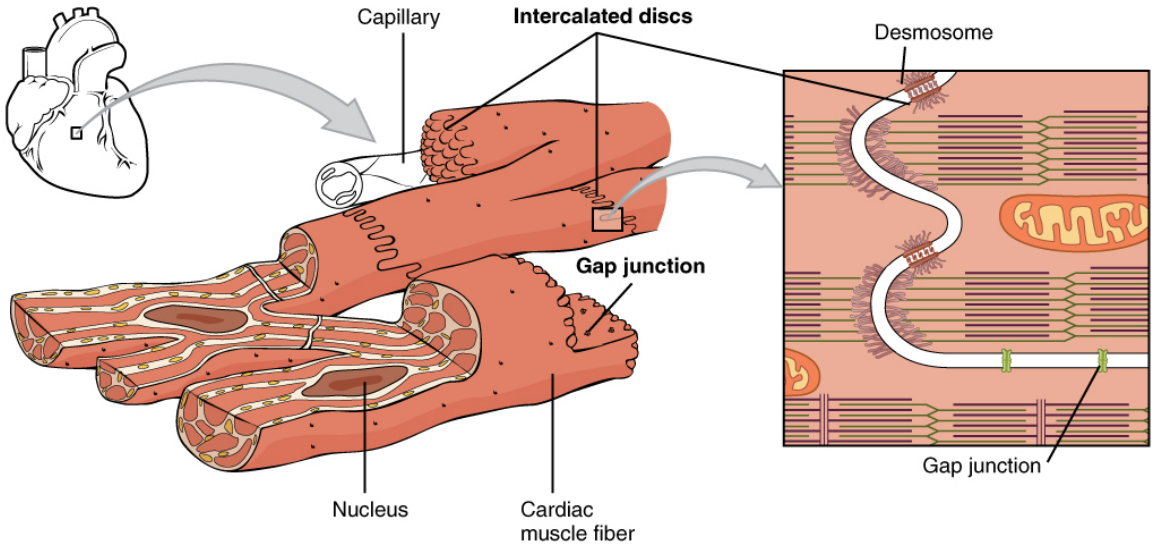

Figure 2.1 Hierarchical structure of heart muscle. (OpenStax College. Anatomy and Physiology. OpenStax CNX. Download free at http://cnx.org/contents/14fb4ad7-39a1-4eee-ab6e-3ef2482e3e22@8.80, accessed on April 1, 2017).

The contraction of individual cardiomyocytes is achieved by simultaneous contraction of myofibrils that spans longitudinally from end to end. Myofibrils alternate with lines of mitochondria, which supply energy for myofibrillar contraction through aerobic metabolic activity. The most basic contractile unit of a myofibril is the sarcomere, which repeats itself along the longitudinal direction of a myofibril. A sarcomere comprises hundreds of ordered protein subunits. [47, 48] These protein subunits are organized in such a way that gives a myofibril the microscopic appearance of repeated interdigitated dark and light bands. The dark bands, or A bands, are primarily constituted of myosin filaments. The light bands, or I bands, mainly comprise actin filaments. Antiparallel actin filaments are cross-linked by α-actinin at the Z discs, which delineate

the boundaries of sarcomeres. [49] Antiparallel myosin filaments are associated with each other by myosin binding protein C [50] and cross-linked by myomesin at the M lines, which have an analogous role to the Z discs [51]. Titin filaments span from Z discs to M lines, and are believed to be a molecular ruler for thick filaments. [52] A spring portion of titin in the I band region contributes to passive cardiac stiffness. [52, 53]

During pressure and/or volume overload, external forces are exerted on individual cardiomyocytes and arouse hypertrophic responses within cardiomyocytes, such as transcription and protein synthesis. Though consensus has not been reached on components that pick up those forces, several structures seem to play important roles in mechanosensing. Intercalated discs are one of those structures because 1) myofibrils insert F actin filaments at their ends to fascia adherens and 2) desmins stabilize Z discs to desmosomes; both fascia adherens and desmosomes are located at intercalated discs. [54, 55] Another candidate is the costameres, which pass mechanical load from ECM to Z discs through integrins. Focal adhesion kinase (FAK) and protein kinase C (PKC) are believed to be involved in initiating and coordinating the downstream signaling pathways. [56] Intracellular signaling converges to proteins at the Z discs, including telethonin, muscle LIM protein, melusin, calcineurin and calsarcins, enigma/ENH/cypher family, and myopalladin [57], or converge to proteins at titin spring segment such as muscle-specific ankyrin repeat protein (MARP) and four-and-a half-LIM domain protein-1(FHL1) [55]. Another mechanosensor is stretch-activated channels, whose function involving sarcomeric addition is yet to be discovered. [58] A schematic representation of

intracellular sarcomeric protein complexes and their connections with membrane structures is shown in Figure 2.2. [55]

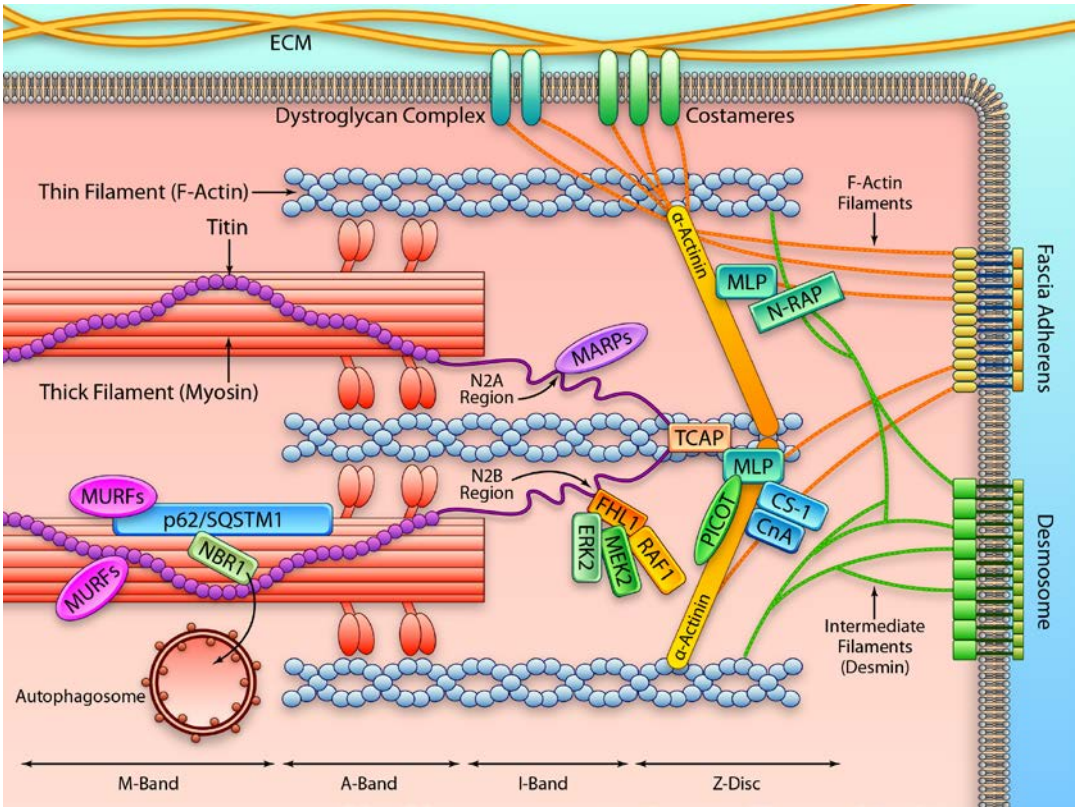

Figure 2.2 A schematic representation of intracellular sarcomeric protein complexes and their connections with membrane structures. Reproduced from [55] with permission from Wolters Kluwer Health, Inc, copyright 2015

2.2 Myofibrillogenesis

De novo myofibrillogenesis

De novo myofibrillogenesis refers to generation of the very first myofibril. De novo myofibrillogenesis is believed to be a relatively simple process when it is compared to myofibrillogenesis under mechanical load because it does not involve disassembly of preexisting sarcomeres. Understanding the process of de novo myofibrillogenesis can

provide insights into myofibrillogenesis under mechanical loads, because both processes involve production of new sarcomeres and thus they may share similar mechanisms.

As we have already known, sarcomeres are delicate structures that comprise hundreds of highly ordered proteins. The assembly of those sarcomeric proteins is expected to progress hierarchically so that erroneous nonfunctional sarcomeres are not produced. Studies based on primary cultures of embryonic chick cardiomyocytes favor a premyofibril model [59] as shown in Figure 2.3. Briefly, IZI complexes, composed of α-actinin and actin, are first formed on spreading edges of a cultured cardiomyocyte. Space between these IZI complexes is held by non-muscle myosin IIB. These structures are

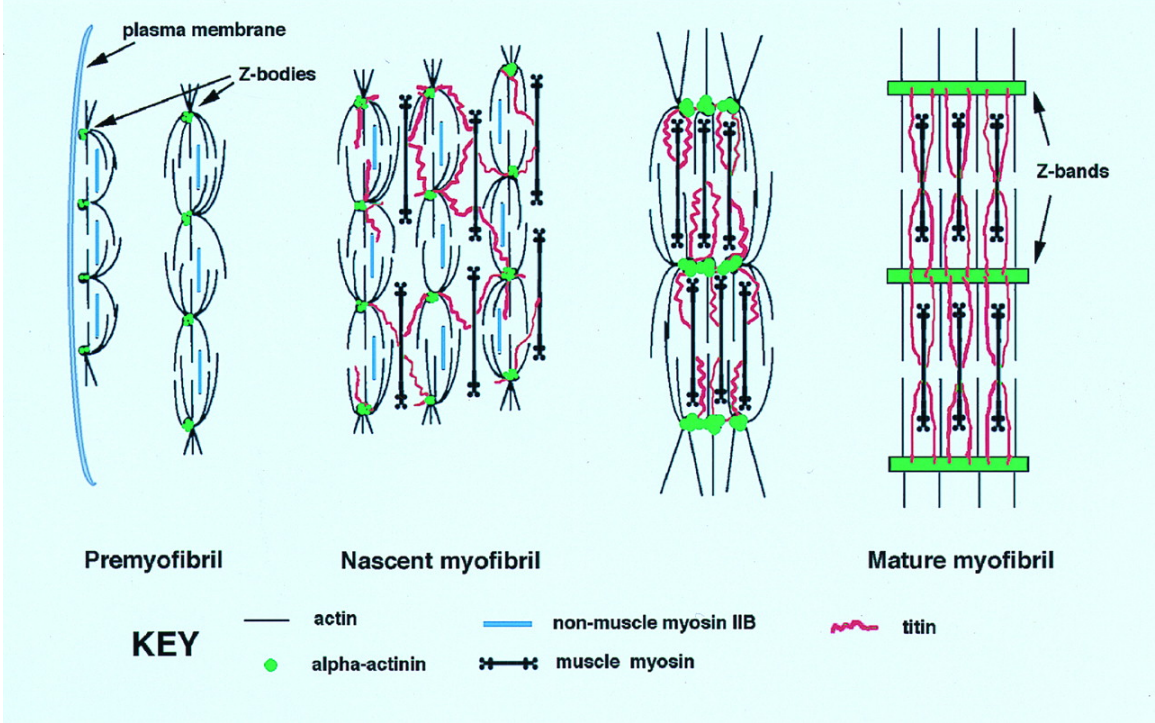

Figure 2.3 A illustration of the premyofibril model for myofibrillogenesis. Reproduced from [59] with permission from National Academy of Sciences, copyright 1997.

named as premyofibrils. The premyofibrils then move away from the cell membrane towards the cell nucleus, during when muscle myosin is incorporated to replace the non-muscle myosin IIB and α-actinin-rich Z bodies begin to laterally associate. The myofibrils in this stage are named as nascent myofibrils. In the last stage, Z bodies fuse together laterally to form striated Z discs and non-muscle myosin IIB is completely replaced by muscle myosin. A mature myofibril is hence formed.

Plausible though the premyofibril model for de novo myofibrillogenesis in primary culture of embryonic chick cardiomyocytes is, it is challenged by studies performed with embryonic chicken heart explants. Several studies reported that no premyofibril-like structures could be detected in myofibrillogenesis in situ. [30, 60, 61] Instead, α-actinin, actin and titin fragment with only its N terminal epitope colocalized near the cell membrane, representing IZI like complexes. Myosin-containing thick filaments and actin-containing thin filaments were also found to be assembled independently before being associated together with titin. These studies have posed serious challenges on application of primary cultures of cardiomyocytes in studying myofibrillogenesis because doubts have been raised that whether it faithful reflects myofibrillogenesis in vivo.

Myofibrillogenesis under mechanical loads

Myofibrillogenesis in cardiomyocytes with preexisting sarcomeric structure is more complex than de novo myofibrillogenesis because cardiomyocytes needs to1) be remodeled to make room for sarcomeres that are going to be added and 2) keep contraction integrity during sarcomeric addition [62]. It can be induced by both

neurohormonal and mechanical stimuli. In this project, we try to investigate sarcomeric addition process under mechanical loading, so myofibrillogenesis under neurohormonal stimuli is not discussed in here. In native hearts, mechanical loads come in forms of pressure and/or volume overloads, which act as longitudinal and transverse strains on individual cardiomyocytes. [63] To study this issue, researchers either select to use heart samples from animals that are affected by pressure or volume overloads, or apply longitudinal and/or transverse strains directly to cultured cardiomyocytes or cardiac explants.

Early studies exclusively use heart samples from animals with disease- or personally induced hypertrophy. Researchers examine those samples under a transmission electron microscope (TEM) and look for any alterations that occur only in hypertrophied heart samples. These alterations will be judged personally and may be hypothesized as indicators for potential sarcomeric addition or damage. For example, in normal hearts, Z discs always display as striated dark lines under TEM, while in hypertrophic hearts aberrant morphologies that are not seen in normal hearts, such as broadened Z discs (Figure 2.4A) [64], split Z discs (Figure 2.4B) [65] and misregistered Z discs (Figure 2.4C) [66], are hypothesized to be indicators of new sarcomere nucleation, because they appears to be making rooms for or generating extra sarcomeres. Other alterations are at the intercalated discs. Frequency of close packed intercalated discs that are separated by ten sarcomeres or less is significantly increased in hypertrophied heart samples than that in normal. Therefore intercalated discs are postulated to be involved in new sarcomeric addition at cell ends. [67] There are also

reports that folds of intercalated discs become exceptionally larger (1.5-3μm) in hypertrophied heart than in normal (0.5μm-1 μm), and myosin filaments are seen in this

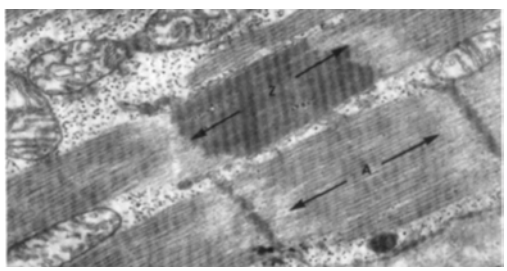

(A)

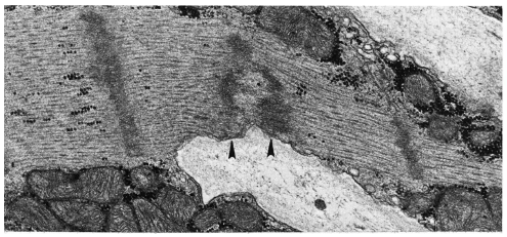

(B)

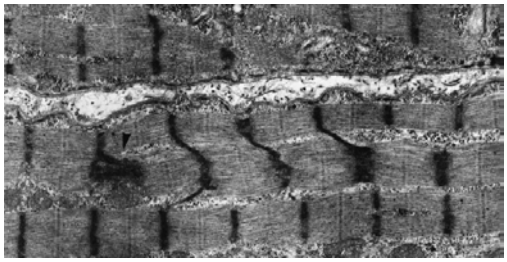

(C)

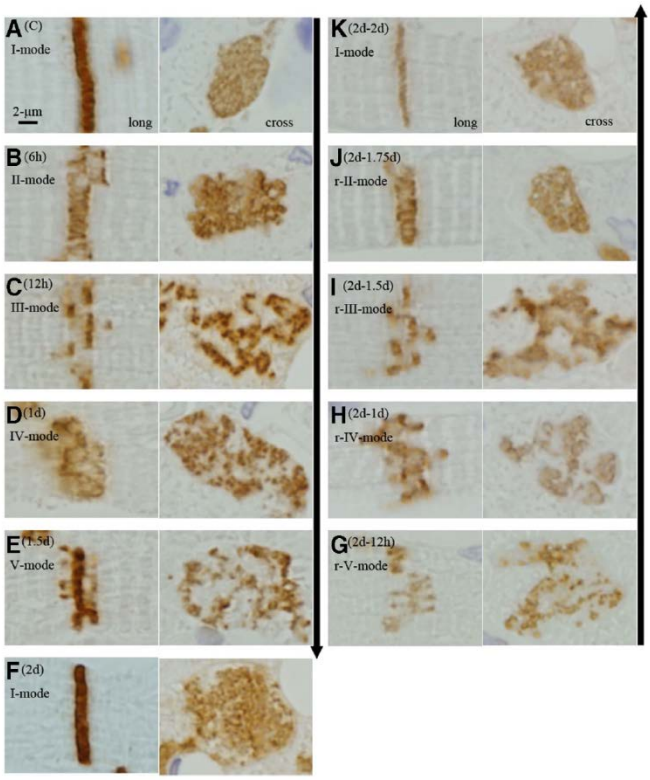

(D)

Figure 2.4 Structural alterations that are hypothesized to be related to sarcomeric addition . (A) Broadened Z disc, adapted from [64] with permission from Elsevier, copyright 1970. (B) Split Z disc [65]. (C) Misregistered Z disc, adapted from [66] with permission from Nature Publishing Group, copyright 1969. (D) Transformation of intercalated discs during volume overload and overload removal. Reproduced from [70] with permission from American Society for Investigative Pathology, copyright 2010

enlarged folds. [66] Recently, researchers have found that Z disc proteins, α-actinin, and N terminal titin could be identified at the axial level of the fold apices, which would be a Z disc of the terminal sarcomere in the myofibril although Z disc-like structures are not present. [68, 69] This domain is hypothesized to permit elastic positioning of new sarcomeres during cardiomyocyte growth because introduction of new sarcomeres would not squeeze preexisting myofibrils. Yoshida et al provided supporting evidence for this elastic addition of sarcomeres at intercalated discs that cardiomyocyte elongation after acute volume overload was accompanied by periodic broadening and narrowing of intercalated discs (Figure 2.4D). [70]

Later studies are predominantly based on direct application of mechanical loads on cardiomyocytes cultured on elastic substrates or cardiac explants. Hypertrophic response of cardiomyocytes is induced by both longitudinal and transverse stretch at transcriptional, translational and post-translational levels. [23-27] Yu et al found that sarcomeres were added to preexisting myofibrils by insertion and that this could occur throughout the cell's length. [27] Yang et al directly captured the dynamics of sarcomeric addition in uniaxially and statically stretched cardiomyocytes in culture. Their results show that new sarcomeres could be added to the end (Figure 2.5A) and/or in the middle (Figure 2.5C) of preexisting myofibrils, thus elongating them. Lateral expansion of myofibrils was achieved mainly by longitudinal splitting (Figure 2.5D) of and sarcomeric addition to the side (Figure 2.5B) of preexisting myofibrils. [28] Guterl et al found that cardiomyocyte thickening was accompanied by cardiomyocyte shortening in isometrically stretched papillary muscle, indicating that myocyte thickening might have

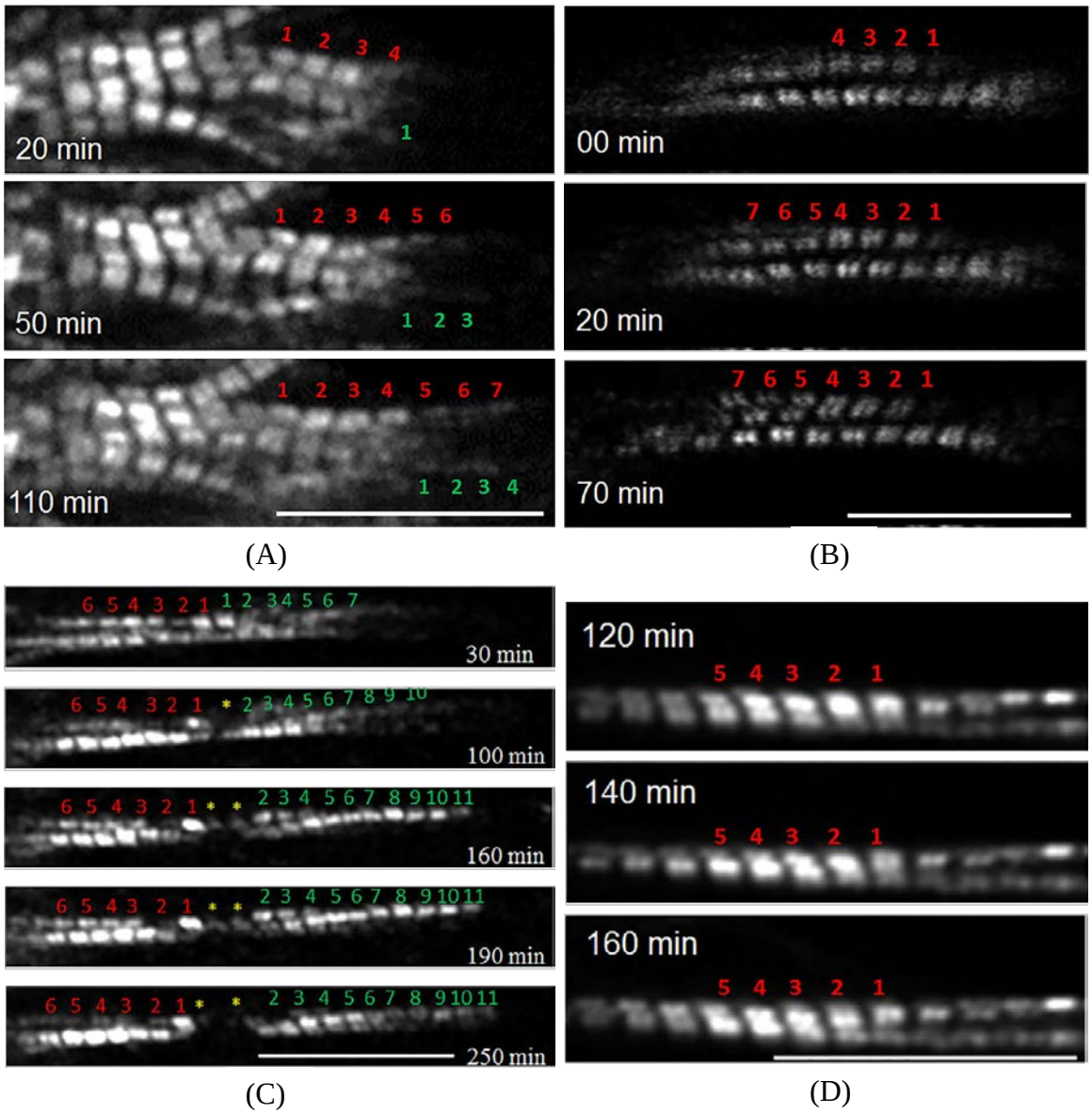

Figure 2.5 Modes of sarcomeric addition observed in isolated single cardiomyocytes. (A) Sarcomeric addition in series at cell end. (B) Sarcomeric addition in parallel using an existing myofibril as template. (C) Sarcomeric insertion in the middle of a myofibril. (D) Myofibrillar splitting. Adapted from [28] under Creative Commons Attribution 4.0 International License

occurred partially by rearrangement of existing sarcomeres. [31]

Studies on de novo myofibrillogenesis provide insights into the correct sequence of sarcomeric assembly which may be shared by myofibrillogenesis under increased mechanical loads. Studies on myofibrillogenesis under mechanical loads are concentrated on revealing the locations and modes of sarcomeric addition, which may or may not be shared by de novo myofibrillogenesis. For example, researchers report that myofibril elongation during de novo myofibrillogenesis is achieved by a lateral coalescing of adjacent shorter myofibrils [59]; this is yet to be discovered in myofibrillogenesis under increased mechanical loads. Despite the progress that has been made, many results are supported by few studies if not one. A lack of experimental evidences has posed serious concerns to the conclusions that have been made. There is still no agreement between researchers on the most fundamental questions such as when, where and how sarcomeric addition occurs under mechanical loading, not to mention the effects of different mechanical loading conditions on sarcomeric addition and the functional outcomes of sarcomeric addition. More systematic investigations are needed.

2.3 Engineering cardiomyocyte alignment on PDMS substrates

Cardiac function is directly related to cellular orientation and elongation. [71] Therefore, alignment of cardiomyocyte in culture is not only a metric of in-vivo similarity [72], but also a prerequisite for direction-controllable mechanical assays. There are many techniques for engineering cell alignment in vitro as review by Li et al, including topographical patterning, surface chemical treatment, mechanical loading and

electrical stimulation. [29] Experiments have shown that cardiomyocytes can be aligned using any of these techniques.

Topographical patterning

Topographical patterning is the most widely used and most efficient method for engineering cell alignment. The mechanism underlying cell alignment with topographical features is contact guidance, which was first described by Weiss 70 years ago. [73] Different types of cells have different preferential topographical patterns. For example, cardiomyocytes show astonishing alignment on parallel patterns such as grooves and wrinkles, while they barely align to upright pillars, which neurons prefer. [29]

Grooves usually refer to the type of grooves with upright walls, though some irregular grooves are also used [74, 75]. Grooves for cell alignment are on micro/nano-scale. These miniaturized features are made with micro/nano-fabrication techniques such as deep reactive ion etching, electron beam lithography, direct laser writing, photolithography, replica molding and microfluidics. [29] Similar effective though micro and nano grooves are in cell alignment, their underlying mechanism are different. Cell alignment on microgrooves is due to physical constrictions, while cell alignment on nanogrooves is related to more fundamental signaling pathways. [76]

Dimensions of grooves play an important role in directing the guidance of cell alignment, especially the depth of grooves [77, 78]. Various studies have shown that different cells have different sensitivity to depth of grooves [79], though no agreements have been made on the responsive threshold for any cells. For effective alignment of cardiomyocytes, the smallest depth of grooves is about 140nm. [75]

Groove topography has been reported to affect the morphology and function [80] of cultured cardiomyocytes. Motlagh et al found that cardiomyocytes cultured in 10 X 10 X 5μm (groove width X ridge width X groove depth) grooves with interspersed pillars showed increased myofibrillar height and well-established myofibrillar structure at cell ends. They believed that the presence of a vertical surface would promote the myofibrillar assembly at the interface. [81] Kim et al found that cardiomyocytes cultured on nanogrooves were significantly elongated and expression of connexin 43 (Cx43), one gap junctional proteins, was increased with increased widths of grooves and ridges. [82] The significant elongation could be attributed to both the facilitation of anisotropic features in cell extension and the inhibition in cell lateral expansion across nanogrooves. [83]

Precisely periodic micro/nano grooves does not represent in vivo extracellular matrix, because native extracellular matrix such as collagen fibers is on several orders of scale. [84] To address this problem, researchers develop substrates with unidirectional multi-scale wrinkled substrates for cell alignment, which is first introduced by Bowen. [85] Unidirectional wrinkles are usually formed by unidirectional compressing a stiff layer. As a consequence, the stiff layer buckles in the direction of the compressive strain, thus forming perpendicular wrinkles. The stiff layer can be made by metal sputtering or oxidization in a plasma or UV ozone chamber. The compressive stress can be delivered by differential thermal contraction, externally applied compressive force, and differential swelling or shrinkage. [86] The dimensions of wrinkles depend on the thickness of the stiff layer and the strength of the compressive strain. Studies have shown that: 1) periods

and amplitudes of wrinkles increase with thickness of the stiff layer [87]; and 2) increased compressive strain is related to increased amplitudes, decreased periods and increased degree of wrinkle orientation. [86] Most wrinkles in literature have periods ranging from submicron to about ten microns and amplitudes less than 2 μm [84, 85, 87-89] , with one exception from Efimenko et al that wrinkle periods ranges from 50 nm up to 400 μm and amplitude ranges from 10 nm up to 10 μm [90].

Studies have shown that wrinkled features have a clear alignment effect on various cells, including human embryonic stem cell (hESC), hESC-derived cardiomyocytes, neonatal cardiomyocytes, etc. Wrinkles are reported to induce an enhanced anisotropic electrical signal propagation [84] and an enhance distribution of Cx43, N cadherin and vinculin at cell-cell junctions [89] in cardiomyocyte culture, which implies the potential benefits of using wrinkles with respect to cardiomyocyte function.

Chemical patterning

Chemical patterning for cell alignment refers to patterning of culture substrates with cytophoblic and/or cytophilic molecules. When cells are seeded to chemically patterned substrates, cells can only adhere and grow in areas with cytophilic molecules. If the dimensions of the patterns are appropriate, cells will align. A direct and specific cell-sensing mechanism such as integrin-ligand binding governs the chemical patterning process. [91] Selection of cytophobic and/or cytophilic molecules depends on cells and substrates. Common cytophilic molecules include poly-L-lysine (PLL), peptides, fibronectin, laminin and other ECM proteins. Common cytophobic molecules are poly(ethylene glycol) (PEG)-graft polymers and serum albumin. [29]

There are several approaches for chemical patterning, including microcontact printing, dry lift-off technique, selective molecular assembly patterning, microfluidic patterning, dip-pen technology, and nanopipetting. [91-93] Among these techniques, microcontact printing (μCP) is the most widely used method for cell alignment. Microcontact printing generally involves four steps: stamp fabrication using soft lithography technique, stamp inking with cytophilic or cytophobic molecules, printing molecular inks to substrates [94], and releasing stamps from substrates as shown in Figure 2.6. New μCP techniques stem from the common μCP, such as affinity μCP [95], aqueous μCP [96], enzyme-etching μCP [97], etc.

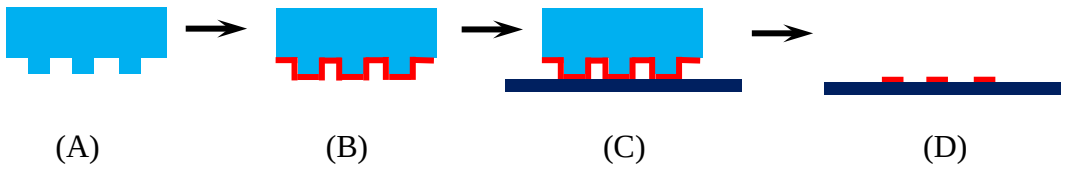

Figure 2.6 General procedure for microcontact printing. (A) Stamp fabrication. (B) Inking. (C) Printing to substrata. (D) Releasing.

The quality of cardiomyocyte alignment on microcontact printed substrates depends on the dimension of patterns. Cardiomyocytes show the best alignment on 5-15 μm lanes, which support only one cell spanning the width of each lane. Besides, patterned cardiomyocytes display an in vivo-like bipolar distribution of N cadherins and Cx 43. [98] Badie et al used microcontact printing to produce a cardiomyocyte culture with realistic ventricular micro and macro structure, with which they found that electrical signal transduction in ventricles is closely related to the alignment of cardiomyocytes and is sensitive to local variations in cell alignment. [99]

Mechanical loading

Mechanical loading for cardiomyocyte alignment comes in forms of uniaxial cyclic stretch, and is widely used in cardiac tissue engineering. Application of cyclic stretch to cardiomyocytes cultured on silicone dishes results in alignment of cardiomyocytes in parallel to the direction of stretch. N-cadherin and Rac1 are involved in the response of cardiomyocyte alignment to uniaxial stretch. Alignment of cardiomyocytes to mechanical stretch is time-dependent. Cardiomyocytes fail to align in the direction of stretch when stretch is applied 24 hours after cultivation. [100, 101]

Electrical Stimulation

Cardiomyocytes, as one of the electrical sensitive and responsive cells, are able to align parallel to the externally applied electric field. [102] Alignment of cardiomyocytes can be promoted by electrical field as low as 2.3V/cm. When electrical field stimulation is applied to cardiomyocytes cultured on microgrooved or micro-abraded surfaces, cardiomyocytes will predominantly follow the guidance of the topographical features, which indicates that electrical cues is a significantly weaker determinant of cardiomyocyte alignment than topographical cues. [103] When electrical field stimulation is applied in the direction of underlying topographical cues, it will enhance cardiomyocyte elongation and electrical properties. [104] Cardiomyocyte alignment in the direction of electrical field results in a larger field potential on individual cardiomyocytes and hence larger contraction amplitude; this might be the mechanism underlying alignment of cardiomyocyte.

Though topographical patterning, chemical patterning, mechanical loading and electrical stimulation are all effective techniques for cardiomyocyte alignment, the strength of their alignment effects is different. Topographical cues are the strongest for cell alignment. [104-107] Chemical cues are only slightly weaker than topographical cues. Mechanical and electrical cues sometimes fail to induce alignment of cardiomyocytes. Topographical and chemical patterning techniques are the most widely used methods in aligning cardiomyocytes in vitro.

2.4 Time-lapse imaging

Time-lapse imaging is imperative for understanding cellular and molecular mechanisms underlying living organisms, such as cell migration, molecular transportation, protein synthesis and assembly, and so on. [108, 109] Traditional time-lapse imaging relies on widefield microscopy and image contrasts derive from phase, differential interference and polarization. Advances in optical theories and microscopic techniques have provided plenty of alternative strategies, an important one of which is fluorescence microscopy. [110, 111]

The increasingly broad application of fluorescence microscopy envisioned in the last several decades is partially due to the advances in fluorescent probes and labeling method. Green fluorescent protein (GFP) and its color variants, since their discovery, have profoundly changed the way in which proteins and cells are studied, because they can be fused with almost any protein and expressed in almost any cell. Another attractive fluorophore is fluorescent naonocrystals, or quantum dots. They can also be coupled to

various proteins. They are highly photostable and the emission spectra can be easily tuned by adjusting the particle size. [111]

Fluorescence microscopy is compatible with many new microscopic techniques including confocal, multiphoton, harmonic generation, total internal reflectance and super-resolution microscopy. In studies on sarcomeric dynamics using time-lapse imaging, one-photon excitation, two-photon excitation and second harmonic generation are the most widely used microscopic techniques. One-photon excitation microscopy generally works on a thin layer of cell culture, and it is limited by out-of-focus light (for widefield microscopy) and scattering (for confocal microscopy). Two-photon excitation fluorescence (TPEF) is a nonlinear process, in which a fluorophore simultaneously absorbs two photons with the same wavelength and yield one photon with a shorter wavelength. TPEF microscopy is inherently confocal because simultaneous absorption of two photons can only occur in the focal volume. Therefore, phototoxicity induced by out-of-focus light is reduced. Another advantage of TPEF microscopy over one-photo microscopy is the large penetration depth. [109] The disadvantage is the low spatial resolution. SHG is a polarization based nonlinear scattering process, in which simultaneously arrived two photons with the same wavelength lead to emission of one photon with exactly half of the wavelength and double energy. Therefore, there is no energy loss during SHG and hence no phototoxicity. Similar to TPEF, SHG also has the advantages of large penetration depth and 3D sectioning ability. It also shares the optics of TPEF microscopy and can be easily built into an existing TPEF microscope with minimal modifications. SHG is intrinsic to noncentrosymmetric structures, which reside

in several biological samples [112] including collagen, myosin, tubulin, glial fibrillary acidic protein, starch, and cellulose, and some synthetic chemicals such as potential-sensitive dyes, e.g. di-4-ANEPPS [113-115]. SHG microscopy endows these samples with free contrast so that they can be detected without protein labeling. The Jablonski diagrams of one-photon excitation, two-photon excitation and second harmonic generation are shown in Figure 2.7. [116]

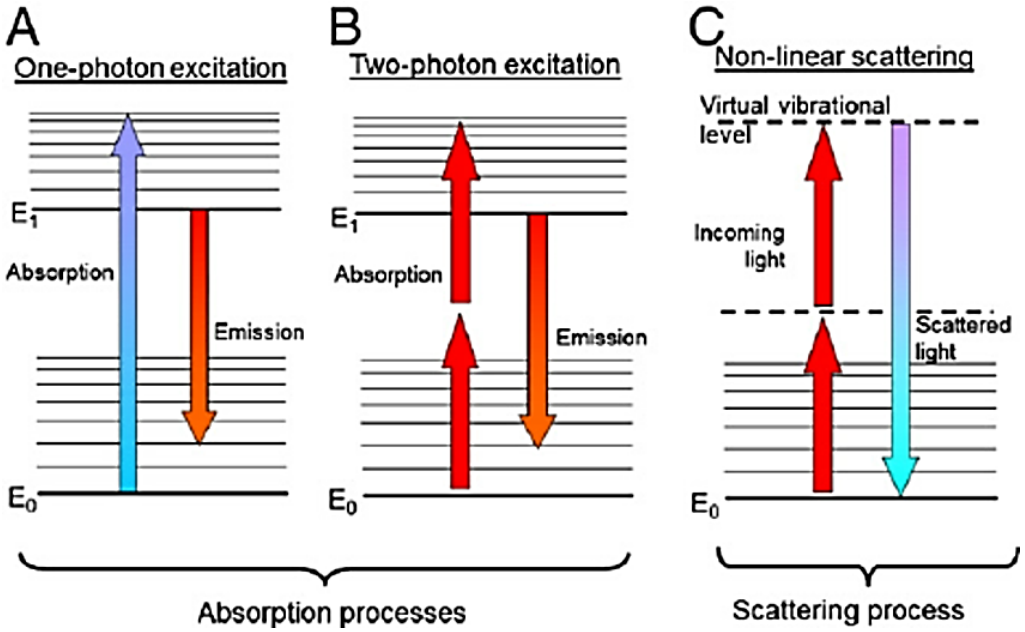

Figure 2.7 Jablonski diagram of one-photon excitation fluorescence (A), two-photon excitation fluorescence (B), and second harmonic generation (C). Adapted from [116] with permission from Elsevier, copyright 2012.

Application of fluorescence microscopy together with one-photon excitation, two-photon excitation and second harmonic generation techniques has revealed amounts of information on sarcomeric dynamics. Srikakulam et al found that GFP-myosin emerged as globular foci at cell peripheries, evolved to short filamentous structures and was finally

replaced by myofibrils; these conformational changes are attributed to the folding of the head and coiled-coil domains of myosin filaments. [117] Dabiri et al expressed GFP-conjugated α-actinin in spreading chicken cardiomyocytes and found that longitudinal growth of myofibrils was accomplished by lateral coalescing of adjacent shorter myofibrils. [59] Manisastry et al simultaneously observed fluorescent protein-conjugated N-RAP and α-actinin/actin, and discovered the function of N-RAP as scaffolds for α-actinin assembly. [118] SHG signal arises from the coiled-coil domain of myosin filaments [119]. The use of SHG microscopy on studies of myosin filaments does not require exogenous protein labeling. SHG microscopy permits dynamic observation of sarcomeric addition, and leads to discovery of many modes of sarcomeric addition, including sarcomeric addition at myofibril end, side, and middle part, or through myofibril splitting. [28, 120, 121]

Photodamage is a primary concern of live-cell imaging because it can adversely affect the cellular and molecular processes being studied. Except for potential thermal damage, laser radiation also lead to reactive oxygen species, free radicals, direct DNA damage, and plasma formation. [122] Photodamage from nonlinear microscopy depends on configuration of the incident laser, including pulse duration, pulse repetition rate, center wavelength, etc. Ji et al believed that photodamage decreases more rapidly with decreased laser intensity than does the signal. With this belief, they introduced a passive pulse splitter into a TPEF microscope. The passive pulse splitter increases the pulse repetition rate and decreases the energy of each pulse. They found that addition of a 64X pulse splitter reduced photodamage in a live sample by an order of magnitude. [123]

Consistent with Ji et al' results, our experiment with live cardiomyocytes showed a 13 times decrease in photodamage when a 64X pulse splitter was introduced. [43] On the other hand, Donnert et al found that photobleaching could be reduced to a similar extent by decreasing pulse repetition rate from 40M Hz to 0.5MHz. They attributed it to the increased separation of individual pulses, which allowed excited fluorophores to return to the ground state before being excited again. [124, 125] Saytashev et al found that photodamage linearly depended on the energy fluence per pulse, and at the same TPEF signal-yielding level, it was smaller with shorter pulse. [122] Photodamage was reduced by local fluorophore density-based non-uniform exposing: area with weak fluorescence was exposed intensely while area with strong fluorescence was exposed lightly. This non-uniform exposing method maintained adequate image quality with low dose of radiation. [126, 127]

CHAPTER III ESTABLISHMENT OF A CARDIOMYOCYTE-CULTURE MODEL ON A POLYDIMETHYLSILOXANE SUBSTRATE WITH IN VIVO-LIKE MECHANICAL LOADING ENVIRONMENT

3.1 Introduction

Clinical-relevant mechanobiological studies of cardiac muscle in vitro require an in vivo-like cardiomyocyte culture that recapitulates at least the native mechanical loading environment. This mechanical environment can be viewed into an active and a passive part: the active stress is caused by the contractile force of cardiomyocytes along their long axes; the passive stress comes from the deformation gradient of myocardium. [128] To allow a cultured cardiomyocyte to experience a mechanical loading equivalent to the in vivo active and passive stress, the cell culture must be specifically designed to ensure appropriate force transmission between connected cardiomyocytes and between cardiomyocytes and their surrounding extracellular matrix (ECM); such a special design is not attained in the currently used cardiomyocyte culture models for mechanobiological studies.

The most prevalent cardiomyocyte culture models for mechanobiological studies are established on deformable silicone substrates using neonatal cardiomyocytes [23, 24, 40, 129-131]. These culture models are advantageous over animal models due to their simplicity, accessibility and controllability. However, cardiomyocytes are cultured randomly in these models, lacking the in vivo-like cell-cell and cell-ECM coupling. In the past two decades, researchers have become increasingly aware of the importance of a culture, with elongated cardiomyocytes aligned along their long axes and end-to-end connected in recapitulating the in vivo organization of cardiomyocytes and thus

mimicking the native mechanical loading environment. For example, Simpson et al aligned collagen fibrils on a silicone substrate to induce cardiomyocyte alignment so to investigate myocyte protein turnover under specific directions of stretch [25]. Yu et al, studied the cardiomyocyte remodeling process under uniaxial and static strain by aligning cardiomyocytes on microgrooved polydimethylsiloxane (PDMS) substrates. [27] However, synchronous active contraction and end-to-end coupling between cardiomyocytes were not attained or characterized in these cultures.

In this study, we developed a cardiomyocyte culture model on a PDMS substrate that recapitulated several aspects of the in vivo-like mechanical loading on cardiomyocytes, including synchronous active contraction, aligned organization, end-to-end coupling between cardiomyocytes as well as cell-ECM coupling. We compared the effects of several state-of-the-art techniques for aligning cardiomyocytes and utilized electrical field stimulation to reinforce synchronous active contraction of cardiomyocytes. The techniques compared for cardiomyocyte alignment include microgroove pattering [132], wrinkle patterning [90], and microcontact printing [99]. Our study not only provides a useful tool for mechanobiological studies but also sheds light on formation and maintenance of mechanical coupling of cardiomyocytes in vivo.

3.2 Materials and Methods

Substrate preparation and characterization

All substrates for cell culture were made with PDMS (Sylgard 184 silicone elastomer kit, Dow Corning). PDMS base and crosslinker were mixed at 10:1 ratio (w/w), and degased by centrifugation at 2000rpm for 5min. The mixture is referred to as PDMS

hereafter. To keep experimental consistency and to reduce variables, baking procedures for curing PDMS were the same for all substrates (65 °C overnight). Thickness of all PDMS membranes for cell culture was set to 75μm; thickness of PDMS membranes could be controlled by adjusting the spinning speed of a spinner (Laurell WS-400B). PDMS thickness as a function of spin speed (Figure 3.1) was well-described by Zhang et al. [133] As indicated in the chart, spinning speed was set to 1000rpm and spin time was set to 60s.

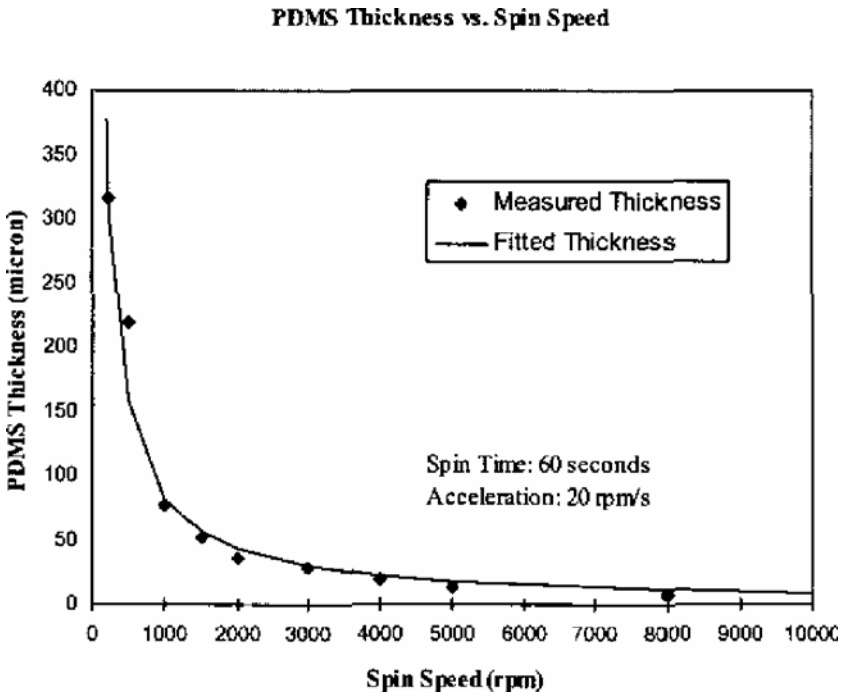

Figure 3.1 Plot of PDMS thickness as a function of spin speed. Reproduced from [136] with permission from IEEE, copyright 2004.

To optimize performance of PDMS as substrates for cell culture, all PDMS substrates for cell culture would be subject to triple solvent extraction, vacuum oven

baking, and sonication if not noted otherwise. PDMS membranes would first be soaked in triethylamine (TEA), ethyl acetate (EA) and acetone, each for 2h. This was designed to remove trapped uncrosslinked PDMS monomers, and improve the biocompatibility of PDMS. [134, 135] Membranes were then baked at 100 °C vacuum oven overnight to remove any residual solvent and further crosslink residual PDMS monomers, if any. These PDMS membranes were bonded to a rectangular PDMS frames (interior dimension: 60mm X 16mm, border width: 3mm, frame thickness: 3mm) to make the final culture chambers. These culture chambers were autoclave, and activated by oxygen-plasma (PDC 32G, Harrick Plasma) or UV-ozone treatment (PSD-UV, Novascan Technologies) as needed before being used for adhesive protein coating and cell culture.

Fabrication of wrinkled PDMS membranes

PDMS was spin-coated to a 4-inch wafer (University Wafer) at 500 rpm for 60s and baked at 80 °C for 2h. A 250 μm membrane was produced and used for fabrication of the first wrinkled PDMS membrane. Fifty percent of strain was applied to the membrane with a custom-made membrane stretcher (Figure 3.2), which was then oxygen-plasma treated for 30min. Strain was released gradually and wrinkles formed on top of the membrane. A polyurethane (PU) master was fabricated from the first wrinkled PDMS membrane using the method described by Desai et al [136], from which subsequent wrinkled PDMS membranes were fabricated. In detail, the PU master was first silanized with trimethylchlorosilane, and then spin-coated with PDMS at 500 rpm for 60s. The PU master was baked at 65 °C overnight and then soaked in TEA for 30min to enable

automatic release of the PDMS membrane. A schematic representation of the fabrication process of wrinkled PDMS membranes is shown in Figure 3.3.

Dimensions of wrinkles were characterized by a scanning electron microscope (SEM). To visualize the top view, wrinkled PDMS membranes were placed directly on top of an aluminum support. To get the side view, wrinkled PDMS membranes were bonded to 1mm thick PDMS, and placed upside down on additional supporting PDMS. This sandwich configuration was important for reducing generation of cracks during cutting. PDMS sandwiches were cut in the middle with two closely spaced blades, and slices were flipped on their sides and bonded to aluminum supports. Wrinkled PDMS membranes were sputter-coated with platinum for 2min, and viewed with Hitachi S4800.

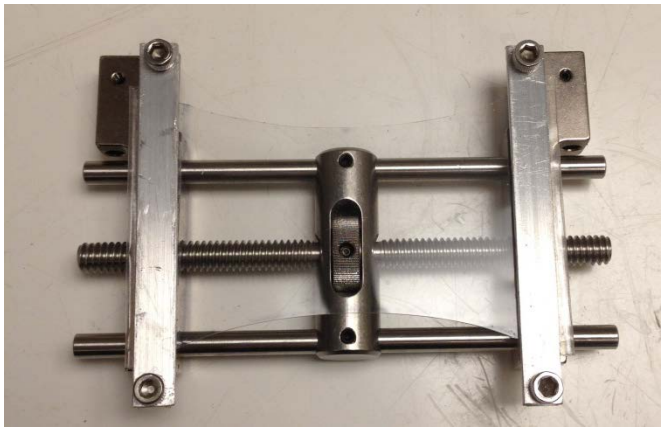

Figure 3.2 Custom-made membrane stretcher

Fabrication of microgrooved PDMS

Microgrooved PDMS substrates were fabricated in three major steps ―mask design, master fabrication, and PDMS membranes fabrication. A mask with a microscale two-dimensional layout of geometries was designed with commercial software such as

AutoCAD, Solidworks, etc. and was laser-plotted to plastic films by commercial companies (CAD/Art Services, Inc). Masks printed on plastic films were used in this project because 1) they were less expensive than that printed on glass substrates; and 2) the resolution (10μm) was sufficient for the application presented here. The geometries used for cell culture in this project was the same as those reported by Motlagh et al [81] : 10μm wide, 10μm spaced lines (Figure 3.4).

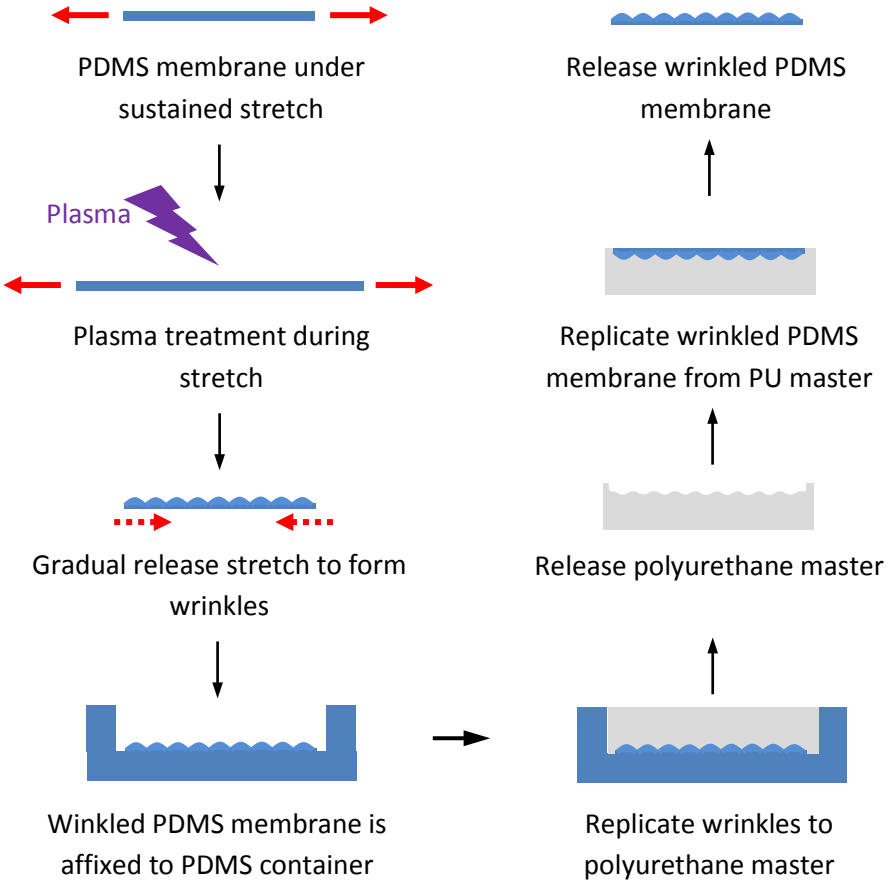

Figure 3.3 A schematic representation of the fabrication process of wrinkled PDMS membrane.

The depth of microgrooves was designed to be 1.5 µm to reduce preferential attachment of cardiomyocytes to the side walls and to increase attachment of cardiomyocytes to substrates. Because no commercially available series of SU-8 photoresist (MicroChem, Corp) allows the production of the specific height of 1.5 µm (Figure 3.5), a customized formulation was developed by mixing SU-8 2005 and cyclopentanone (Acros Organics) at equal weight, which we named as SU-8 2001. SU-8 2001 was poured onto a 2-inch wafer (1 ml per inch of wafer diameter) and was spun at 2000 rpm for 30s to produce a thin even film of 1.5 µm. The wafer was soft-baked at 95 °C for 2min to evaporate residual solvent and to solidify photoresist. Subsequently, the wafer was transferred to the stage on the Karl-Suss MJB3 mask aligner, and was exposed to UV radiation (75mJ/cm^2) through the designed mask. The emulsion side of the mask

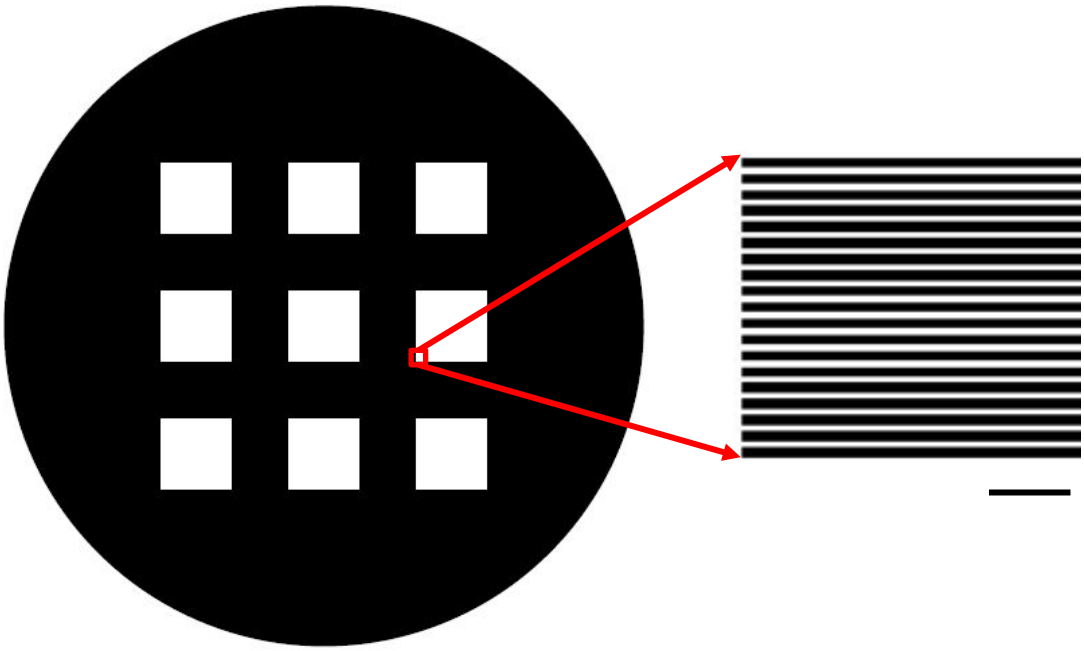

Figure 3.4 The mask for fabrication of microgrooved features. Scale bar = 100µm

was placed downward in direct contact with the photoresist layer to reduce dimensional aberrations that might occur during exposure. After exposure, the wafer was hard-baked at 95 °C for 2min to complete the process of UV-initiated crosslinking of SU-8. Unexposed SU-8 was rinsed off with developer for 1min. The wafer was further hard-baked at 150 °C for 30min to enhance bonding of microgrooves. The processing parameters for different film thickness of SU-8 photoresist were shown in Table 3.1.

PDMS was spin-coated to the master, baked and cleaned using aforementioned method. The top and side view of fabricated microgrooved PDMS membranes were prepared in the same way as wrinkled PDMS membranes, and the dimensions were measured with a conventional widefield microscope (Axiovert 200M, Zeiss).

Microcontact printing

A general microcontact printing process involves creating PDMS stamps, inking stamps with cytophilic/cytophobic molecules, applying stamps to substrate, and stamp releasing. To compare the effects of microgroove patterning and microcontact printing on cell culture, the same mask was used for fabrication of microgrooves and stamps for microcontact printing. The microgrooves on stamps were made deep (7 μm) so that roof collapse [137] was minimized. Considering the depth of grooves on stamp, SU-8 2005 was selected. SU8-2005 was spun at 1000rpm and parameters for lithography were adjusted accordingly (Table 3.1): soft-bake time 3min, exposure energy 120mJ/cm^2, hard-bake time 4min, development time 2min. The master was further baked at 150 °C for 30min to enhance bonding of the microstructures. The master was placed in a 60mm petri dish and 8ml PDMS was poured into the petri dish. The PDMS was vacuumed to

release air bubbles entrapped in microgrooves and cured at 80°C overnight. These stamps had a final thickness of about 3mm. Square PDMS block (8 X 8 mm^2) were cut out and used as stamps for microcontact printing without triple solvent extraction and cleaning. Their surface hydrophobicity/hydrophilicity was found to be optimal for protein transfer from PDMS stamps to UV-ozone activated PDMS membranes in the printing step.

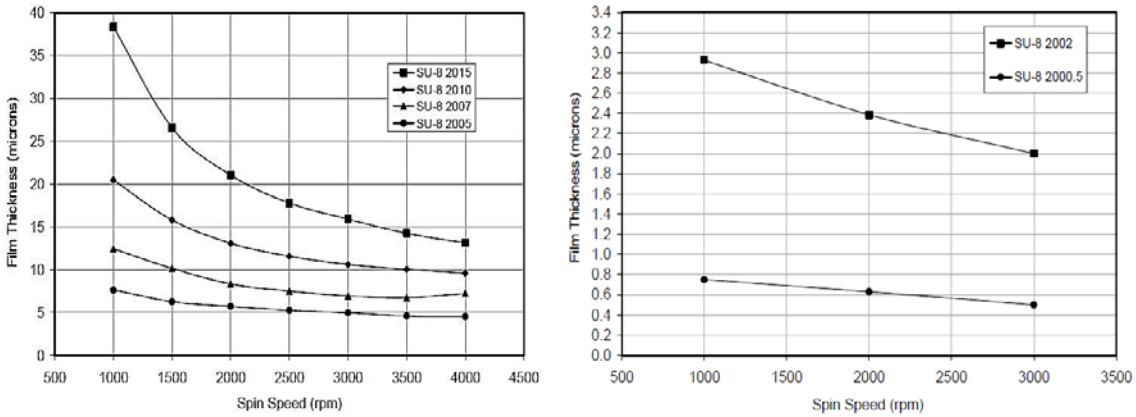

Figure 3.5 Plots of SU-8 photoresist thickness as a function of spin speed. Reproduced from manufacturer's (MicroChem) processing guidelines.

Table 3.1 Processing parameters for different film thickness of SU-8 photoresist

Thickness microns	Soft Bake Time minutes @ 95°C	Exposure Energy (mJ/cm^2)	Hard Bake Time minutes @ 95°C	Development Time (minutes)
0.5-2	1	60-80	1-2	1
3-5	2	90-105	2-3	1
6-15	2-3	110-140	3-4	2-3
16-25	3-4	140-150	4-5	3-4
26-40	4-5	150-160	5-6	4-5

In the printing step, PDMS stamps were coated with freshly prepared 50 μg/ml fibronectin in deioned water for 1h. During that time, the featureless PDMS membrane in a culture chamber was activated by UV-ozone for 15min, which increases the affinity of PDMS substrates to fibronectin. UV-ozone treatment was found to be better than oxygen-plasma treatment at enhancing fibronectin transfer. Timing of fibronectin coating and UV-ozone treatment were carefully adjusted so that both finished nearly simultaneously. Excess fibronectin solution was aspirated and stamps were blown dry with compressed nitrogen. With sterile tweezers, stamps were immediately brought into contact with PDMS substrates. A 50g weight was applied to the back of the stamps to enforce conformal contact. The printing process lasted for 30min at room temperature. After printing, stamps were lifted off carefully.

The printed PDMS substrates were rinsed with PBS and covered with normal culture medium for 1h to enhance cell spreading between printed fibronectin lines. The PDMS substrates were then store in PBS at 4 °C until cell seeding. Normal culture medium is high-glucose Dulbecco's modified Eagle's medium (Gibco) with 10% fetal bovine serum (VWR) and 1% antibiotics (Gibco). To view printed lines on PDMS substrates, fibronectin was conjugated to fluorescein isothiocyanate (FITC) using FluoroTag FITC conjugation kits (Sigma Aldrich). The labeled fibronectin was mixed with unlabeled fibronectin at a ratio of 1:4 and was used to coat the stamp in regular microcontact printing.

Cell isolation and culture

Ventricular cardiomyocytes were isolated from 3-day-old neonatal Sprague-Dawley rats using a two-day protocol as described by Yang et al [28], which was approved by Clemson University Institutional Animal Care and Use Committee. All substrates for cell culture were prepared on the day of cell seeding. Wrinkled and microgrooved PDMS membranes were coated with freshly prepared 20 μg/ml fibronectin overnight before cell seeding. Culture chambers with untreated PDMS were used as control. All culture chambers were set on PDMS frames so that cardiomyocytes were cultured on hanged membranes, eliminating resistive stress from stiff supporting surfaces. When cells were ready, they were seeded to substrates at a density of $2 \times 10^5/cm^2$ in normal culture medium. Medium was replaced next day with normal culture medium plus β cytosine-arabinoside (AraC) (Sigma Aldrich) and was replaced every other day thereafter. The effect of Arac on fibroblast proliferation was investigated and is shown in Appendix A.

Electrical field stimulation

Electrical field stimulation was performed using two pure carbon rods (Ladd Research Industries). The carbon rods were connected to a stimulator via platinum wires. The stimulator comprises a stimulation generator (STG1008, Multi Channel Systems) and a power amplifier (model UT01, Marchand Electronics). Cells were stimulated with a biphasic pulse train (1ms pulse duration at 2Hz) at 3 V/cm.

Immunocytochemisty

Cells were fixed with 4% paraformaldehyde (pH 7.4) for 10 to 15min, rinsed thoroughly with PBS, penetrated with 0.25% Triton X-100 for 10 to 15min, and blocked with 10% (v/v) donkey serum plus 0.1M glycine for 30min at room temperature (RT). Glycine was used for blocking uncrosslinked paraformaldehyde. Cells were then incubated with rabbit anti pan cadherin primary antibody (Abcam, 1:200) at 4°C overnight. The next day, cells were rinsed with PBS, and incubated with Alexa Fluor 488-conjugated Donkey anti rabbit IgG (H+L) (Invitrogen, 1:200) for 2h in a dark room. Cells were then rinsed thoroughly and incubated with mouse anti α-actinin (Sigma Aldrich, 1:500) followed by Alexa Fluor 594-conjugated Donkey anti mouse IgG (H+L) (Invitrogen, 1:200). Cells were rinsed thoroughly with PBS and mounted with ProLong Gold antifade mounting solution with DAPI (Invitrogen). Cardiomyocytes cultured on different substrates were imaged with a spinning disc confocal microscope (DSU, Olympus).

Evaluation of cardiomyocyte alignment

Cell alignment was evaluated using an adaption of the weighed orientation order parameter (OOP) as described by Pasqualini et al [138]. Maximum intensity projected α-actinin images were used as substrate for calculation. A structure-tensor orientation histogram was generated using an imageJ plugin—OrientationJ Distribution. OOP was then calculated by:

$$OOP = \frac{1}{N}\left|\sum_{1}^{N} e^{i2\vartheta_j}\right|$$

where $i = \sqrt{-1}$ is the complex unit, e is Euler's number, and ϑ_j is the jth orientation in $\{\vartheta_1, \vartheta_2, \ldots, \vartheta_N\}$, which is bounded by 0 and π. OOP is bounded by 0 (for completely isotropic structures) and 1 (for completely anisotropic structures). Further, the orientation histogram was fitted with a linear mix of Von Mises Distributions

$$f(\vartheta; \mu_1, \delta_1, \gamma_1, \mu_2, \delta_2, \gamma_2) = \gamma_1 \frac{exp[\delta_1 \cos(2\vartheta - 2\mu_1)]}{2\pi I_0(\delta_1)} + \gamma_2 \frac{exp[\delta_2 \cos(2\vartheta - 2\mu_2)]}{2\pi I_0(\delta_2)}$$

where $\mu_{1,2}$and $\delta_{1,2}$represent the localization and spread parameters for the Z-disks and Z-bodies, respectively, and $I_0$is the modified Bessel function of order 0. Each item represents the probability density function (pdf) of the designated structure. The weighed OOP was determined by:

$$OOP_1 = 2\sum_1^N pdf_1(\vartheta)\cos(\vartheta - \mu_1)^2 \Big/ \sum_1^N pdf_1(\vartheta) - 1$$

$$OOP_2 = 2\sum_1^N pdf_2(\vartheta)\cos(\vartheta - \mu_2)^2 \Big/ \sum_1^N pdf_2(\vartheta) - 1$$

$$\eta = \sum_1^N pdf_1(\vartheta) \Big/ \sum_1^N f(\vartheta; \mu_1, \delta_1, \gamma_1, \mu_2, \delta_2, \gamma_2)$$

$$wOOP = \eta \times OOP_1 + (1 - \eta) \times OOP_2$$

Statistics

All data were presented as mean ± standard deviation (SD). The quality of cardiomyocyte alignment on treated PDMS substrates were compared with that on untreated PDMS substrates using Student's T-test. A probability value that was less than 0.05 was considered statistically significant.

3.3 Results

Substrates with different alignment cues (Figure 3.6) were prepared with the aforementioned methods. Releasing a piece of pre-stretched and plasma-treated PDMS membrane led to formation of wrinkles on the top of the PDMS membrane that went perpendicular to the applied strain. The wrinkles showed normally distributed periods (3.85 ± 1.16 μm) and depths (0.80 ± 0.30 μm), and their periods and depths are positively correlated ($R^2 = 0.63$) by a relating coefficient of 0.2. This coefficient suggests that a percentage of slightly greater than 20% of applied strain was fixed onto the PDMS membrane (mathematical calculations shown in Appendix B), which led to the formation of wrinkles. The microgroove features were designed to have equivalent groove and ridge widths of 10 μm. The produced microgroove features showed 2.75% to 5% shrinkage, inversely depending on the thickness of the supportive base. For example, when

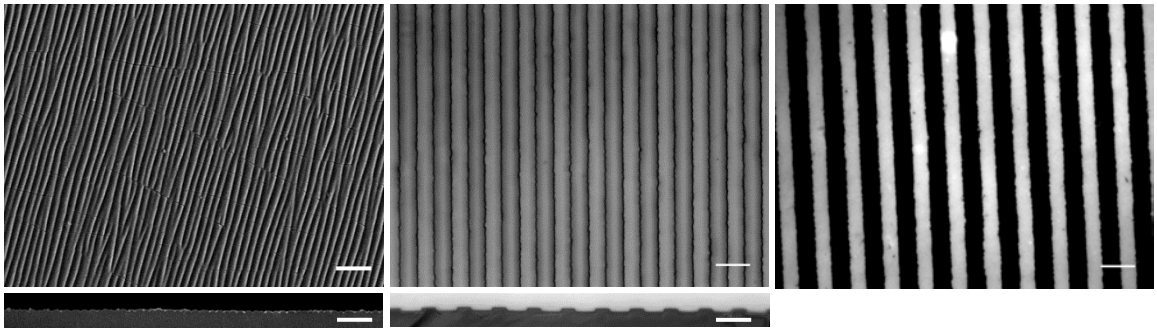

(A) (B) (C)

Figure 3.6 PDMS substrates prepared with different techniques. (A) Wrinkled PDMS membrane. (B) Microgrooved PDMS membrane. (C) Microcontact-printed fibronectin lines on blank PDMS membrane. Top and side views are shown for both (A) and (B). Scale bars = 20μm.

microgrooves were produced on thin PDMS membrane (about 75μm) for direct cell culture, the groove and ridge widths were 11.09 ± 0.27 μm and 7.87 ± 0.23 μm, with a total shrinkage of 5%; when microgrooves were produced on thick PDMS stamps (about 3mm) for microcontact printing, the groove and ridge widths were 10.07 ± 0.28 μm and 9.38 ± 0.20 μm, with a total shrinkage of 2.75%. Grooves with different depths were prepared for different purposes: for direct cell culture, groove depth was 1.50 ± 0.08 μm; for microcontact printing, groove depth was 7.0 ± 0.22 μm. Fibronectin could be transferred to UV ozone activated PDMS substrates at high resolution, resulting in a relief pattern of the grooves on the printing stamps.

When cardiomyocytes were cultured on treated PDMS substrates , they consistently elongated in the direction of the underlying alignment cues and assumed rod shapes (Figure 3.7A-C). On untreated PDMS membranes, cardiomyocytes spread randomly and developed polygonal shapes (Figure 3.7D). The quality of alignment was quantitatively evaluated by weight OOP (Figure 3.7E); results show that the presence of alignment cues significantly improved the quality of alignment on most culture stages. While chemmical cues (microcontact-printed fibronectin lines) induce better alignment during an early stage of culture (3 days in vitro, DIV3), they were not capable of maintaining the alignment to the degree that topographical cues (microgrooves and wrinkles) did at later stages of culture (DIV5 and 7). Further, the quality of alignment was consistently better for cell cultured microgrooved PDMS membranes than that on wrinkled PDMS membranes.

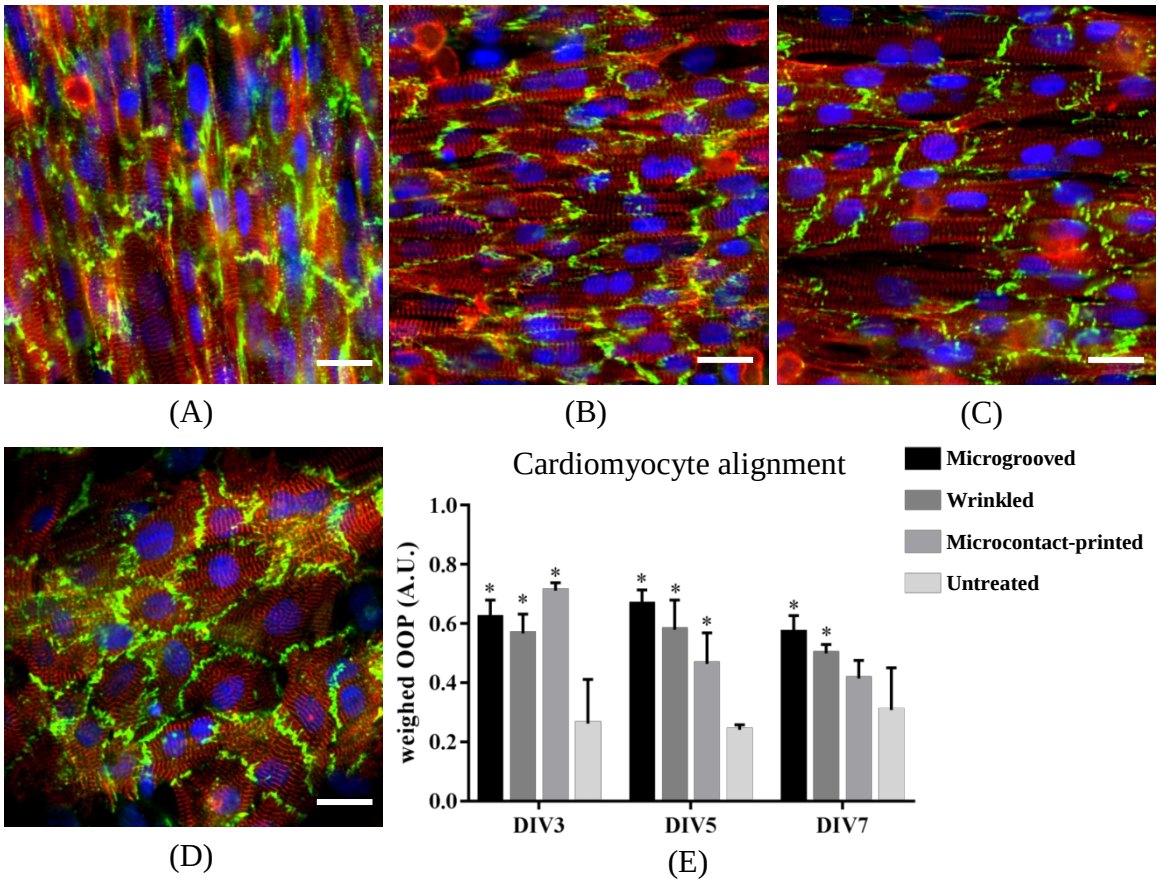

Figure 3.7 Immunocytochemistry for DIV3 cardiomyocytes cultured on (A) microgrooved (B) winkled (C) microcontact-printed and (D) untreated PDMS membranes (green: N cadherin, red: α-actinin, blue: nuclei). Scale bars = 20 μm. (E) Cardiomyocytes alignment on substrates evaluated at different stages by weighed OOP.

Immunocytochemistry results show a polarized distribution of N cadherin to the longitudinal ends of cardiomyocytes (Figure 3.7B-D), resembling the distribution of N cadherin in adult cardiac muscle. The steplike profile of cell-cell interfaces suggests the formation of in vivo-like intercalated discs between connected cardiomyocytes. However, these steplike cell-cell interfaces remodeled in subsequent culturing and returned to

sigmoidal cell-cell interfaces (Figure 3.8A) that naturally occur during culture [139]. The remodeling process was inhibited by electrical stimulation, and sigmoidal cell-cell interfaces were able to return to steplike cell-cell interfaces after application of electrical stimulation for 2 days (Figure 3.8B). Occasionally, cells in these aligned cultures showed automatically synchronous contraction, which macroscopically deformed the supporting membrane. In these cultures, the steplike intercalated discs were maintained without

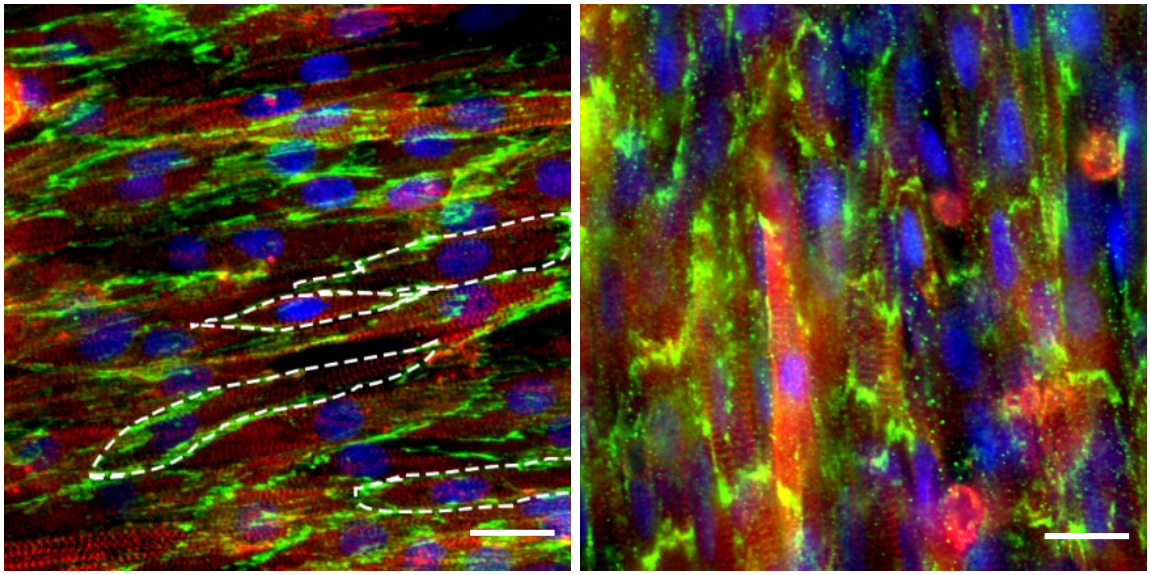

(A) (B)

Figure 3.8 Morphological changes of cell-cell interface in cardiomyocyte cultures on microgrooved PDMS membranes. (A) Sigmoidal cell-cell interface (white dash lines) shown in DIV5 culture without electrical stimulation. (B) Steplike cell-cell interface re-formed after application of electrical stimulation for 2 days from a cardiomyocyte culture with sigmoidal cell-cell interfaces. Green: N cadherin, red: α-actinin, blue: nuclei. Scale bars = 20 μm

electrical stimulation. These results suggest that the formation and maintenance of intercalated discs in vitro depend on mechanical coupling between cardiomyocytes.

Abundant extracellular matrix proteins were expressed in these aligned cardiomyocyte cultures, such as collagen type IV (Figure 3.9A). Collagen type IV is a major component of basement membrane, which wraps around each cardiomyocyte in adult hearts. The expression of ECM proteins by cardiomyocytes suggests an in vivo-like interaction of cardiomyocyte with extracellular matrix and maturation of cardiomyocytes. Though cells are cutured on a 2D PDMS substrate , a 3D cell construct with 3 to 4 layers of cardiomyocytes was formed (Figure 3.9B). When treated PDMS substrates for alignment were bounded to stiff surfaces such as the bottom of a petri disc,

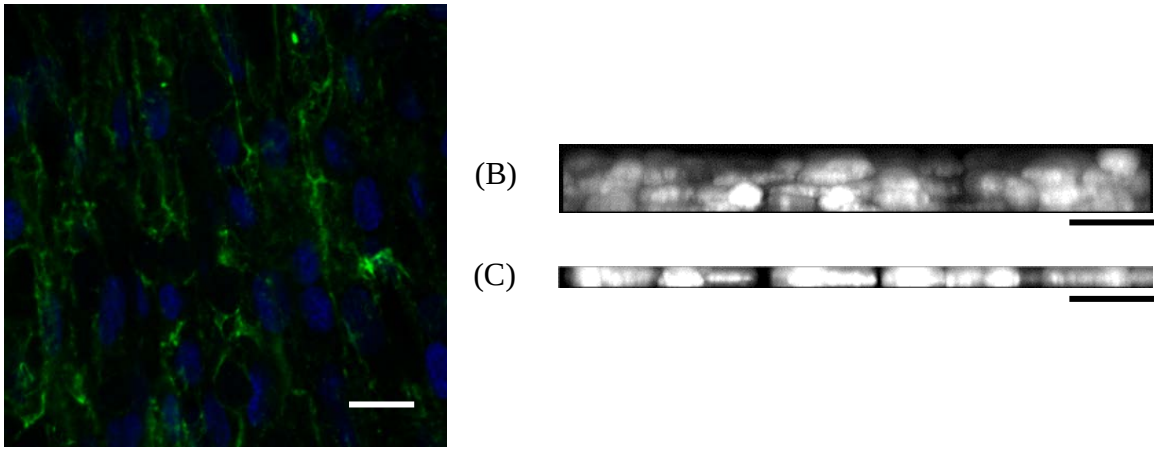

(A)

Figure 3.9 Cardiomyocyte culture on a hanged microgrooved PDMS membrane under electrical stimulation showed abundant collagen type IV (green in A) and multiple layers of nuclei (white in B).On the contrary, cardiomyocyte culture on a bounded microgrooved PDMS membrane showed a monolayer of cell nuclei (white in C). Scale bars = 20 μm

cardiomyocytes failed to form the 3D cell construct (Figure 3.9C), which suggests that formation of such a in vivo-like cell contruct depend on the hanging culture arrangement, which mechanically mimicking a heart muscle with matched compliance.

3.4 Discussion

In this study, we established a 3D cardiomyocyte culture model on a 2D PDMS substrate that recapitulated several aspects of in vivo-like mechanical loading environment. Cardiomyocytes were aligned using various state-of-the-art techniques to form a cell construct that resembled the anisotropic organization of cardiomyocytes in vivo. Electrical field stimulation reinforced the active contraction of cardiomyocytes along their long axes, mimicking the active stress of native cardiomyocytes. Cardiomyocytes showed intercalated disc-like cell-cell interfaces between longitudinally connected cardiomyocytes, implying formation of mechanical coupling and appropriate force transmission between cardiomyocytes. Abundant collagen type IV was expressed in the cell construct, indicating the establishment of an integrated basement membrane around cardiomyocytes and implying the formation of cell-ECM mechanical interaction. Multiple layers of nuclei were distributed in the construct, suggesting the establishment of a 3D cell culture on a 2D PDMS substrate, which recapitulated the force transmission in the third dimension that is usually missing in a traditional 2D culture. In summary, the culture model established in this study closely imitates the in vivo-like mechanical loading environment and may serve as a promising tool for mechanobiological studies of cardiac muscle in vitro.

To recapitulate the anisotropic organization of cardiomyocytes, several state-of-the-art techniques were used and compared, including microgroove patterning, wrinkle patterning, and microcontact printing, all of which induced effective alignment of cardiomyocytes on PDMS membranes. Consistent with previous reports, our results show that topographical cues had a stronger constraining effect than chemical cues. [105] Results show that the techniques used to achieve cardiomyocyte alignment did not affect cell-cell interaction. Among the three techniques, microgroove patterning and microcontact printing are widely used methods for engineering cardiomyocyte alignment. Winkle patterning, a new technique that has come into use in the past two decades, allows the use of multiple scales of the wrinkle patterns [90] that mimic the hierarchical structure of collagen type I fibers [140, 141]. However, the wrinkles produced in this study ranged from 1.7 to 6.4 μm and did not appear in multiple scales. We attribute this to the discrepancies of fabrication, among which the fixed amount of strain might be an important contributor.

Intercalated disc-like cell-cell interfaces were formed in the culture model presented here. Usually, “intercalated discs” refers to the steplike membrane appositions between two longitudinally connected cardiomyocytes, where important structures such as adherens junction, desmosome, gap junction, ion channels are located.[54] Though the development of intercalated discs is described in both in vivo and in vitro studies [142, 143], how intercalated discs establish the steplike profile is largely unknown. In an aligned cell culture, cardiomyocytes in physical contact naturally form sigmoidal cell-cell interfaces [144], and stabilized cell-ECM adhesions [139]. Adherens junctions are then

established and they grow under increasing tugging force [145] exerted by the contractile myofibrillar cytoskeleton; the force directs the initial formation of cell-cell interface perpendicular to the long axes of cells [146]. Our results show that steplike intercalated discs can be re-formed after application of electrical stimulation, which reinforces the synchronous contraction of cardiomyocytes, suggesting that the formation and maintenance of steplike intercalated discs depends on the tugging force on adherens junctions. However, this needs to be confirmed by more extensive studies.

A 3D cardiomyocyte construct can be formed on a 2D PDMS substrate as shown in this study; however, the mechanism underlying the formation of a cardiac tissue with multiple layers of cells in vitro remains elusive. Guo et al reported that cardiomyocytes can migrate away from an explanted neonatal cardiac tissue and spread on stiff surfaces while they remain merged on soft substrates. [147] Therefore, we hypothesize that the hanging PDMS membranes for cell culture matched the compliance of native hearts, and allowed synchronous contraction of cardiomyocytes that generated the necessary mechanical forces between cell-cell and cell-ECM interactions for formation and maintenance of tissue-like structure [147]. What is in agreement with this hypothesis is that when bounding the PDMS membrane to a petri dish, cardiomyocytes failed to form the multiple layer cell construct. Supportive evidences from experiments that use stiffness-tunable PDMS substrates, as describe by Palchesko et al [148], are needed though. Besides, the formation of a 3D cell culture might synergistically enhance the formation of steplike intercalated discs.

3.5 Conclusion

A 3D cardiomyocyte culture model that recapitulates key aspects of in vivo-like mechanical loading environment was established on a hanged PDMS substrate. Formation of intercalated disc-like cell-cell interfaces and 3D tissue like structure may depend on the substrate stiffness directly or indirectly. The culture model may serve as a tool for mechanobiological studies of cardiac muscle in vitro.

CHAPTER IV DYNAMIC OBSERVATION OF SARCOMERIC MYOSIN FILAMENTS IN CARDIOMYOCYTES UNDER STATIC STRETCH

4.1 Introduction

When the heart experiences increased mechanical loads, cardiomyocytes hypertrophy by adding sarcomeres in series or in parallel, to compensate the increase in work load. However with different inducing factors (physiological or pathological), this compensatory growth of cardiomyocytes can either enhance or deteriorate heart function. It is hypothesized that sarcomeric addition, the most obvious structural remodeling process during cardiomyocyte hypertrophy, must be different for the different functional outcomes. However, what the differences of sarcomeric addition are that lead to different outcomes remains unknown. Furthermore, sarcomeric addition processes in response to general mechanical stimuli remain elusive. Understanding the sarcomeric addition process under mechanical loading conditions is beneficial because it is likely to shed light on therapeutic strategies that may alleviate and cure cardiac hypertrophy or gear a pathological hypertrophy toward physiological hypertrophy [1, 3].

Though sarcomeric addition under mechanical stimuli is not well understood, studies on de novo sarcomerogenesis have provided information on sequences of sarcomeric assembly [30, 59, 61], which is likely to be shared by sarcomeric addition under mechanical stimuli. However, sarcomeric addition during pathological cardiac hypertrophy usually occurs in adult cardiomyocytes, whose cytosolic space is packed with myofibrillar crystalline structures. Addition of new sarcomeres cannot compromise the integrity of existing sarcomeric structure and the contractile function. When, where and how sarcomeric addition in mechanical-loaded adult cardiomyocytes occurs, is

unknown. Such studies are hindered by lack of in vivo-like cell culture model for mechanical assays and adequate methods of evaluation.

Early studies are primary based on animal models of various kinds of induced cardiac hypertrophy. Samples from hypertrophic hearts are fixed and examined under a transmission electron microscope for structural aberrations. Aberrations are frequently found in two structures— Z discs and intercalated discs. Several such aberrations, including broadened Z discs [64], split Z discs [65], misregistered Z discs [66], fold amplitude-increased intercalated discs [70], and multiple intercalated discs [67], are hypothesized to be involved in sarcomeric addition. However, sarcomeric damage is also a frequent phenomenon in cardiac hypertrophy and it is difficult to exclude from investigation without time-lapse imaging, which reveals the entire process of sarcomeric addition.

Recently Yang et al [28] have successfully performed time-lapse imaging for uniaxially and statically stretched cardiomyocytes and have confirmed several modes of sarcomeric addition. They find that under longitudinal stretch sarcomeres are added to the end, by the side or in the middle of an existing myofibril and under transverse stretch sarcomeres are added by the side of or by splitting longitudinally in the middle of an existing myofibril. Additions to the end of and by the side of an existing myofibril occur at cell peripheries and are similar to de novo sarcomerogenesis. Sarcomeric addition in the middle is similar to that on the end because the myofibril is broken and myofibrillar ends are exposed. Addition by longitudinally splitting of an existing myofibril supports the hypothesis that misregistered Z discs are involved in sarcomeric addition under

increased mechanical loads. Because time-lapse imaging is performed on single cardiomyocytes, no sarcomeric addition at intercalated discs can be observed. Whether the observed modes of sarcomeric addition occur in the native heart can be clarified only in an in vivo-like cardiomyocyte culture or cardiac explants.

In this study, we used the cardiomyocyte culture model established by our lab on microgrooved polydimethylsiloxane (PDMS) for studying the sarcomeric addition process under mechanical stimuli with time-lapse imaging using our custom-built two photon excitation fluorescence (TPEF) and second harmonic generation (SHG) microscope [43]. We aimed to clarify 1) if modes of sarcomeric addition under mechanical stimuli observed in single cardiomyocytes exist in an in vivo-like cardiomyocyte construct; 2) if intercalated discs play a role in sarcomeric addition under mechanical stimuli; and 3) if other hypothesized modes of sarcomeric addition exist.

4.2 Materials and Methods

Design and calibration of a uniaxial cell stretching device

A uniaxial cell stretching device was designed and fabricated to fit a commercial on-stage incubator (Okolab) to be installed on the TPEF-SHG microscope during time-lapse imaging for maintenance of a physiological culture environment, as shown in Figure 4.1D. The frame of the stretching device (Figure 4.1C) was machined from biocompatible polyether ether ketone (PEEK) material. It comprises a supporting part, a fix mount and a moveable mount for the PDMS culture chamber. The moveable mount was attached to a fine pitch threaded shaft (Thorlabs) and was to slide on parallel rails

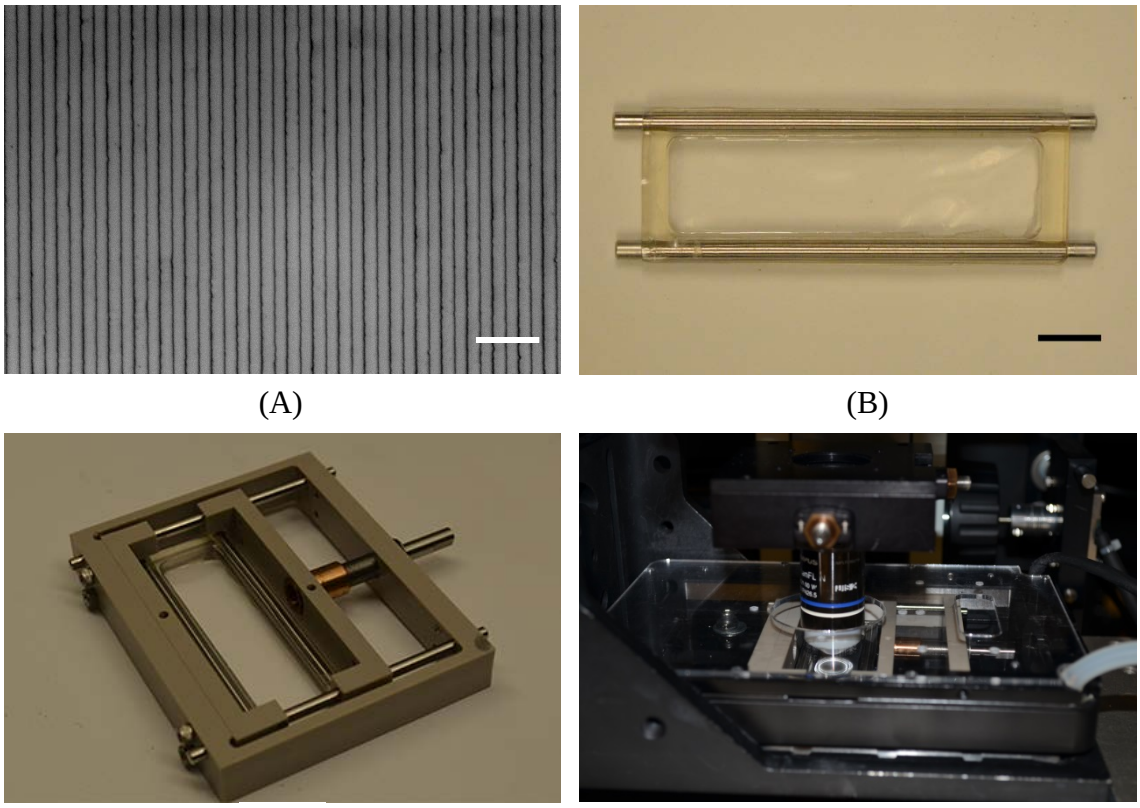

(A) (B)

(C) (D)

Figure 4.1 Uniaxial cell stretching device. (A) Phase image of microgrooved substrate of cell culture chamber. Scale bar = 20μm. (B) PDMS culture chamber. Scale bar = 10mm. (C) PEEK frame of cell stretching device with culture chamber mounted. (D) Cell stretching device housed in the on-stage incubator.

when the shaft was turned. The sliding of the moveable mount relative to the fixed mount deformed the PDMS culture chamber accordingly. The culture chamber (Figure 4.1B) had a large aspect ratio (about 3.6:1) to ensure the delivery of uniaxial strain across the short axis of the substrate. The frame of the culture chamber was fabricated with PDMS from acrylic modes with relieved structures. Microgrooved PDMS membranes (Figure 4.1A) that were fabricated independently as described in CHAPTER III were bonded to

the frame to make the final culture chamber. The reasons for using microgrooved PDMS were that 1) it was efficient in inducing and effective in maintaining cardiomyocyte alignment; and 2) cardiomyocytes on microgrooved PDMS form a 3D cell construct with intercalated cell-cell interfaces. Culture chambers for longitudinal stretching experiments were made by orienting the underlying microgrooves in the direction of the short axis, while culture chambers for transverse stretching experiments were made by orienting microgrooves perpendicular to the short axis.

Strain applied with the designed cell stretching device was calibrated to revolutions of the fine pitch threaded shaft using an image-based method. Briefly, one phase image of the microgrooved substrate was acquired before strain application and after each turn of the threaded shaft. Deformation field was obtained by comparing landmarks on images with and without stretch using BUnwarpJ, an imageJ plugin. Strain was calculated by averaging strain in each deformation grid.

Cardiomyocyte culture and immunocytochemistry

PDMS culture chambers were sonicated in 70% ethanol for 1h and activated by UV ozone for 15min before being mounted to the cell stretching device. A light stretch was applied to culture chambers to keep substrates tight. The culture substrates were coated with 20 μg/ml fibronectin at 37°C overnight. When cardiomyocytes were ready, they were plated to culture substrates at a density of 2 X 10^6/chamber in normal culture medium. Cardiomyocytes were allowed to adhere for 4h and were rinsed with normal culture medium (DMEM + 10% FBS + 1% AA). After overnight culture, medium was changed to normal culture medium supplemented with 2μM β cytosine-arabinoside

(AraC). Medium was then changed every other day. Cardiomyocytes were electrically stimulated as described in CHAPTER III, starting 48h after cell plating.

On the fifth day in vitro (DIV5), cardiomyocytes cultured in PDMS chambers were fixed with 4% paraformaldehyde (pH 7.4) for 10 to 15min, rinsed thoroughly with PBS, penetrated with 0.25% Triton X-100 for 10 to 15min, and blocked with 10% (v/v) donkey serum plus 0.1M glycine for 30min at room temperature (RT). They were then incubated with rabbit anti pan cadherin primary antibody (Abcam, 1:200) at 4 °C overnight. The next day, cells were rinsed with PBS, and incubated with Alexa Fluor 488-conjugated Donkey anti rabbit IgG (H+L) (Invitrogen, 1:200) for 2h in a dark room. Cells were rinsed thoroughly with PBS and mounted with ProLong Gold antifade mounting solution without DAPI (Invitrogen). The cardiomyocyte culture was imaged with the TPEF-SHG microscope with laser setting at 880nm. The filter for the TPEF channel is 530/43 nm (Semrock); the filter for the SHG channel is 440/40 nm (Semrock).

Time-lapse imaging of cardiomyocytes under mechanical stretch

The lab-built TPEF-SHG microscope was modified by introducing a passive pulse splitter to reduce photodamage, and the modified microscope was verified for live cell imaging using randomly cultured cardiomyocytes on glass bottom dish (Appendix C). [43] To image sarcomeric addition under mechanical stretch, cardiomyocytes were cultured in a culture chamber with microgrooved PDMS substrate for 5 days before time-lapse imaging. On the day of imaging, the cell stretching device was transferred to the on-stage incubator that had been installed on the TPEF-SHG microscope. The TPEF channel was left idle due to absence of fluorescence; the SHG channel was used for

collecting signals from myosin filaments. The center wavelength of the laser was set to 830nm and SHG signals were collected through a band-pass filter (414/46, Semrock). An area with well-aligned sarcomeric structures was selected as a region of interest (ROI) by visual judgment and a stack of images of this ROI was acquired before and immediately after stretch application, from which the actual strain of cardiomyocytes was determined. Then, images of this ROI were taken at a predefined interval (20min to 120min) for up to 24h. The stretch to cardiomyocytes in either longitudinal or transverse direction was delivered stepwise to avoid damage to cardiomyocytes.

Synchronized imaging

After 3 days of electrical stimulation, cardiomyocytes beat at a pacing frequency of 2 Hz, which exceeds the 3D imaging speed (on the order of 0.1 Hz depending on size of stack) of the TPEF-SHG microscope. The beating of cardiomyocytes leads to motion artifact, which compromises interpretation of acquired images. To eliminate motion artifact, a method of synchronized recording was developed as described below. The beating of cardiomyocytes was overridden by external triggering, generated by a custom Matlab program (Appendix D) using the NI card for image acquisition. Imaging was only active for the period of time when cardiomyocytes was at rest. The trigger sequence is shown in Figure 4.2. Scanimage [149] was revised accordingly to achieve synchronized imaging (code not shown).

Western blotting

Cardiomyocytes were stretched longitudinally or transversely for 24h starting from DIV5. Stretched cardiomyocytes in each culture chamber were lysed with 300ml

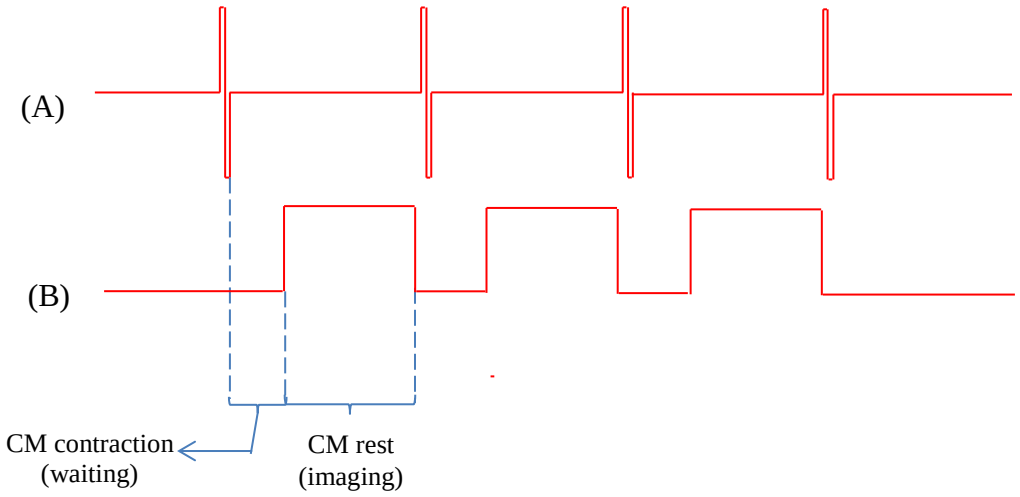

Figure 4.2 Trigger sequence: (A) Trigger for CM beating; (B) Trigger for time-lapse imaging.

ice-cold RIPA buffer (Thermo Scientific) for 20min; the lysate was collected by scraping and was centrifuged for 20min (14000rcf, 4°C). The supernatant was collected and used as a sample for sodium dodecyl sulfate polyacrylamide gel electrophoresis (SDS-PAGE). Before SDS-PAGE, total protein concentration was quantified with a BCA Protein Assay Kit (Pierce). Equal amounts of sample were mixed with Laemmli buffer (Bio-Rad) and were boiled for 5min at 95°C before loading onto a 4−20% precast gradient polyacrylamide gel (Bio-Rad). After SDS-PAGE, proteins were blotted onto a PVDF membrane (Bio-Rad). The membrane was blocked for 2h at RT with 2% non-fat milk or 3% bovine serum albumin (Bioworld). They were incubated with two primary antibodies: mouse anti heavy chain cardiac myosin (Abcam, 1:500), and mouse anti GAPDH (Abcam, 1:1000), which were relayed with an HRP-conjugated goat anti mouse IgG secondary antibody (Novus, 1:2000). A chemiluminescence reaction was performed with

a commercial product (Santa Cruz), and results were obtained with a UVP detection system. The brightness of each band was measured in ImageJ. Brightness of myosin heavy chain bands was normalized with that of GAPDH bands. The normalized myosin heavy chain bands were further compared to those obtained from cardiomyocytes under no stretch to determine if the expression of myosin heavy chain were altered by mechanical stretch.

Statistics

All data was analyzed in GraphPad Prism 7.0 and was presented as mean ± standard deviation (SD). The slope of linear regression between strain and revolution was compared to the theoretical value by an F-test. Student's T-test was used to determine whether concentration of myosin was significantly increased by mechanical stretch. A probability value that was less than 0.05 was considered statistically significant.

4.3 Results

Uniaxial cell stretching device was fabricated as designed. Longitudinal and transverse stretch was easily delivered to cardiomyocytes by turning the fine pitch threaded shaft on the cell stretching device. For simple strain management, strains of cell culture substrates were first calibrated to revolutions of the threaded shaft. Results (Figure 4.3C) show a linear correlation between revolution and strain (R^2=0.9996), which is related by a coefficient of 0.0181 ± 0.0001. This coefficient was close to, but significantly smaller than, the theoretical value (0.0199), which can be calculated by pitch size (1/80 inch) over width (0.628 inch) of PDMS substrates. The initial strain was

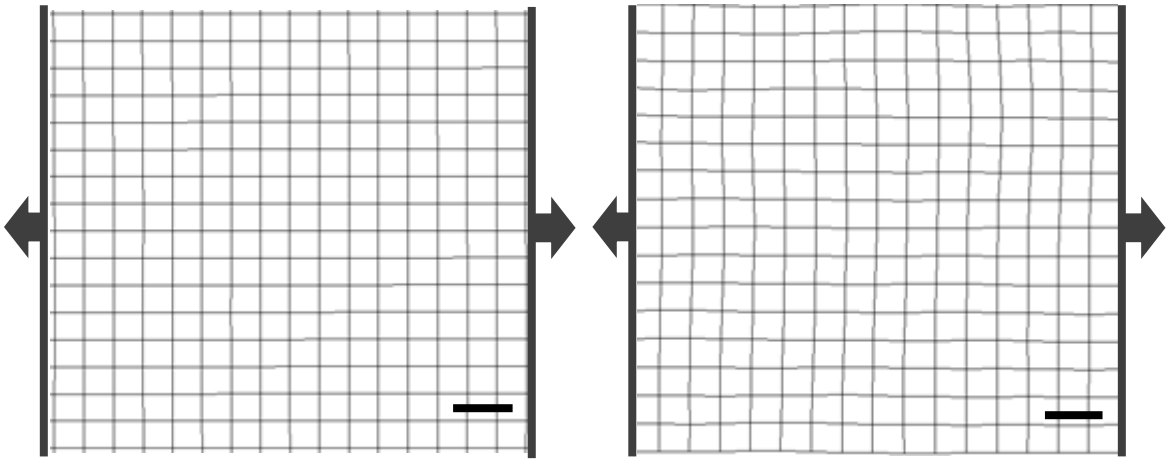

(A) (B)

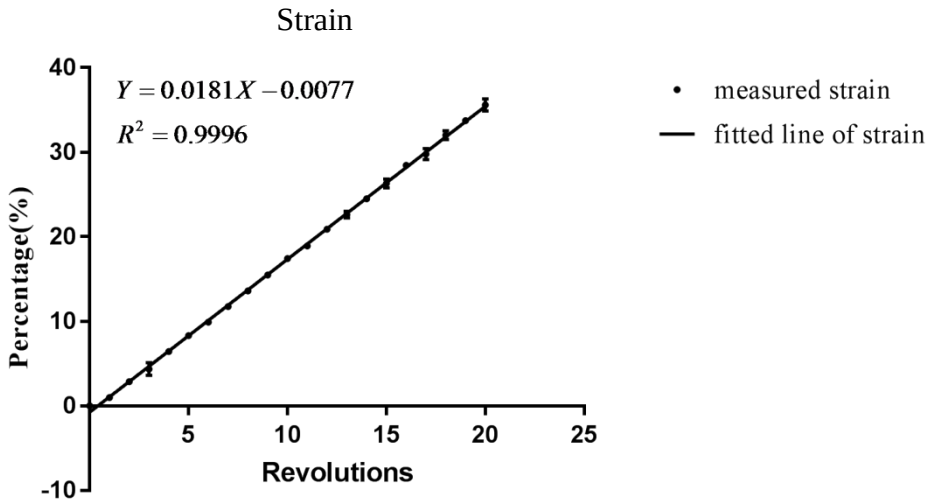

(C)

Figure 4.3 Characterization of strain delivered with the uniaxial cell stretching device. (A) Deformation field of microgrooved substrate under 5-revolution stretch (~9%). Scale bar = 10μm. (B) Deformation field of sarcomeric structures within cardiomyocytes under 5.5-revolution stretch (~10%). Scale bars = 10μm. (C) Plot of strain as a function of revolution. Dots are experimental data and solid line is fitted line of linear regression. Arrows in (A) and (B) show the direction of applied stretch.

estimated to be about 5 revolutions (~1.6mm) from the slope difference. Strain of PDMS substrates as indicated by the deformation field (Figure 4.3A) was uniaxial and uniform. When cardiomyocytes were cultured on top, the deformation field (Figure 4.3B) was slightly altered. Strains on PDMS substrates were conveyed to cardiomyocytes with a minimal deviation of (2.5 ± 3.7%).

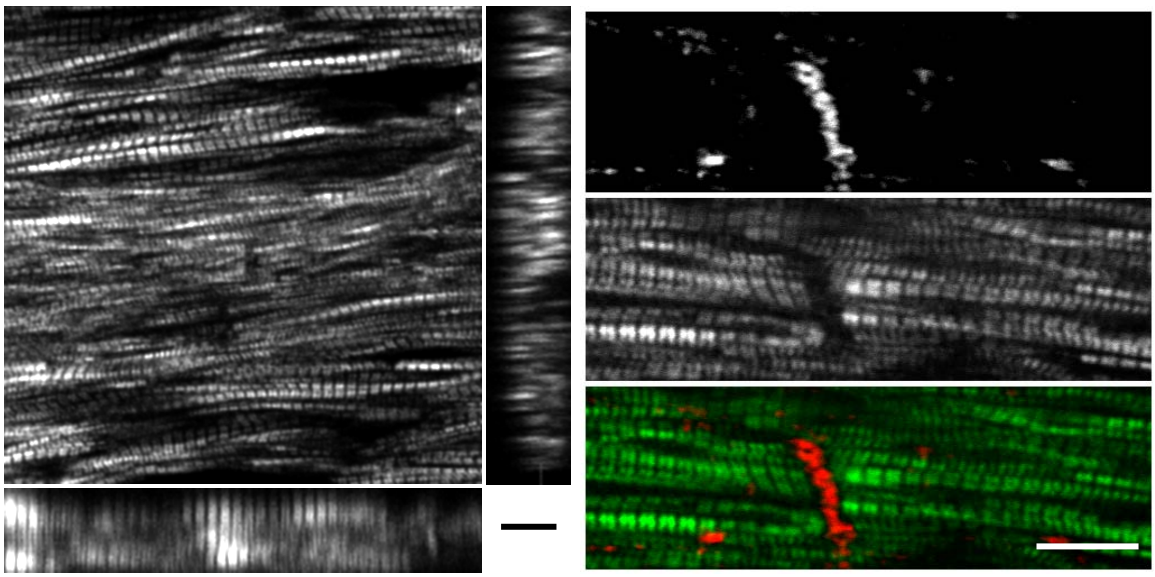

(A) (B)

Figure 4.4 Cell culture characterization. (A) Top and side views of myofibrillar structures in the cell culture. (B) Colocalization of N cadherin and sarcomeric gaps. Top: N cadherin staining, middle: SHG image of sarcomeric A band, bottom: merge of N cadherin and sarcomeric A band image. Scale bars = 10 μm.

An aligned cardiomyocyte culture was formed on a microgrooved PDMS substrate in a culture chamber that had been mounted on the uniaxial cell stretching device. The presence of the cell stretching device did not induce cytotoxicity to the cardiomyocytes. After 5 days in culture, a 3D cardiomyocyte construct was formed on

the microgrooved PDMS membrane (Figure 4.4A) and myofibrils within cardiomyocytes were parallel to underlying microgrooves. The average myofibrillar height of the construct was 11.83 ± 0.78μm. Cardiomyocytes in the 3D construct showed intercalated disc-like cell-cell interface with the polarized distribution of N cadherin, which frequently colocalized with sarcomeric gaps in myofibrils (Figure 4.4B).

To determine the appropriate strains for inducing sarcomeric addition for dynamically imaging, cardiomyocyte sensitivities to strains with respect to sarcomeric damage was evaluated. Cardiomyocytes were exposed to different extents of longitudinal strains, 3h after which cardiomyocytes with sarcomeric structure disruption were counted. Cardiomyocytes showed no sarcomeric damage when they were stretched less than 6%. At stretch over 6%, the percentage of sarcomeric damage became larger and larger as strains increased. When strains exceeded 14%, sarcomeric damage occurred in 100% of cardiomyocytes (Figure 4.5). We noticed that cardiomyocyte sensitivities to strain-caused damage were direction-dependent and were larger in the transverse than longitudinal direction. In practical experiments, we found 6% transverse stretch and 8% longitudinal stretch could efficiently perturb dynamics of sarcomeric assembly with low amount of sarcomeric damage; therefore, 6% transverse and 8% longitudinal stretch were primarily used in the following mechanical assays.

When cardiomyocytes were longitudinally or transversely stretched, sarcomeric length or intermyofibrillar space was found to instantly increase to the same extent. During longitudinal stretch, sarcomeres were added in the middle of an existing myofibril beside a preexisting sarcomeric gap (Figure 4.6A). New sarcomeric nucleation did not

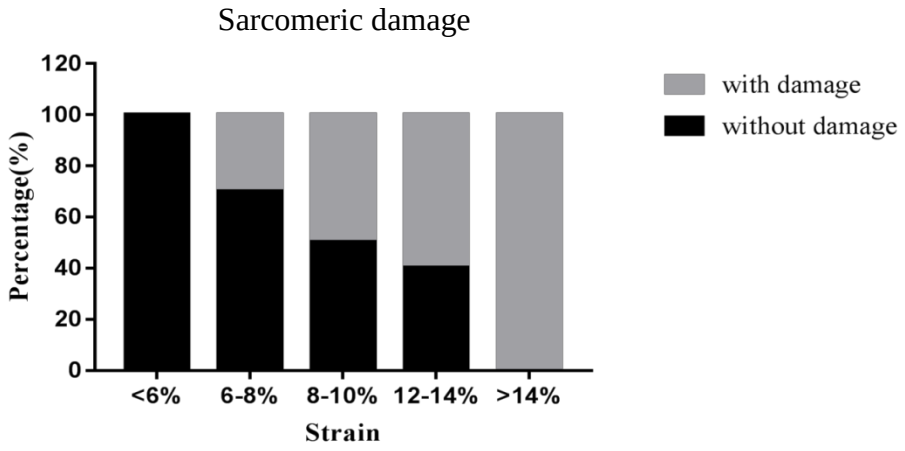

Figure 4.5 Relationship between sarcomeric damage and external strain.

begin until 8h after stretch application. The space between the two sarcomeres gradually increased to about the size of a regular A band. During or after the increase, a thin A band appeared in the middle of the space. A new sarcomere was completely added 14h after stretch. Because sarcomeric gaps denote cell-cell interfaces at longitudinal ends of cardiomyocytes, it may be that new sarcomeres were inserted at an intercalated disc. During transverse stretch, the sarcomeric insertion at an intercalated disc was found to be reverted; this we define as sarcomeric deletion (Figure 4.6B). Similar to sarcomeric insertion at intercalated discs, sarcomeric deletion did not begin until 8h after stretch application. A sarcomeric A band was removed from the intercalated disc area during the process, which was completed within an hour.

Several modes of sarcomeric addition, first described by Yang et al [28] in single cardiomyocytes, were also observed (Figure 4.7). At the intermyofibrillar spaces between two existing myofibrils, sarcomeres were added during both longitudinal and transverse

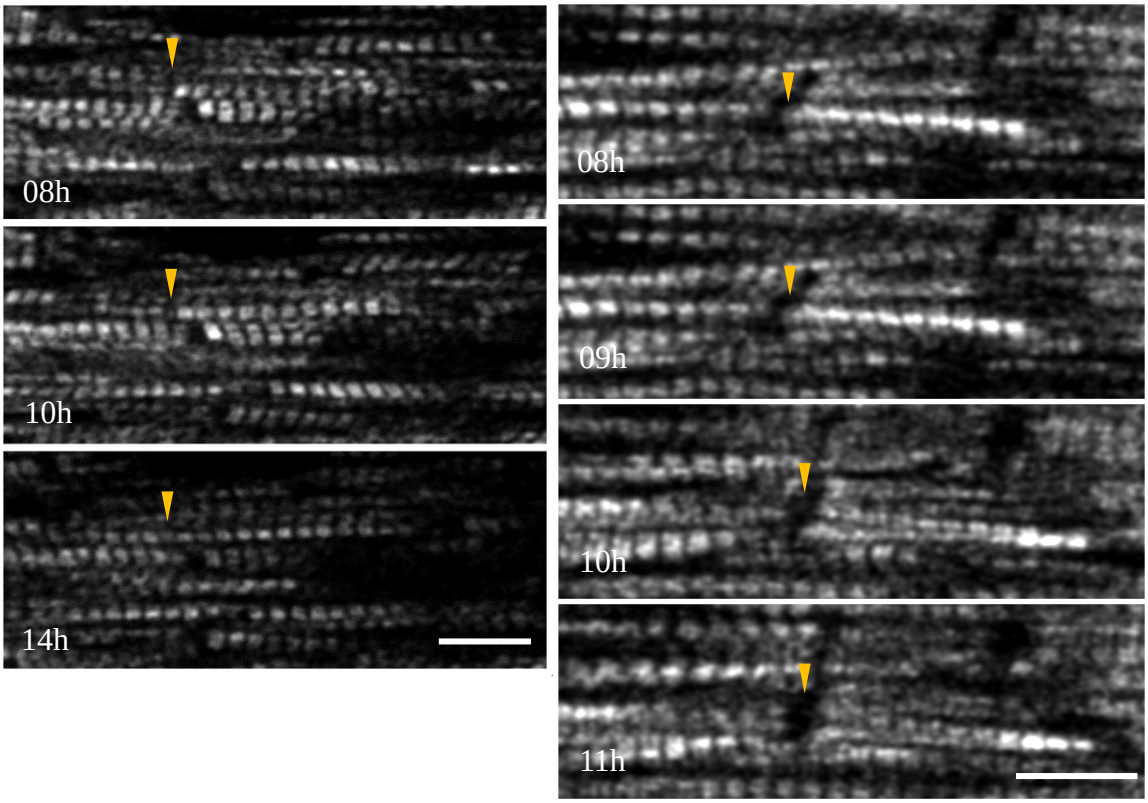

(A) (B)

Figure 4.6 Sarcomeric insertion and deletion at intercalated discs. (A) Sarcomeric insertion into preexisting myofibrils under longitudinal stretch near an area that is likely to be the intercalated disc between two cells. (B) Sarcomeric deletion at intercalated discs. Gold arrow heads indicate the location of sarcomeric insertion and deletion. Time = hours after stretch application. Scale bars = 10μm.

stretch, increasing the number of myofibrils (Figure 4.7A). The number of myofibrils could also be increased through myofibrillar splitting (Figure 4.7B), which was only observed during transverse stretch.

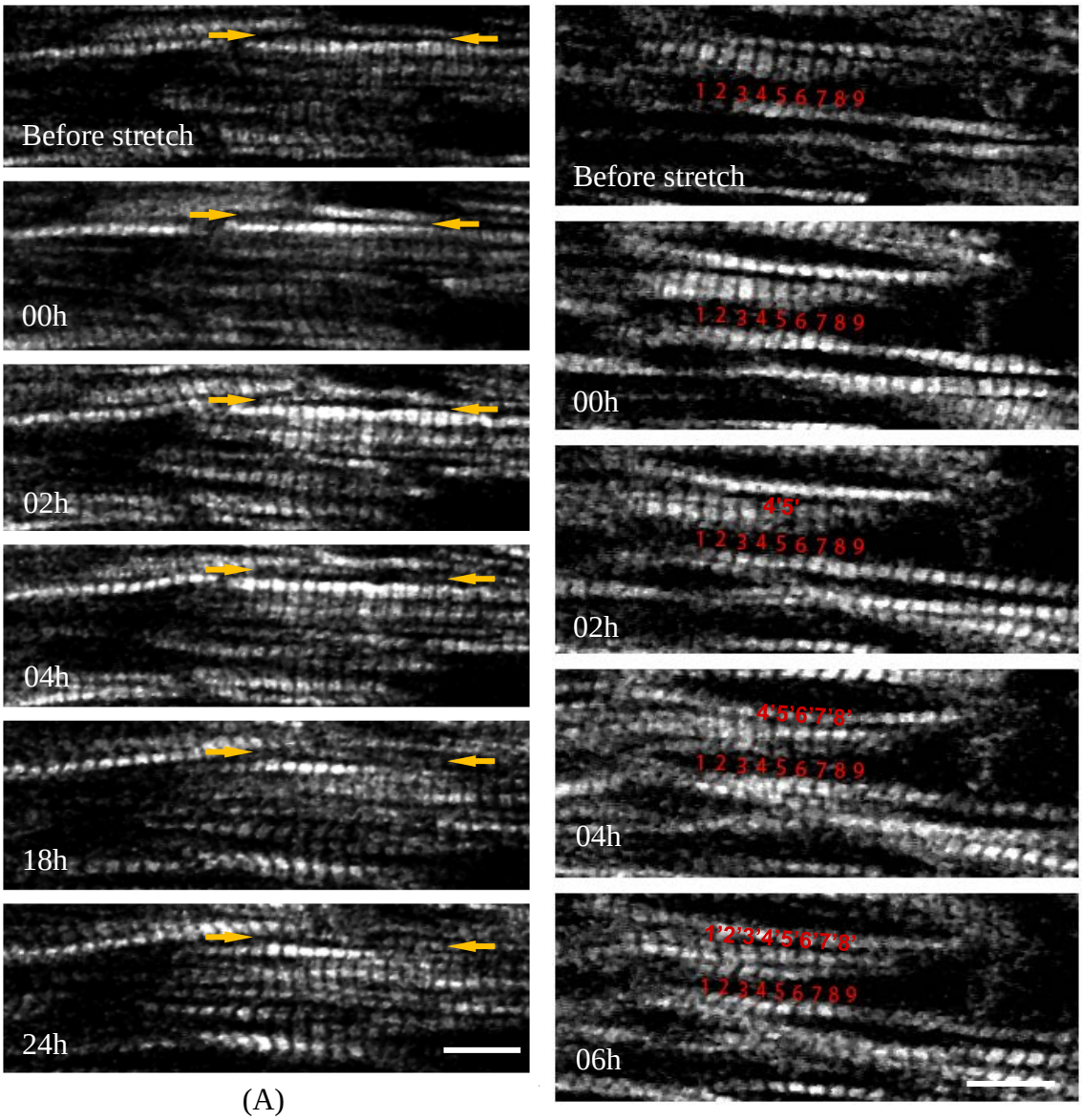

(A)

Figure 4.7 Sarcomeric addition that leads to more myofibrils. (A) Sarcomeric addition to intermyofibrillar space (gold arrows) between two existing myofibrils during 6% transverse stretch. (B) Myofibrillar splitting during 6% transverse stretch. Red numbers denote the original myofibril, and prime numbers denote split sarcomeres. Time = hours after stretch application. Scale bars = 10 µm.

Next, we examined if mechanical stimulation increased myosin synthesis on translational level. The concentration of cellular myosin was measured by western blotting for cardiomyocytes being stretched for 24h and was compared with the concentration for unstretched cardiomyocytes (Figure 4.8). When cardiomyocytes were stretched transversely by 6%, expression of myosin heavy chain increased by 118% (statistically insignificant); when cardiomyocytes were stretched longitudinally by 8%, expression of myosin heavy chain increased by 64% (statistically insignificant). The results suggest that cardiomyocytes are more sensitive to transverse stretch than longitudinal stretch with respect to myosin synthesis.

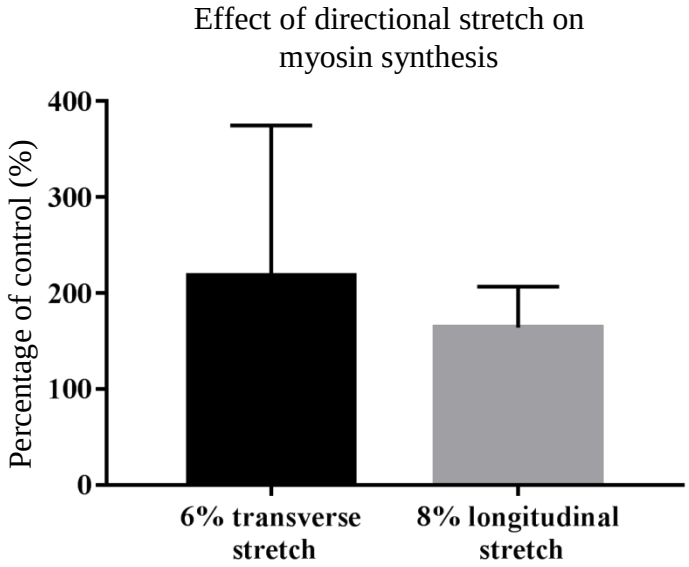

Figure 4.8 Concentration of cellular myosin 24h after stretch application. Data is presented as percentages of control (no stretch).

4.4 Discussion

Sarcomerogenesis under mechanical loading is one of the most important processes in cardiomyocyte remodeling during cardiac hypertrophy. Though many hypotheses have been proposed regarding sarcomerogenesis under mechanical loading, the process remains largely unknown due to a shortage of studies that reveal the dynamic process. In this study, we used a passive pulse splitter-based TPEF-SHG microscope to observe the dynamic sarcomeric addition process within cardiomyocytes in an in vivo-like 3D cell culture during mechanical stretching. We, for the first time, observed the dynamic processes of sarcomeric insertion and sarcomeric deletion at intercalated disc-like cell-cell interfaces. We also confirmed the modes of sarcomeric addition to the side of an existing myofibril and by myofibrillar splitting [28]. Our study depicts modes of sarcomeric addition under mechanical stretch that have not been observed before. This may advance the understanding of cardiomyocyte remodeling under mechanical loading conditions such as cardiac hypertrophy.

Intercalated discs, among the most frequently altered structures in a hypertrophic heart, are hypothesized to play an important role in sarcomeric addition during mechanical stimulation. [66, 67] Bennett et al [68] defined a spectrin-rich domain at the apex of the folds at intercalated discs, which occurs at the axial level of what would be the final Z-disc of the terminal sarcomere. This spectrin-rich domain is named as transitional junction and is supposed to be related to sarcomeric addition at cell ends during growth. Yoshida et al reported transformation of intercalated discs among five modes during volume load and load removal, which they hypothesized to be related to

sarcomeric addition. [70] The hypothesis of sarcomeric addition at intercalated discs was inconclusive due to the use of fixed samples in these studies. Our dynamic observation showed the sequential events during the entire addition process, from the space clearing to the complete addition of sarcomeres. Because the uniaxial stretching device we used provides uniform strain to the whole cell body, the selective addition of sarcomeres to intercalated discs is thought to be native to cardiomyocytes. Because the structural integrity and the contractile function of the myofibril that were added with a sarcomere were not affected, we theorize that intercalated discs allow elastic addition of sarcomeres during mechanical stimulation. Beside sarcomeric insertion, our study showed that sarcomeric deletion can also occur at intercalated discs during transverse stretch. Deletion of sarcomeres at intercalated discs suggests that rearrangement of sarcomeres, which Guterl et al [31] hypothesized based on the phenomenon of accompanied widening with shortening of isometrically stretched cardiomyocytes, may begin by recycling sarcomeric proteins at intercalated discs.

Yang et al [28] first described several modes of sarcomeric addition in a mechanically stretched single cardiomyocyte. Two of these modes were also observed in our in vivo-like 3D cardiomyocyte culture; they are sarcomeric addition to the side of an existing myofibril and by myofibrillar splitting. Sarcomeric addition in the 3D in vivo-like cardiomyocyte culture occurred at a much slower rate than sarcomeric addition in single cardiomyocytes. The typical sarcomeric addition rate in a single cardiomyocyte [28]or a 2D cardiomyocyte culture [27] is 1 sarcomere or myofibril per hour, while in the 3D in vivo-like cardiomyocyte culture, the sarcomeric addition rate is 1 sarcomere or

myofibril per several (6-24) hours. Sarcomeric addition in living rat hearts is 1 sarcomere per day [70]. Our 3D in vivo-like cardiomyocyte culture better represents the sarcomeric addition process in vivo regarding sarcomeric addition rate than single cardiomyocyte cultures and 2D cardiomyocyte cultures.

Synthesis of cytoskeletal proteins accompanies sarcomerogenesis under mechanical stretch. Our western blotting results show a 118% increase of cellular myosin concentration in cardiomyocytes under 6% transverse stretch and a 64% increase in cardiomyocytes under 8% longitudinal stretch. Simpson et al [25] reported an ~50% increase in cardiomyocytes under 5% transverse stretch and no increase in cardiomyocytes under 5% or 10% longitudinal stretch. Our results show a consistent direction-dependent sensitivity of cardiomyocytes, and that cardiomyocytes are more sensitive to transverse than longitudinal stretch. We attribute the difference in synthesis levels of cellular myosin to the difference in cell culture, as studies have proven that a 3D culture environment enhances expression of some cellular protein including α-actinin and desmin when compared to 2D culture. [150] Given the potential influences of in vivo versus in vitro culture environment [30], we believe the results presented in this study more faithfully reflect the in vivo cardiomyocyte response to mechanical load.

4.5 Conclusion

With the 3D cardiomyocyte culture and passive pulse splitter-based TPEF-SHG, sarcomeric addition stimulated by longitudinal and transverse stretch was produced and dynamically observed. For the first time, addition and deletion of sarcomeres at intercalated discs were dynamically captured. Addition of sarcomeres to the side of

existing myofibrils and addition through myofibrillar splitting were confirmed in an in vivo-like cell culture. This study supports the long-standing hypothesis of sarcomeric addition at intercalated discs, and may shed light on cardiomyocyte remodeling to cardiac hypertrophy on sarcomeric level.

CHAPTER V DYNAMIC OBSERVATION OF SARCOMERIC Z DISCS IN CARDIOMYOCYTES UNDER STATIC STRETCH

5.1 Introduction

The Z disc is one of the most important sarcomeric structures. They delineate sarcomeric boundaries, and stabilize sarcomeric structures by interacting with nonsarcomeric and other sarcomeric proteins. They bind barbed ends of sarcomeric actin filaments and connect with myosin filaments through titin filaments, thus holding together major sarcomeric components. Z discs play an important role in mechanotransduction. Intercellular forces exerted on N cadherin and desmosomes at intercalated discs are relayed to Z discs through F actin and desmin; forces between sarcolemma and ECM are passed to Z discs through costameres. Studies have shown that many Z-disc proteins are involved in mechanotransduction signal pathways, including telethonin, muscle LIM protein, melusin, calcineurin and calsarcins, enigma/ENH/cypher family, myopalladin, and so on [57, 151].

Z discs actively participate in de novo sarcomerogenesis and are hypothesized to participate in sarcomerogenesis under increased mechanical load, e.g., in cardiac hypertrophy. Z bodies, which fuse laterally to form Z discs during de novo sarcomerogenesis, are the first detectable sarcomeric structures in spreading cardiomyocytes cultured in vitro [59] and in cardiomyocytes of developing hearts [30, 61]. Z discs are among the most frequently altered cardiomyocyte sarcomeric structures in adult hypertrophic hearts, and some alterations of Z discs are hypothesized to be interphases of sarcomeric addition as a response of cardiomyocytes to increased mechanical load. These alterations include broadened Z discs [64], split Z discs [65] and

misregistered Z discs [66]. However, direct evidence of the role of Z discs in sarcomeric addition under increased mechanical load is missing.

Time-lapse imaging is one of the most direct strategies for clarifying the roles of Z discs in sarcomeric addition. However, conventional widefield microscopy suffers from low contrast because Z discs are very thin (100-140nm in width [151]). Discovery of green fluorescent protein and its variants and advances in fluorescence microscopy in the past several decades have overcome the contrast challenge and made such studies feasible. [111] Simultaneous observation of Z discs and other sarcomeric structures such as thick and thin filaments will help identify the roles of these structures and the fashion of their interactions during mechanical load-induced sarcomerogenesis.

In this study, we expressed EYFP-conjugated α-actinin in cardiomyocytes by transfection and simultaneously observed dynamics of Z discs and myosin filaments with the passive pulse splitter-based TPEF-SHG microscope. The reason for using α-actinin as a probe of Z discs is that α-actinin is the major component and the scaffolding protein of Z discs. [151] We aimed to find 1) whether Z disc alterations seen in adult hypertrophied heart are present in mechanically loaded cardiomyocytes and 2) whether these alterations are involved in sarcomeric addition.

5.2 Materials and Methods

Transfection

Transient transfection was used in this study because primary cardiomyocytes is nonproliferative. Transient transfection expresses a transgene for a limited period of time, typically several days. In transient transfection, the transgene is usually subcloned into a

plasmid vector. In the study we report here, plasmid with a cDNA sequence of EYFP-conjugated sarcomeric α-actinin was provided as a kind gift from Dr. Sanger's lab [59]. Chicken sarcomeric α-actinin was subcloned into the *HindIII* site of the pEYFP-N1 vector (Clontech). The resulting plasmids were amplified in E coli and purified with Qiagen Mega Kit according to the manufacturer's instruction. Final plasmids were quantified with a plate reader (Synergy 2, BioTek); the concentration was estimated to be 0.1μg/μl.

Transfection reagent (TR) is an important determinant of transfection efficiency. To determine the optimal TR for cardiomyocytes, transfection efficiencies of several commercial TR products were compared, including Viromer Red (Lipocalyx), Viromer Yellow (Lipocalyx), lipofectamine 2000 (Invitrogen), TransIT-LT1 (Mirus Bio), Xfect (Takara), Viafect (Promega) and Fugene HD (Promega). Dilutions of each TR and the incubation time with plasmid were optimized as suggested by the manufacturer. Transfection was performed for cardiomyocytes on the first day in vitro (DIV1), and transfection efficiency was checked 24h and 48h after transfection. The highest transfection efficiency of each TR was used for comparison. The detailed protocol for each TR is shown in Appendix E.

Fluorescence recovery after photobleaching

Because expression of EYFP-conjugated α-actinin is transient, the presence of EYFP-conjugated α-actinin expression at the time of time-lapse imaging needs to be determined. A fluorescence recovery after photobleaching (FRAP) experiment was performed for cardiomyocytes on the day of time-lapse imaging. The laser was set to

850nm to maximally approach the excitation spectra of EYFP, in an effort to optimize the bleaching and image acquisition. The laser power was set to full (~200mW) for photobleaching and to 30mW for image acquisition. A rectangular ROI was selected with Scanimage and bleached for 1min. Fluorescence images were taken before bleaching, immediately after bleaching (0min), and at user-defined time points thereafter. Analysis of FRAP data was performed as described by Manisastry et al [118]. Intensity of fluorescence in the ROI was normalized to intensity of the whole image by

$$I_n = \frac{I_{roi} - I_{background}}{I_{image} - I_{background}}$$

Then the normalized intensity was scaled to 0 and 1 by

$$I_{ns} = \frac{I_n - I_{n,min}}{I_{n,max} - I_{n,min}}$$

The exponential recovery part of data was fitted to the curve function

$$I_{ns} = b + p\left(1 - e^{-\frac{t}{\tau}}\right)$$

where p equals to the percentage of recovery, τ is the time constant.

Time-lapse imaging of cardiomyocytes under mechanical stretch

Cardiomyocyte culture was prepared as described in CHAPTER IV. Cardiomyocytes were transfected on DIV1 with the best TR determined previously. A time-lapse imaging experiment was performed as described in CHAPTER IV except that 1) the laser was set to 850nm for excitation of EYFP; and that 2) fluorescence images from EYFP were acquired through the TPEF channel with a 530/40nm band-pass filter (Semrock).

Statistics

All data were presented as mean ± standard deviation (SD) if not noted otherwise.

5.3 Results

Among the seven compared transfection reagents, Xfect transfection reagent showed the highest transfection efficiency for neonatal cardiomyocytes; the transfection efficiency is 5.0 ± 0.6% (Appendix E). A FRAP experiment was performed for cardiomyocytes on the day of time-lapse imaging (DIV5) to determine the presence of EYFP-α-actinin expression in cardiomyocytes that were transfected on DIV1. As shown in Figure 5.1, fluorescence in the bleached region was recovered, suggesting that cardiomyocytes were still expressing EYFP-α-actinin on the day of time-lapse imaging.

Next we examined if morphological changes of Z discs were induced by mechanical stretch. Prior to mechanical stretch, three distributive patterns of fluorescent α-actinin existed. They were uniformly spaced striations, which represents the normal Z discs, diffuse distribution, which represents erroneous assembly of α-actinin, and continuous distribution, which represents the stress fiber-like structures that usually appear at the cell periphery [152]. After stretch application, the percentages of uniformly spaced striations and continuous distribution were decreased. Two new distributive patterns of fluorescent α-actinin appeared. They were broadened distribution, which corresponds to the broadened Z discs [64] that are present in the hypertrophied heart, and nonuniformly spaced striations, which represents an enlarged sarcomere. The percentage of diffuse distribution was not significantly altered, suggesting that sarcomeric damage was not induced by mechanical stretching. Because sarcomeric addition and

morphological changes in Z discs both occurred after stretch application, Z discs may actively participate in the stretch-induced sarcomeric addition. The distributive patterns before and after stretch application are shown in Figure 5.2.

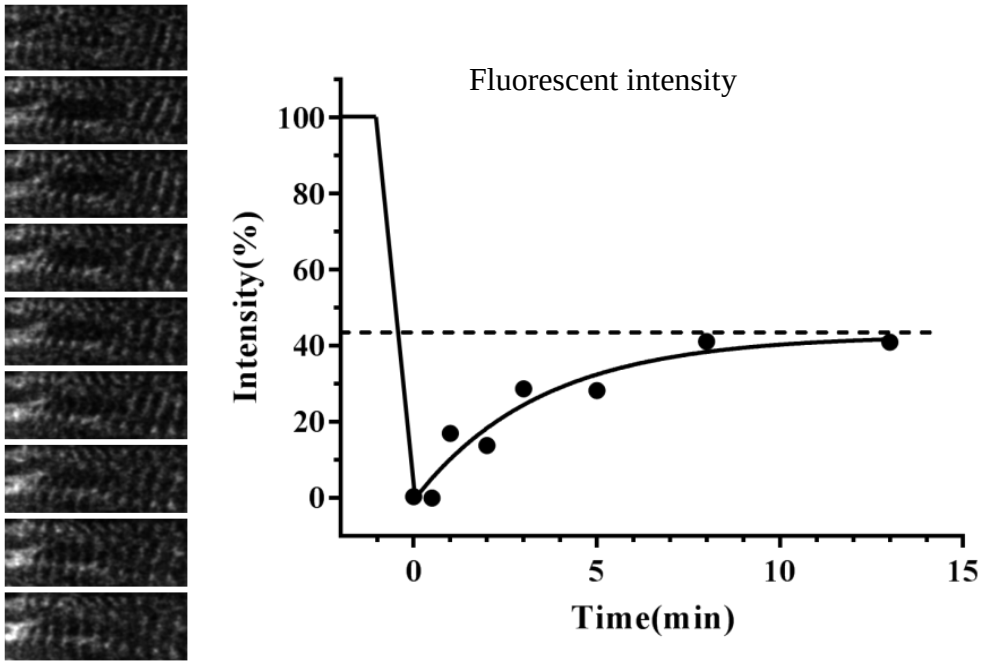

(A) (B)

Figure 5.1 FRAP process in cardiomyocytes. (A) TPEF images showing the FRAP process within a cardiomyocyte. (B) Intensity plot of FRAP process shown in (A).

Application of mechanical stretch resulted in transformation of distributive patterns of α-actinin. In one experiment (Figure 5.3A), the original continuously distributed α-actinin began to cluster 4h after 6% longitudinal stretch and appeared as broadened striations thereafter. The broadened striations had a width equivalent to the length of a normal sarcomere. The broadened striation gradually thinned back towards normal, when a thin sarcomeric A band was added to the longitudinal side. However,

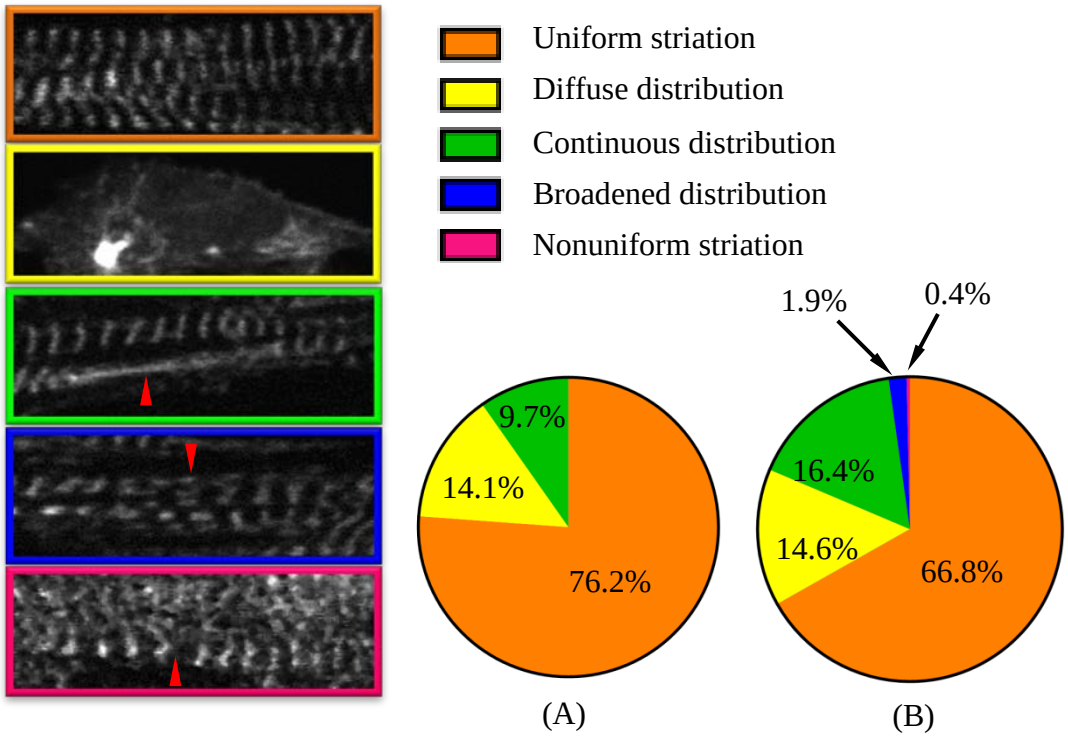

Figure 5.2 Distributive patterns of α-actinin before (A) and after (B) stretch application. Red arrow heads denotes the distributive pattern. The image for each distributive pattern has borders of the same color as each part in the pie graph, which is denoted by the legend on top.

addition of a normal sized sarcomeric A band was not accomplished before complete loss of sarcomeric structures within the imaged cardiomyocyte. In another experiment (Figure 5.3B), a normal sized sarcomeric A band was formed on the lateral side of a broadened striation, into which it was partially inserted. The insertion of the sarcomeric A band split the broadened striation in the middle, and after the split, the broadened striation converted to two uniformly spaced striations. In spite of the fact that a complete sarcomeric addition process was not observed, these results suggest that a sarcomere can

be added to Z discs to elongate a myofibril, and broadened Z discs are interphases during sarcomeric addition.

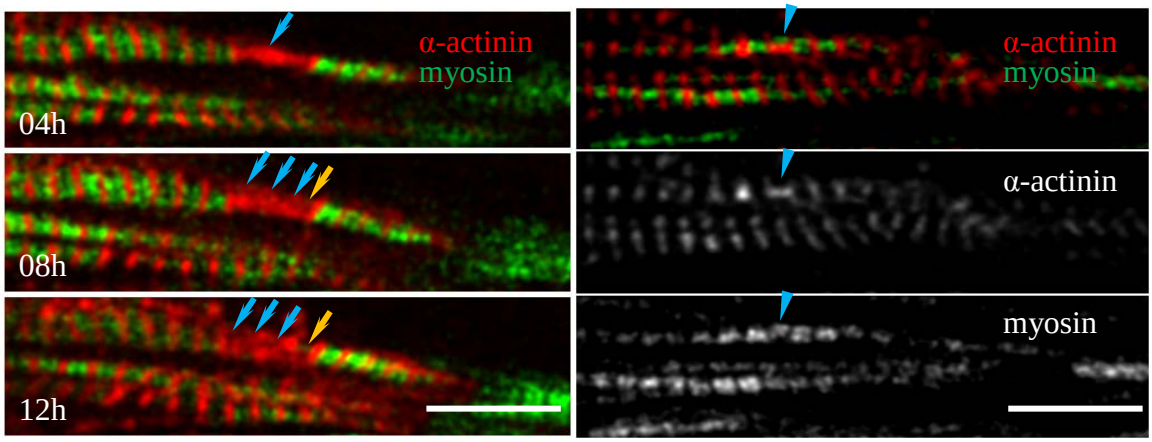

(A) (B)

Figure 5.3 Transition of distributive patterns from continuous to broadened striation (A) and from broadened to uniform striation (B) under longitudinal stretch. (A) The continuous distribution is broadened to the size of a regular sarcomere (blue arrows), and the addition of a thin sarcomeric A band (gold arrow) in the longitudinal direction returns broadened striation to normal. Time = hours after stretch application. (B) A sarcomeric A band is added to the lateral side of a broadened striation, which is split in the middle and was returned to uniform striation. The top image is a merge of the bottom two images. Scale bars = 10μm

Transformation from uniformly to nonuniformly spaced striations was observed under transverse stretch (Figure 5.4). A myofibril broke up longitudinally in the middle after application of 6% transverse stretch. The cardiomyocyte neither widened the Z disc to fill the free space at the break, nor nucleated a new Z disc and a sarcomeric A band.

The Z disc attached to the sarcomere on only one side of the break, leaving a free-end on the sarcomere on the other side. Despite the free end, the sarcomere maintained its integrity at the break. This caused an increase in local sarcomeric length to twice the length of a normal sarcomere, as if a new sarcomere were going to be added. This result suggests that locally enlarged sarcomeres are potential sites for sarcomeric addition.

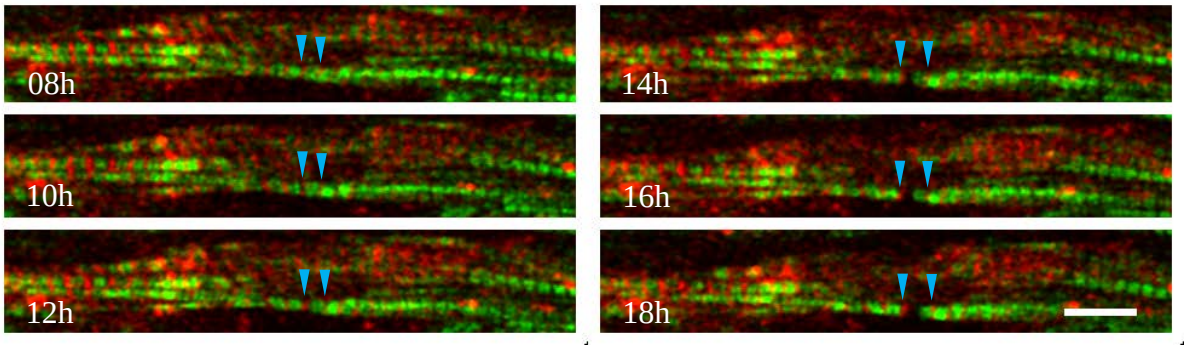

Figure 5.4 Transformation of distributive patterns from uniformly to nonuniformly spaced striations during transverse stretch. Blue arrows denote where the transition occurs. No Z disc broadening, Z disc nucleation and/or sarcomeric A band nucleation was found at the denoted space. Time = hours after stretch application. Scale bar = 10μm.

5.4 Discussion

In this study, we simultaneously and dynamically observed two important sarcomeric structures, Z discs and A bands, during mechanical stimulation using a combined technique of fluorescent protein fusion and TPEF-SHG microscopy. We found that Z discs actively participated in sarcomeric addition under mechanical stimulation, and variants of Z disc morphologies are interphases during sarcomeric addition. Our results support the long-standing hypothesis that broadened Z discs are active sites for

sarcomeric addition, and imply that sarcomeres with distance-increased Z discs are potential sites for sarcomeric addition. The combinative use of fluorescent protein fusion technique with TPEF-SHG microscopy is an intriguing attempt for simultaneous observation of two cytosolic proteins, which is usually achieved by bi-transfection that may suffer from doubled interference from protein fusions [118].

Z discs are among the most frequently altered sarcomeric structures in cardiomyocytes during cardiac hypertrophy, and some alterations of Z discs have long been hypothesized to be interphases of sarcomeric addition, a response by cardiomyocytes to increased mechanical loads, such as broadened Z discs [64]. Our results show the dynamic sarcomeric addition process at broadened Z discs, suggesting that the Z disc act as a structural support during sarcomeric addition. However, under what condition a Z disc broadens itself to support sarcomeric addition remains unknown. For example, during transverse stretch, the distance between two successive Z discs was increased without broadening. The absence of Z disc broadening is not due to depletion of EYFP conjugated α-actinin, which has been ruled out by a FRAP experiment. Because the integrity of sarcomeres was not compromised by the absence of a broadened Z disc, it is postulated that something other than a Z disc acts as a structural support for sarcomeric addition.

The results of our study suggest that variants of Z disc morphologies can be interphases of sarcomeric addition stimulated by mechanical load (Figure 5.5). During mechanical stretch, normal Z discs are transformed directly or indirectly to stress fiber-like structures [152], broadened Z discs, or Z discs with increased spaces such as in an

enlarged sarcomere, to allow sarcomeric addition, after which Z disc morphology is returned to normal. During these morphological changes, sarcomeric damage can occur as a result of sarcomeric addition, mechanical stress, or another cause. More studies are needed to verify the existence of sarcomeric addition-related transformations of Z disc morphologies, e.g., from sarcomeres with distance-increased Z discs to sarcomere with normal-spaced Z discs.

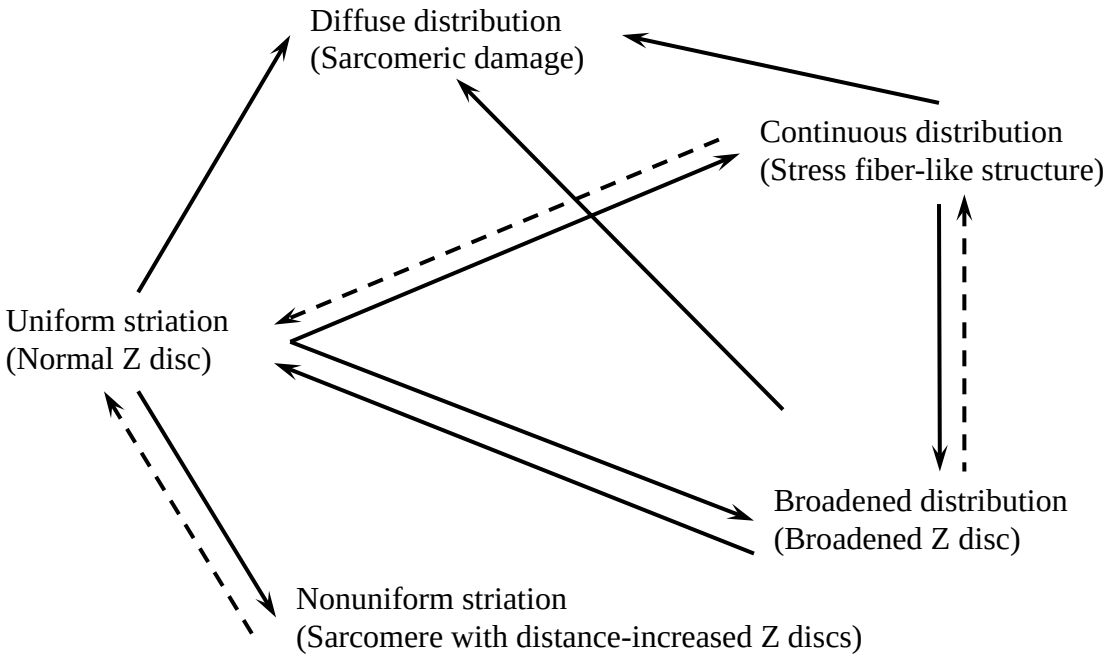

Figure 5.5 Transformation of distributive patterns of α-actinin. Arrows indicate direction of transitions. Solid lines indicate proved transitions. Dash lines indicate potential but unproved transitions. Text in parentheses indicates the corresponding state of Z discs or sarcomeres

Although the Z disc can actively participate in sarcomeric addition and act as a structural support, the role of the Z disc in sarcomeric addition may be much larger. The

Z disc plays an important role in mechanotransduction, not only in that they mechanically sense the intercellular and extracellular force but also because many Z disc proteins are involved in mechanotransduction signal pathways. The crystalline structure of the Z disc may indicate that it work more as a mechanical sensor than a structural support for sarcomeric addition. The inflexibility of the crystalline structure makes Z discs more likely to fail than intercalated discs, which are membrane-based.

5.5 Conclusion

Two sarcomeric structures, Z discs and A bands, were simultaneously and dynamically observed with a combined technique of fluorescent fusion protein and TPEF-SHG microscopy. Z discs were shown to actively participate in sarcomeric addition during mechanical stimulation and variants of Z disc morphologies were found to be interphases of sarcomeric addition. For example, broadened Z discs were found to be active sites for sarcomeric addition, during when they served as structural supports. Sarcomeres with distance-increased Z discs were also suggested as potential sites for sarcomeric addition. These findings have provided fundamental knowledge for understanding the role of Z discs in sarcomeric addition, and may advance understanding of cardiomyocyte remodeling during cardiac hypertrophy with respect to Z discs.

CHAPTER VI CONCLUSION, LIMITATION AND FUTURE WORK

Heart failure is a huge public health concern; it affects about 5.7 million adults and contributes to 1 out of every 9 death in the United States. Of the 900,000 people diagnosed with heart failure annually, half die within 5 years of diagnosis [6]. Heart failure usually appears as a result from cardiac hypertrophy, during which individual cardiomyocytes are enlarged in both size and mass. The enlargement is achieved by addition of sarcomeres, the basic contractile units. Cardiomyocytes elongate by adding sarcomeres in series and thicken by adding sarcomeres in parallel. It is generally accepted that sarcomeric addition can be initiated by increased mechanical loading; however, the sarcomeric addition process under various mechanical overloads on molecular level remains largely unknown. Previous researches on sarcomeric addition largely rely on animal models with induced cardiac hypertrophy; those experiments provide little direct evidence for sarcomeric addition process as a response to increased mechanical loading, aside from the start and end point conditions. Studies showing the dynamic addition process of sarcomeric addition are rare, due to lack of in vivo-like cardiomyocyte culture models for mechanical assays and limited choice of live imaging techniques.

The scope of this project is therefore to develop an in vivo-like cardiomyocyte culture model and utilize it for real-time observation of sarcomeric addition process triggered with externally applied mechanical loads. Our long-term goal is to understand how sarcomeric addition is regulated by mechanical-loading conditions. The objective of this project is to test the hypotheses that longitudinal stretch will cause sarcomeric addition through sarcomeric protein insertion at Z-discs and that transverse stretch will

cause sarcomeric addition either through longitudinal splitting of an existing myofibril or sarcomeric addition using an existing myofibril as a template.

To test these hypotheses, we first established an in vivo-like cardiomyocyte culture model on a deformable polydimethylsiloxane (PDMS) substrate, which recapitulated key features of in vivo-like mechanical loading environment, including synchronous active contraction, aligned organization, end-to-end coupling between cardiomyocytes as well as cell-ECM coupling. In vivo-like alignment of elongated cardiomyocytes was achieved using various state-of-the-art techniques including microgroove patterning, wrinkle patterning, and microcontact printing. Synchronous active contraction along the long axes of cardiomyocytes was reinforced by electrical field stimulation. Cardiomyocytes showed intercalated disc-like cell-cell interfaces, with expression of abundant collagen type IV. A 3D cell culture with multiple layers of cells was formed on a 2D PDMS substrate. Next, we used the in-vivo-like cardiomyocyte culture model to study the dynamics of sarcomeric A bands during mechanical stretching. A custom-built cell stretching device was developed for delivery of uniaxial and uniform stretch to cardiomyocytes. Sensitivity of cardiomyocyte to stretch induced damage was evaluated, and appropriate strains for observation of sarcomeric addition were determined. A synchronized recording scheme was designed to remove motion artifacts. Cardiomyocytes were either longitudinally or transversely stretched and the dynamic process of sarcomeric addition was recorded with a passive pulse splitter-based two-photon excitation fluorescence (TPEF) and second harmonic generation (SHG) microscope. Cardiomyocyte remodeling on translational level during sarcomeric addition

was evaluated by western blotting. Following that, we used the same culture model and studied the morphological changes of Z discs during mechanical stretching. To visualize Z discs, cardiomyocytes were transfected with plasmid carrying a gene of enhanced yellow fluorescent protein (EYFP) conjugated α-actinin. Variants of Z disc morphologies were determined before and after stretch application, and those Z disc morphologies that appeared after stretch application, was closely investigated with the passive splitter-based TPEF-SHG microscope.

We found that cardiomyocytes could form a multiple layer cell culture with intercalated disc-like cell-cell interfaces on a 2D substrate. The formation of 3D cell culture and intercalated disc-like cell-cell interfaces showed no dependence on techniques used to achieve alignment of elongated cardiomyocytes, but may depend directly or indirectly on the substrate stiffness. With this in vivo-like culture model, we, for the first time, observed the dynamic processes of sarcomeric insertion and sarcomeric deletion at intercalated disc. We also confirmed the modes of sarcomeric addition to the side of an existing myofibril using it as a template and through myofibrillar splitting, which was first dynamically observed in single cardiomyocytes. Simultaneous and dynamical observation of Z discs and A bands results in the discovery of the role of the Z disc during sarcomeric addition as a structural support. Variants of Z disc morphologies, such as continuous Z discs, broadened Z discs, and distance-increased Z discs were found to be interphases of sarcomeric addition. Our results provide direct evidences supporting two long-standing hypotheses: 1) intercalated discs are active sites for sarcomeric addition; and 2) broadened Z discs are active sites for sarcomeric addition. These findings

may advance the understanding of cardiomyocyte remodeling on sarcomeric level to mechanical overloads during cardiac hypertrophy.

The major limitation of the presented work is the insufficiency of data. Most conclusions about sarcomeric addition are supported by only a few observations if not one. This is due to: 1) sarcomeric addition rate is low; 2) occurrence of sarcomeric addition is temporally diverged; and 3) long-term cell culture in on-stage incubator is challenging. The problem of data insufficiency is exacerbated by the low efficiency of data analysis, which is achieved by visual determination of sarcomeric addition from 3D + t data sets. In future, I will be devoted to: 1) finding ways to increase the detection rate of sarcomeric addition by increasing the imaging field, and 2) developing an automated method for analyzing sarcomeric addition from 3D + t data sets.

IN CONCLUSION, a 3D cardiomyocyte culture model that recapitulates the in vivo-like mechanical loading environment, was established in vitro on a 2D PDMS substrate. With this culture model, we, for the first time, revealed the dynamic sarcomeric addition process at intercalated discs and Z discs with custom-built passive pulse splitter-based TPEF-SHG microscope, which confirmed the long-standing hypotheses of sarcomeric addition at intercalated discs and Z discs. These findings may advance the understanding of cardiomyocyte remodeling process on sarcomeric level during development of cardiac hypertrophy.

APPENDICES

Appendix A

Inhibition of fibroblast proliferation

Fibroblast over-proliferation is a big problem in long-term cardiomyocyte culture.[153] Because β cytosine-arabinoside (AraC) interferes the synthesis of DNA, Arac is widely used as an inhibitory drug for fibroblast proliferation. Fibroblast proliferation is accompanied by a proportional increase in metabolic activity, especially in the log phase of cell proliferation curve; therefore, fibroblast proliferation can be evaluated by proliferation assays that measure the metabolic activity, such as MTT assay. MTT (3-(4,5-dimethylthiazol-2-yl)-2,5-diphenyltetrazolium bromide) is a water soluble reagent that can be reduced to insoluble purple formazan in the mitochondria of living cells. The insoluble formazan can be rapidly quantified with a spectrometer or plate reader.

AraC stock solution (1mM) was prepared by dissolving AraC in autoclaved deioned water. Fibroblasts were obtained during cardiomyocyte isolation, and were purified by repetitive passaging. Purified fibroblasts were seeded to 96 well plate at a density of 1×10^4 per well. On the first day in vitro (DIV1), MTT assay was performed for one set of wells. AraC was then added to other sets of wells to make a final concentration of 0 µM, 0.1 µM, 0.5 µM, 1 µM, 2 µM, and 5 µM. MTT assay was performed on DIV2, DIV4, DIV6, DIV8 and DIV10. Metabolic activities were compared to that measured on DIV1.

MTT assay was performed as described by Ciapetti et al [154]. Briefly, MTT (Sigma Aldrich) stock solution (5 mg/ml) was prepared by dissolving MTT in PBS, which was filtered through 0.22 µm syringe filter to remove undissolved crystals. When cells were ready, 50 µl 5 mg/ml MTT were added to each well and incubated for 3 to 4h in incubator, including one set of wells with no cells (control). Medium was then removed and 150 µl dimethyl sulfoxide (DMSO) (Fisher Chemical) was added to each well to dissolve the reduced product. The well plate was shaken on an orbital shaker for 15min in a dark room. Absorbance was measured at 590nm with a commercial plate reader (Synergy 2, BioTek) with a reference filter set to 620nm. Results were corrected by blank (results from control) subtraction.

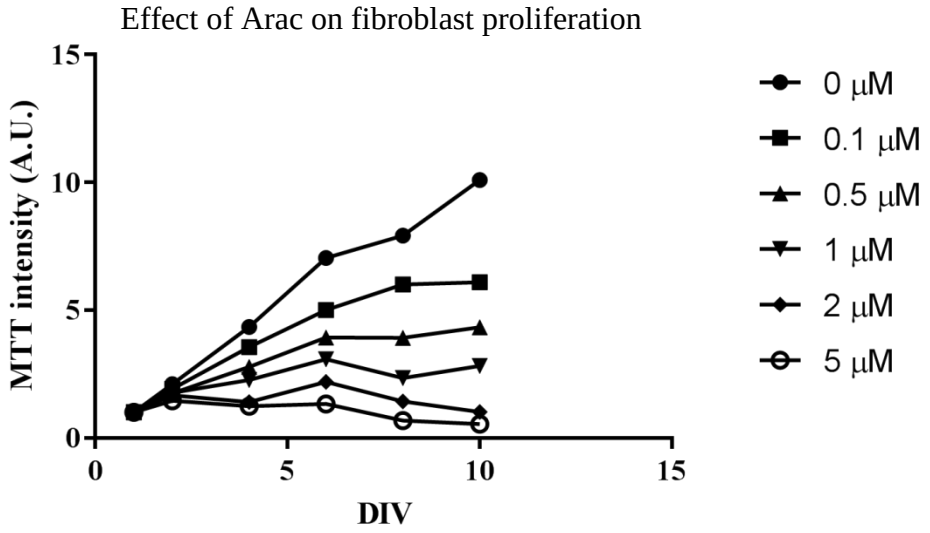

Figure A-1 MTT assay for fibroblast cultured with AraC.

Results (Figure A-1) show a log growth of fibroblasts in control (0 µM) from DIV1 to DIV6 and a decreased growth rate from DIV8 to DIV10. Fibroblast proliferation rate decreased with increased AraC concentration. A concentration of 2 µM AraC kept

number of fibroblasts nearly unchanged from DIV1to DIV8. Higher concentration of AraC (5 μM) decreased the number of fibroblasts. For long-term cardiomyocyte culture, we want to inhibit fibroblast proliferation without cytotoxicity to fibroblasts and cardiomyocytes. Therefore, a concentration of 2 μM was considered optimal for the purpose of inhibiting fibroblast proliferation.

Appendix B

Calculation of fixed strain by plasma treatment

Wrinkle depths and wrinkle periods were found to be positively correlated (R^2 = 0.63) by a coefficient of 0.2. According to the circular geometry of wrinkles on the side view, the length of the arc was calculated based on the depth (D) and period (P) of wrinkles. Assuming the radius of the circle that fits the border of wrinkles is R, the relation of R to D and P is described by

$$R^2 = (R - D)^2 + (\frac{P}{2})^2$$

The angle (θ) of the arc of wrinkle is calculated by

$$\tan(\frac{\theta}{2}) = P/2(R - D)$$

The length (L) of the arc of wrinkle is calculated by

$$L = \theta R$$

According to these formulas, we found that L equaled to 1.10P. According to the fabrication process, a thin PDMS membrane was stretched 50%, which means that a portion of PDMS membrane with a length of P would increase to 1.50P. Oxygen plasma treatment stiffened the surface of the membrane. After stretch release, the PDMS

membrane with a length of 1.50*P* was shortened to 1.10*P*. This indicates that 80% of the initial strain dissipated in the membrane during stretch release. Taking into account that the final period of the wrinkle is longer than the original length in the PDMS membrane, the dissipated strain is less than 80%.

Appendix C

Passive pulse splitter and sarcomeric addition during cell spreading

The passive pulse-splitter was designed as described by Ji et al. [123] The optical scheme of the pulse-splitting unit is shown in Figure C-1. The fundamental 4X pulse-splitting unit (Figure C-1C) was two mirrors separated by a low dispersion fused-silica plate and a layer of air. One beam entering the unit was split into two subbeams with equal energy at the interface of the fused-silica and air, where a half-transmission and half-reflection optical coating was present. At the designed incident angle, these subbeams met again at the interface after being reflected by the two precisely separated mirrors, and was split one more time. This resulted in two subbeams, each with two pulses with a temporal offset determined by the light path difference in the pulse-splitting unit as shown by

$$\Delta t = \frac{2}{c}\sqrt{(n_1^2 - n_0^2)(d_1^2 - d_0^2)}$$

where $n_{0,1}$ and $d_{0,1}$ represent the reflective index and the thickness of silica plate and air layer. Splitting capacity was increased by incorporating more 4X pulse-splitting units, and it was only limited by pulse length, repetition rate and group delay dispersion. In this application, a 64X pulse-splitting unit (Figure C-1B) was constructed with two 4X pulse-

splitting units and two half-transmission, half-reflection beam splitters. The two 4X pulse splitter unites were designed to have different internal pulse delay and the paths of laser were precisely controlled to avoid overlay of subpulses. The two subbeams were combined in the end by a polarized beam splitter. The alignment quality of each subbeam would affect the final resolution. For best result, each recombined beam was required to have a spot coincidence of less than 1mm after 10 meters' propagation in free space. This 64X pulse splitter was incorporated in the TPEF-SHG microscope at the very beginning of its light path. The optical scheme of the modified TPEF-SHG microscope is shown in Figure C-1A.

When cardiomyocytes were ready, an aliquot of cardiomyocytes were stained with DiO for cell membrane, which were then mixed with unstained cardiomyocytes. The mixed cardiomyocytes were plated onto a fibronectin coated glass-bottom dish. Cardiomyocytes were cultured in regular incubator for 1 day and were then transferred to an on-stage incubator (Okolab), which was mounted onto the TPEF-SHG microscope. Fluorescence from DiO-stained membrane was collected through standard FITC filter (515-565nm) in the TPEF channel; intrinsic SHG signals from myosin filaments were collected through another band-pass filter (414/46, Semrock) in the SHG channel. A DiO-stained cardiomyocyte surrounded by unstained cardiomyocytes was selected for time-lapse imaging so that the shape of the cardiomyocyte could be delineated by fluorescence images acquired with the TPEF channel. Images were taken hourly with the 830nm laser and the entire imaging process lasted for 24h.

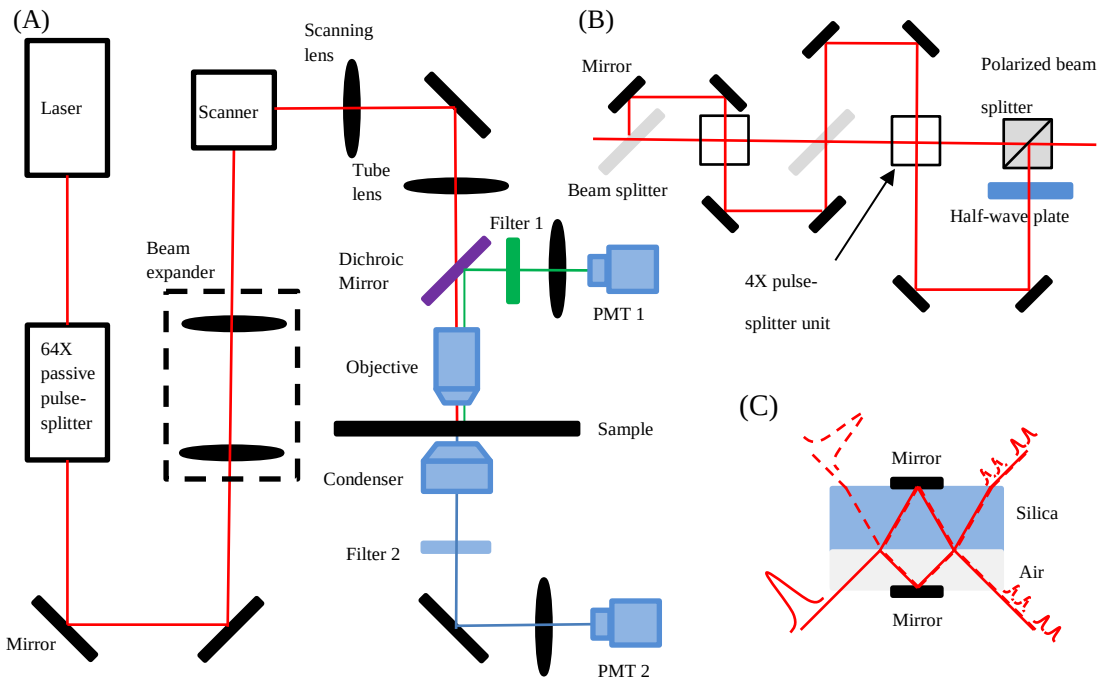

Figure C-1 Schematic representation of (A) passive pulse splitter-based TPEF-SHG microscope, (B) 64X passive pulse splitter, (C) 4X passive pulse splitter. TPEF: two-photon excitation fluorescence. SHG: second harmonic generation.

Results show that the presence of 64X passive pulse splitter reduced photodamage and increased amiable laser power for time-lapse imaging from 2.8mW [120] to several tens of miliwatts, which substantially increased feasibility of the TPEF-SHG microscope. As a trade-off, resolution of the modified TPEF-SHG microscope was compromised. The lateral resolution decreased from 0.47μm [155] to 0.55μm, and axial resolution decreased from 1.2μm [155] to 2.3μm. The lateral resolution was sufficient for resolving sarcomeres (~2μm). When using the modified TPEF-SHG microscope for 3D imaging, an axial step size of 1μm was used to make full use of axial resolution. The amiable laser

power for time-lapse imaging depends on cell age and image acquisition frequency. For a frequency of 1 image acquisition per hour, the recommended power was 15mW for DIV1, 20mW for DIV2, 30mW for DIV3, 40mW for DIV4 or older.

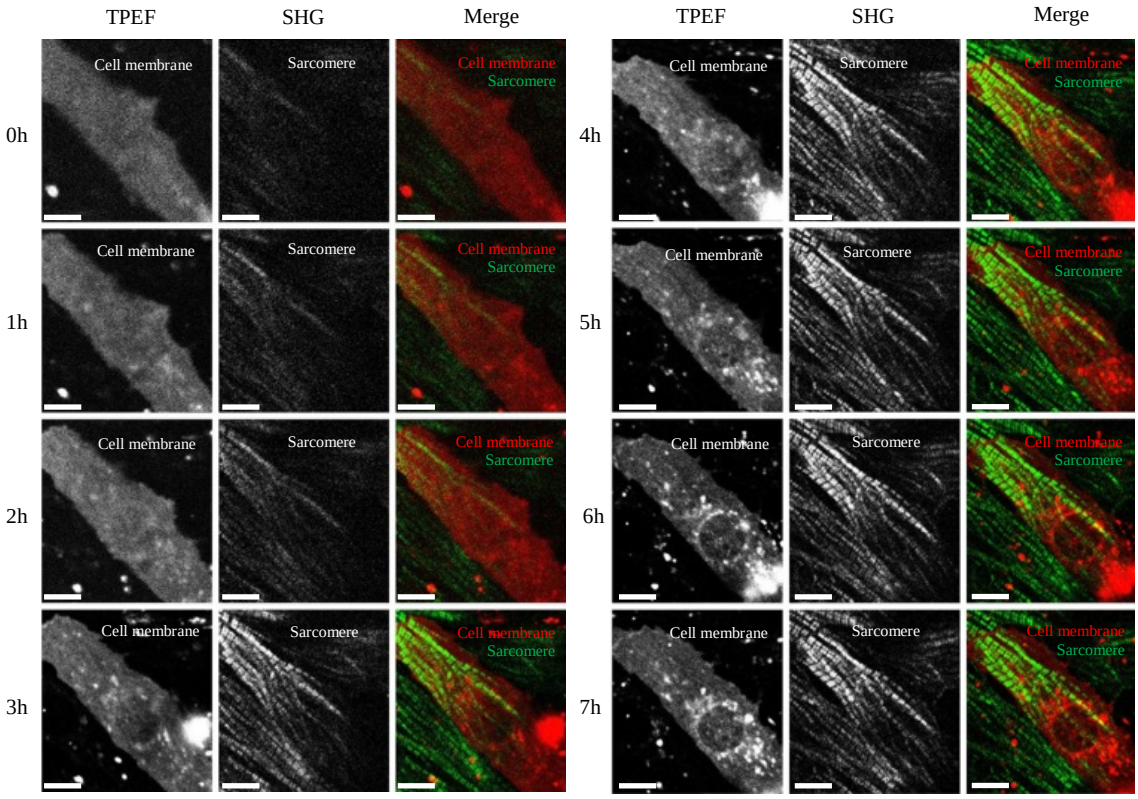

Figure C-2 Sarcomerogenesis process without mechanical stretch. DiO-stained cell membrane is recorded in the TPEF channel and sarcomeric structure is recorded in the SHG channel. Cell membrane is assigned red and sarcomere green in the merged images. Time = hours after stretch application. Scale bars = 10μm.

Dynamics of sarcomerogenesis during cardiomyocyte spreading (Figure C-2), observed with the passive pulse splitter modified TPEF-SHG microscope, showed both supportive and contradictory evidences to premyofibril model as described by Dabiri et al

[59]. Striated sarcomeric A bands faded in all over cardiomyocytes after cardiomyocytes spread out, supporting the replacing mechanism in nascent myofibril phase when non-muscle myosin IIB is replaced by muscle myosin. The exchanging of muscle myosin with non-muscle myosin is believed to be performed in units of myosin molecules and/or oligomers [156] instead of myosin filaments; otherwise, these myosin filaments should have been captured by the SHG imaging. On the other hand, length of sarcomeres and sarcomeric A bands was not increased during the sarcomerogenesis process, which is contradictory to premyofibril model that incorporation of muscle myosin filament increases length of sarcomeres and sarcomeric A bands.

Appendix D

Matlab script for synchronized imaging

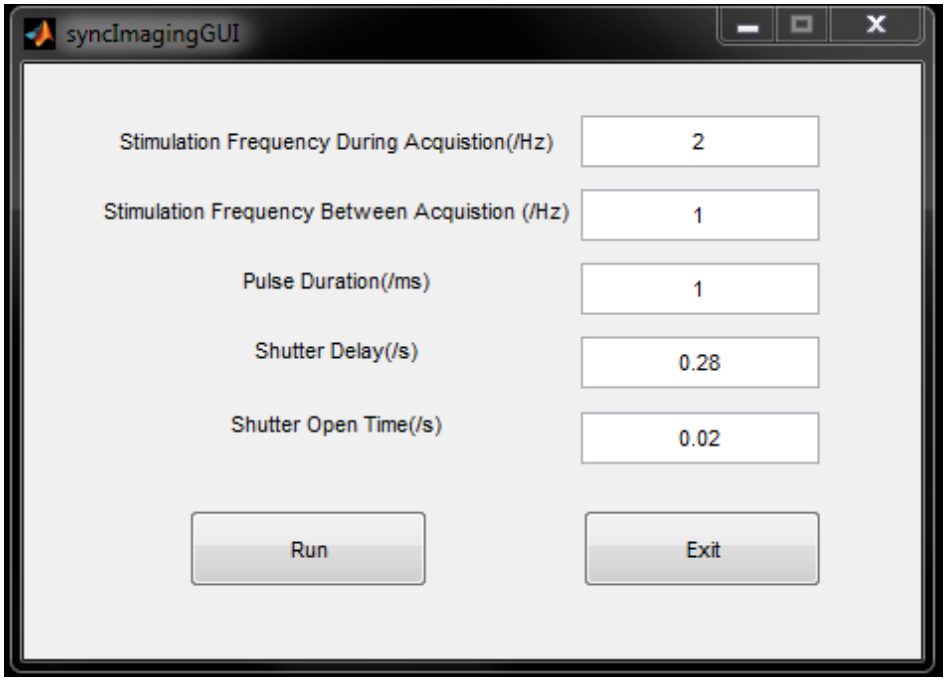

Figure D-1 User interface for synchronized imaging

A MATAB script was coded to generate triggering signal at user specified frequency, duration, and delay. The triggering signal was output by the same NI card used for image acquisition. The user interface is shown in Figure D-1 with the code shown below.

```
function varargout = syncImagingGUI(varargin)
   gui_Singleton = 1;
   gui_State = struct('gui_Name',       mfilename, ...
                      'gui_Singleton',  gui_Singleton, ...
                      'gui_OpeningFcn', @syncImagingGUI_OpeningFcn, ...
                      'gui_OutputFcn',  @syncImagingGUI_OutputFcn, ...
                      'gui_LayoutFcn',  [] , ...
                      'gui_Callback',   []);
   if nargin && ischar(varargin{1})
      gui_State.gui_Callback = str2func(varargin{1});
   end

   if nargout
      [varargout{1:nargout}] = gui_mainfcn(gui_State, varargin{:});
   else
      gui_mainfcn(gui_State, varargin{:});
   end

function syncImagingGUI_OpeningFcn(hObject, eventdata, handles, varargin)

   handles.output = hObject;

   %Add Zhonghai's data to guidata so that it can be passed to other callbacks

handles.parameters.stimFreqDuringAcquisition=str2num(get(handles.stimFreqDuringAcquisition,'String'));%Hz

handles.parameters.stimFreqBetweenAcquisition=str2num(get(handles.stimFreqBetweenAcquisition,'String'));%Hz
   handles.parameters.pulseDuration=str2num(get(handles.pulseDuration,'String'));%ms
   handles.parameters.shutterDelay=str2num(get(handles.shutterDelay,'String'));%s

handles.parameters.shutterOpenTime=str2num(get(handles.shutterOpenTime,'String'));%s

   %initialize tasks based on those parameters
```

```
    import dabs.ni.daqmx.*
    DAQmx_Val_ChanForAllLines=1;

    %create DI task
    handles.daqTasks.hDI=Task('DIline2');

handles.daqTasks.hDI.apiCall('DAQmxCreateDIChan',handles.daqTasks.hDI.taskID,'De
v1/port0/line2','',DAQmx_Val_ChanForAllLines)
    handles.daqTasks.hDI.apiCall('DAQmxStartTask',handles.daqTasks.hDI.taskID)

    %create DOSti task
    handles.daqTasks.hDOSti=Task('CellStimulation');

handles.daqTasks.hDOSti.createDOChan('Dev1','port0/line6:7','','DAQmx_Val_ChanPer
Line');
    handles.daqTasks.hDOSti.start();
    handles.daqTasks.hDOSti.writeDigitalData([0;0]);% set line to 0, means no
stimulation

    %create DOShutter task
    handles.daqTasks.DOShutter=Task('ShutterDO');

handles.daqTasks.DOShutter.createDOChan('Dev1','port0/line4','','DAQmx_Val_ChanPe
rLine');
    handles.daqTasks.DOShutter.start();
    handles.daqTasks.DOShutter.writeDigitalData(0);% set line to 0, means no stimulation

    %create DOShutter task
    handles.daqTasks.DOAcqPauseTrig=Task('PauseTrigDO');

handles.daqTasks.DOAcqPauseTrig.createDOChan('Dev1','port0/line5','','DAQmx_Val_
ChanPerLine');
    handles.daqTasks.DOAcqPauseTrig.start();
    handles.daqTasks.DOAcqPauseTrig.writeDigitalData(0);% set line to 0, means no
stimulation

    % parameters for DI task
    handles.parameters.pNULL=libpointer;
    handles.parameters.pREAD=libpointer('int32Ptr');
    handles.parameters.pBYTESPERSAMP=libpointer('int32Ptr');
    handles.parameters.pDATA=libpointer('uint8Ptr',uint8(0));% pass a pointer to libaray
function, otherwise data will not be changed

    % prepare data for cell stimulation
```

```
    dataVolPer1ms=7228;% data volume per 1 ms
    dataVol=ceil(handles.parameters.pulseDuration*dataVolPer1ms);
    pulseData=zeros(2*dataVol+2,2);
    pulseData(2:dataVol+1,2)=1;
    pulseData(dataVol+2:2*dataVol+1,1)=1;
    handles.parameters.pulseData=pulseData;

    % Update handles structure
    guidata(hObject, handles);

function varargout = syncImagingGUI_OutputFcn(hObject, eventdata, handles)

    varargout{1} = handles.output;

function RunOrStop_Callback(hObject, eventdata, handles)

    set(handles.output,'CurrentCharacter','@');
    DAQmx_Val_GroupByChannel=0;
    acquisitionActiveFlag=false;
    stimFreq=handles.parameters.stimFreqBetweenAcquisition;

    if isequal(get(hObject,'String'),'Run')
      set(hObject,'String','press any key to stop')
    end
    %set gcf to focus
    set(hObject, 'Enable', 'off');
    set(handles.Exit,'Enable', 'off');
    drawnow;
    % run the sync signals
    tStartSti=tic;
    while(strcmp(get(handles.output,'CurrentCharacter'),'@'))

handles.daqTasks.hDI.apiCall('DAQmxReadDigitalLines',handles.daqTasks.hDI.taskID,
1,10.0,DAQmx_Val_GroupByChannel,...

handles.parameters.pDATA,1,handles.parameters.pREAD,handles.parameters.pBYTESP
ERSAMP,handles.parameters.pNULL)
        if isequal(handles.parameters.pDATA.value,0)% acquistion stopped
            if acquisitionActiveFlag% if shutter and pause trig is still active, inactivate it
                handles.daqTasks.DOAcqPauseTrig.writeDigitalData(0);% stop pause trig
before close shutter
                handles.daqTasks.DOShutter.writeDigitalData(0);%close shutter
            end
```

```
        stimFreq=handles.parameters.stimFreqBetweenAcquisition;% switch back to
stimFreqBetweenAcquistion
        acquisitionActiveFlag=false;
        if toc(tStartSti) > 1/stimFreq
          handles.daqTasks.hDOSti.writeDigitalData(handles.parameters.pulseData);
          tStartSti=tic;
        end
      else% data==1, acquistion is active
        stimFreq=handles.parameters.stimFreqDuringAcquisition;% switch frequency of
stimulation
        acquisitionActiveFlag=true;% set flag
        if toc(tStartSti) > 1/stimFreq
          handles.daqTasks.DOAcqPauseTrig.writeDigitalData(0);% stop pause trig
before close shutter
          handles.daqTasks.DOShutter.writeDigitalData(0);%close shutter
          handles.daqTasks.hDOSti.writeDigitalData(handles.parameters.pulseData);%
output another pulse
          tStartSti=tic;
        end
        if toc(tStartSti) > handles.parameters.shutterDelay
          handles.daqTasks.DOShutter.writeDigitalData(1);%open shutter
          pause(handles.parameters.shutterOpenTime);
          handles.daqTasks.DOAcqPauseTrig.writeDigitalData(1);%output pause trig
        end
      end
      %bring figure to focus so that user input can be captured
      figure(handles.output);
  end
  %stop stimulation and sync signal
  handles.daqTasks.DOAcqPauseTrig.writeDigitalData(0);% stop pause trig before close
shutter
  handles.daqTasks.DOShutter.writeDigitalData(0);%close shutter
  handles.daqTasks.hDOSti.writeDigitalData([0;0]);% stop stimulation
  %set back
  set(hObject,'String','Run');
  set(hObject, 'Enable', 'on');
  set(handles.Exit,'Enable', 'on');
  figure(handles.output);

function Exit_Callback(hObject, eventdata, handles)

  handles.daqTasks.hDI.delete();
  handles.daqTasks.hDOSti.delete();
  handles.daqTasks.DOShutter.delete();
```

```
    handles.daqTasks.DOAcqPauseTrig.delete();
    guidata(handles.output,handles);
    close(handles.output);

function stimFreqDuringAcquisition_Callback(hObject, eventdata, handles)

    handles.parameters.stimFreqDuringAcquisition=str2num(get(hObject,'String'));% get
user input
    guidata(handles.output,handles);%update guidata

function stimFreqDuringAcquisition_CreateFcn(hObject, eventdata, handles)

    if ispc && isequal(get(hObject,'BackgroundColor'),
get(0,'defaultUicontrolBackgroundColor'))
        set(hObject,'BackgroundColor','white');
    end

function stimFreqBetweenAcquisition_Callback(hObject, eventdata, handles)

    handles.parameters.stimFreqBetweenAcquisition=str2num(get(hObject,'String'));% get
user input
    guidata(handles.output,handles);%update guidata

function stimFreqBetweenAcquisition_CreateFcn(hObject, eventdata, handles)

    if ispc && isequal(get(hObject,'BackgroundColor'),
get(0,'defaultUicontrolBackgroundColor'))
        set(hObject,'BackgroundColor','white');
    end

function pulseDuration_Callback(hObject, eventdata, handles)

    handles.parameters.pulseDuration=str2num(get(hObject,'String'));% get user input

    dataVolPer1ms=7228;% data volume per 1 ms
    dataVol=ceil(handles.parameters.pulseDuration*dataVolPer1ms);
    pulseData=zeros(2*dataVol+2,2);
    pulseData(2:dataVol+1,2)=1;
    pulseData(dataVol+2:2*dataVol+1,1)=1;

    handles.parameters.pulseData=pulseData;
    guidata(handles.output,handles);%update guidata

function pulseDuration_CreateFcn(hObject, eventdata, handles)
```

```
    if ispc && isequal(get(hObject,'BackgroundColor'),
get(0,'defaultUicontrolBackgroundColor'))
        set(hObject,'BackgroundColor','white');
    end

function shutterDelay_Callback(hObject, eventdata, handles)

    handles.parameters.shutterDelay=str2num(get(hObject,'String'));% get user input
    guidata(handles.output,handles);%update guidata

function shutterDelay_CreateFcn(hObject, eventdata, handles)

    if ispc && isequal(get(hObject,'BackgroundColor'),
get(0,'defaultUicontrolBackgroundColor'))
        set(hObject,'BackgroundColor','white');
    end

function shutterOpenTime_Callback(hObject, eventdata, handles)

    handles.parameters.shutterOpenTime=str2num(get(hObject,'String'));% get user input
    guidata(handles.output,handles);%update guidata

function shutterOpenTime_CreateFcn(hObject, eventdata, handles)

    if ispc && isequal(get(hObject,'BackgroundColor'),
get(0,'defaultUicontrolBackgroundColor'))
        set(hObject,'BackgroundColor','white');
    end
```

Appendix E

Transfection with different transfection reagents

Transfection was performed with plasmid construct of EYFP-conjugated α-actinin (referred to as pDNA hereafter). The concentration of the plasmid was 0.1μg/μl. Cardiomyocytes were seeded to 24-well plate at a density of 1 $X10^5$/well one day before transfection. To find the best transfection reagent for our application, transfection efficiencies of several commercial transfection reagents were compared, including

Viromer Red (Lipocalyx), Viromer Yellow (Lipocalyx), lipofectamine 2000 (Invitrogen), TransIT-LT1 (Mirus Bio), Xfect (Takara), Viafect (Promega) and Fugene HD (Promega). All transfection protocols were adapted from product guides from manufacturers.

Transfection with Viromer Red and Yellow

1) Dilute 1.5µg (15µl) pDNA with 120µl Buffer Red/Yellow. This will result in 135µl pDNA working solution at a concentration of 11ng/µl.>> Tube 1
2) Place a 0.6µl droplet of Viromer Red/Yellow onto the wall of a resh tube. Immediately add 14.4µl of Buffer Red/Yellow and vortex 3-5s. >> Tube 2 **Always add Buffer Red/Yellow to Viromer Red/Yellow, not vice versa!**
3) Pipette 135 µl of the pDNA solution from Tube 1 onto the 15 µl of the Viromer Red/Yellow solution in Tube 2. Mix swiftly and incubate for about 15min at room temperature.
4) Add transfection complexes from step 3 to your cells. Titrate as per the table (Table E-1) to identify optimal conditions.

Table E-1 Recommended mass of pDNA at different transfection scales

Transfection Scale	Transfer Volume per well	pDNA per well
Low 0.5x	25µl	250ng
Standard 1.0x	50µl	500ng
High 1.5x	75µl	750ng

5) Incubate cells under their usual growth conditions. Check fluorescence of cells 24 h after transfection.

Transfection with Lipofectamine 2000

1) Dilute 2µl Lipofectamine reagent to 50µl OPTI-MEM I medium (Gibco). Incubate for 5min at room temperature
2) Dilute 0.5µg (5µl) pDNA to 50 µl OPTI-MEM I medium
3) Add diluted pDNA to diluted Lipofectamine reagent. Mix gently and incubate for 30min at room temperature
4) Add pDNA-lipid complex to cells. Incubate cells for 4h in a regular incubator.
5) Change medium to normal culture medium and incubate under their normal growth condition. Check fluorescence of cells 24 h after transfection.

Transfection with TransIT-LT1

1) Warm TransIT-LT1 reagent to room temperature and vortex gently before using.
2) Place 50µl of Opti-MEM I Reduced-Serum Medium in a sterile tube. Add 0.5µg (5µl) pDNA. Pipet gently to mix completely.
3) Add 1.5 µl TransIT-LT1 reagent to the diluted pDNA solution. Avoid any contact of the TransIT-LT1 reagent with the sides of the plastic tube. Pipet gently to mix completely. Incubate at room temperature for 20min (15–30min).
4) Add TransIT-LT1 reagent: pDNA complexes drop-wise to different areas of the wells. Gently rock the culture vessel to evenly distribute the TransIT-LT1 Reagent: pDNA complexes. Incubate for 4h in a regular incubator.

5) Change medium to normal culture medium and incubate under their normal growth condition. Check fluorescence of cells 24h after transfection.

Transfection with Xfect

1) Change medium of cell to DMEM+10%FBS with no antibiotics
2) Warm Xfect polymer to room temperature before use. Thoroughly vortex Xfect polymer.
3) In a sterile tube, dilute 1µg (10µl) pDNA with 15µl Xfect reaction buffer. Mix well by vortexing for 5s at high speed.
4) Add 0.3 µl Xfect polymer to the diluted pDNA. Mix well by vortexing for 10s at high speed. Incubate for 10min at room temperature to allow nanoparticle complexes to form.
5) Spin down for 1s to collect the contents at the bottom of the tube. Add the nanoparticle complex solution drop-wise to the cell culture medium. Gently rock the plate to mix. Incubate in a regular incubator for 4h.
6) Change medium to normal culture medium and incubate cells under their usual growth condition. Check fluorescence of cells 24h after transfection.

Transfection with Viafect

1) Change medium of cell to DMEM+10%FBS with no antibiotics
2) Warm Viafect transfection reagent to room temperature before use. Thoroughly vortex Viafect transfection reagent.

3) Place 50µl of Opti-MEM I Reduced-Serum Medium in a sterile tube. Add 0.5µg (5µl) pDNA. Pipet gently to mix completely.
4) Add 1.5 µl Viafect tranfection reagent to the diluted pDNA. Mix well by pipetting. Incubate for 10min (5-20min) at room temperature.
5) Add the Viafect transfection reagent: pDNA complex drop-wise to the cell culture medium. Gently rock the plate to mix. Incubate in a regular incubator for 4h.
6) Change medium to normal culture medium and incubate cells under their usual growth condition. Check fluorescence of cells 24h after transfection.

Transfection with Fugene HD

1) Change medium of cell to DMEM+10%FBS with no antibiotics
2) Warm Fugene HD transfection reagent to room temperature before use. Thoroughly vortex Fugene HD polymer.
3) Place 50µl of Opti-MEM I Reduced-Serum Medium in a sterile tube. Add 1µg (10µl) pDNA. Pipet gently to mix completely.
4) Add 3µl Fugene HD transfection reagent to the diluted pDNA. Mix well by peppetting. Incubate for 10min (0-15min) at room temperature.
5) Add the Fugene HD transfection reagent: pDNA complex solution drop-wise to the cell culture medium. Gently rock the plate to mix. Incubate in a regular incubator for 4h.
6) Change medium to normal culture medium and incubate cells under their usual growth condition. Check fluorescence of cells 24h after transfection.

Results

Higher transfection efficiency was obtained by performing transient transfection at an earlier time. In this study, cardiomyocytes were allowed to adhere to and spread on substrates for one day before transfection. After transfection with plasmid construct containing cDNA of EYFP-conjugated α-actinin, cardiomyocytes showed yellow fluorescence after 24h cultivation. Among all tested TRs, Xfect showed the highest transfection efficiency, which equaled to 5.0±0.6% and was significantly larger than that of Viromer Yellow, Lipofectamine 2000, Viafect and Fugene HD. No obvious cytotoxicity was observed for any tested TR when they were used as suggested by manufacturers. Xfect was determined as the best TR for our application and was used in this project. The transfection efficiencies of all tested TRs were shown in Figure E-1.

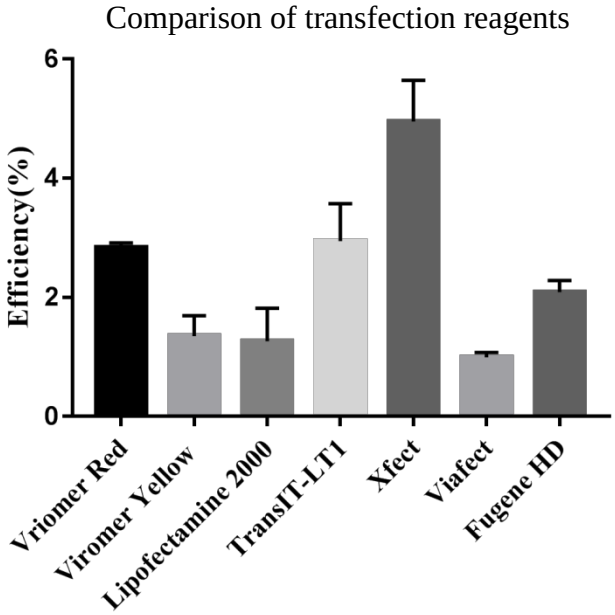

Figure E-1 Transfection efficiencies of several transfection reagents.

REFERENCES

[1] Frey N, Olson EN. Cardiac hypertrophy: the good, the bad, and the ugly. Annual review of physiology. 2003;65:45-79.
[2] Mozaffarian D, Benjamin EJ, Go AS, Arnett DK, Blaha MJ, Cushman M, et al. Heart Disease and Stroke Statistics-2016 Update: A Report From the American Heart Association. Circulation. 2016;133:e38-360.
[3] Gjesdal O, Bluemke DA, Lima JA. Cardiac remodeling at the population level -risk factors, screening, and outcomes. Nat Rev Cardiol. 2011;8:673-85.
[4] Maron BJ, Towbin JA, Thiene G, Antzelevitch C, Corrado D, Arnett D, et al. Contemporary definitions and classification of the cardiomyopathies - An American Heart Association Scientific Statement from the Council on Clinical Cardiology, Heart Failure and Transplantation Committee; Quality of Care and Outcomes Research and Functional Genomics and Translational Biology Interdisciplinary Working Groups; And Council on Epidemiology and Prevention. Circulation. 2006;113:1807-16.
[5] Zak R. Cardiac-Hypertrophy - Biochemical and Cellular Relationships. Hosp Pract. 1983;18:85-97.
[6] Heineke J, Molkentin JD. Regulation of cardiac hypertrophy by intracellular signalling pathways. Nat Rev Mol Cell Bio. 2006;7:589-600.
[7] Zou YZ, Takano H, Akazawa H, Nagai T, Mizukami M, Komuro I. Molecular and cellular mechanisms of mechanical stress-induced cardiac hypertrophy. Endocr J. 2002;49:1-13.
[8] Grossman W, Jones D, McLaurin LP. Wall stress and patterns of hypertrophy in the human left ventricle. The Journal of clinical investigation. 1975;56:56-64.
[9] Morganroth J, Maron BJ, Henry WL, Epstein SE. Comparative left ventricular dimensions in trained athletes. Annals of internal medicine. 1975;82:521-4.
[10] Kerckhoffs RCP, Omens JH, McCulloch AD. A single strain-based growth law predicts concentric and eccentric cardiac growth during pressure and volume overload. Mech Res Commun. 2012;42:40-50.
[11] Holmes JW. Candidate mechanical stimuli for hypertrophy during volume overload. J Appl Physiol (1985). 2004;97:1453-60.
[12] Omens JH. Stress and strain as regulators of myocardial growth. Prog Biophys Mol Bio. 1998;69:559-72.
[13] Goktepe S, Abilez OJ, Parker KK, Kuhl E. A multiscale model for eccentric and concentric cardiac growth through sarcomerogenesis. J Theor Biol. 2010;265:433-42.
[14] Kerckhoffs RCP. Computational modeling of cardiac growth in the post-natal rat with a strain-based growth law. J Biomech. 2012;45:865-71.
[15] Fuchs F, Wang YP. Sarcomere length versus interfilament spacing as determinants of cardiac myofilament Ca2+ sensitivity and Ca2+ binding. J Mol Cell Cardiol. 1996;28:1375-83.
[16] Baker KM, Chernin MI, Wixson SK, Aceto JF. Renin-Angiotensin System Involvement in Pressure-Overload Cardiac-Hypertrophy in Rats. Am J Physiol. 1990;259:H324-H32.

[17] Sasayama S, Ross J, Jr., Franklin D, Bloor CM, Bishop S, Dilley RB. Adaptations of the left ventricle to chronic pressure overload. Circulation research. 1976;38:172-8.
[18] Ross J, Jr. Adaptations of the left ventricle to chronic volume overload. Circulation research. 1974;35:suppl II:64-70.
[19] Lee JD, Sasayama S, Kihara Y, Ohyagi A, Fujisawa A, Yui Y, et al. Adaptations of the left ventricle to chronic volume overload induced by mitral regurgitation in conscious dogs. Heart and vessels. 1985;1:9-15.
[20] Helfant RH, De Villa MA, Meister SG. Effect of sustained isometric handgrip exercise on left ventricular performance. Circulation. 1971;44:982-93.
[21] Schannwell CM, Zimmermann T, Schneppenheim M, Plehn G, Marx R, Strauer BE. Left ventricular hypertrophy and diastolic dysfunction in healthy pregnant women. Cardiology. 2002;97:73-8.
[22] Jacobson SL, Piper HM. Cell-Cultures of Adult Cardiomyocytes as Models of the Myocardium. J Mol Cell Cardiol. 1986;18:661-78.
[23] Komuro I, Katoh Y, Kaida T, Shibazaki Y, Kurabayashi M, Hoh E, et al. Mechanical loading stimulates cell hypertrophy and specific gene expression in cultured rat cardiac myocytes. Possible role of protein kinase C activation. The Journal of biological chemistry. 1991;266:1265-8.
[24] Sadoshima J, Jahn L, Takahashi T, Kulik TJ, Izumo S. Molecular characterization of the stretch-induced adaptation of cultured cardiac cells. An in vitro model of load-induced cardiac hypertrophy. The Journal of biological chemistry. 1992;267:10551-60.
[25] Simpson DG, Majeski M, Borg TK, Terracio L. Regulation of cardiac myocyte protein turnover and myofibrillar structure in vitro by specific directions of stretch. Circulation research. 1999;85:e59-69.
[26] Gopalan SM, Flaim C, Bhatia SN, Hoshijima M, Knoell R, Chien KR, et al. Anisotropic stretch-induced hypertrophy in neonatal ventricular myocytes micropatterned on deformable elastomers. Biotechnology and bioengineering. 2003;81:578-87.
[27] Yu JG, Russell B. Cardiomyocyte remodeling and sarcomere addition after uniaxial static strain in vitro. The journal of histochemistry and cytochemistry : official journal of the Histochemistry Society. 2005;53:839-44.
[28] Yang H, Schmidt LP, Wang Z, Yang X, Shao Y, Borg TK, et al. Dynamic Myofibrillar Remodeling in Live Cardiomyocytes under Static Stretch. Scientific reports. 2016;6:20674.
[29] Li Y, Huang G, Zhang X, Wang L, Du Y, Lu TJ, et al. Engineering cell alignment in vitro. Biotechnology advances. 2014;32:347-65.
[30] Ehler E, Rothen BM, Hammerle SP, Komiyama M, Perriard JC. Myofibrillogenesis in the developing chicken heart: assembly of Z-disk, M-line and the thick filaments. J Cell Sci. 1999;112:1529-39.
[31] Guterl KA, Haggart CR, Janssen PM, Holmes JW. Isometric contraction induces rapid myocyte remodeling in cultured rat right ventricular papillary muscles. American journal of physiology Heart and circulatory physiology. 2007;293:H3707-12.
[32] Mitcheson JS, Hancox JC, Levi AJ. Cultured adult cardiac myocytes: Future applications, culture methods, morphological and electrophysiological properties. Cardiovasc Res. 1998;39:280-300.

[33] Pan J, Singh US, Takahashi T, Oka Y, Palm-Leis A, Herbelin BS, et al. PKC mediates cyclic stretch-induced cardiac hypertrophy through Rho family GTPases and mitogen-activated protein kinases in cardiomyocytes. Journal of cellular physiology. 2005;202:536-53.
[34] Torsoni AS, Marin TM, Velloso LA, Franchini KG. RhoA/ROCK signaling is critical to FAK activation by cyclic stretch in cardiac myocytes. Am J Physiol-Heart C. 2005;289:H1488-H96.
[35] Balle SS, Magnusson SP, McHugh MP. Effects of contract-relax vs static stretching on stretch-induced strength loss and length-tension relationship. Scand J Med Sci Spor. 2015;25:764-9.
[36] Iribe G, Ward CW, Camelliti P, Bollensdorff C, Mason F, Burton RAB, et al. Axial Stretch of Rat Single Ventricular Cardiomyocytes Causes an Acute and Transient Increase in Ca2+ Spark Rate. Circulation research. 2009;104:787-U141.
[37] Kamble H, Barton MJ, Jun M, Park S, Nguyen NT. Cell stretching devices as research tools: engineering and biological considerations. Lab Chip. 2016;16:3193-203.
[38] Brown TD. Techniques for mechanical stimulation of cells in vitro: a review. J Biomech. 2000;33:3-14.
[39] Pan J, Fukuda K, Saito M, Matsuzaki J, Kodama H, Sano M, et al. Mechanical stretch activates the JAK STAT pathway in rat cardiomyocytes. Circulation research. 1999;84:1127-36.
[40] Yamazaki T, Komuro I, Kudoh S, Zou YZ, Nagai R, Aikawa R, et al. Role of ion channels and exchangers in mechanical stretch-induced cardiomyocyte hypertrophy. Circulation research. 1998;82:430-7.
[41] Webb AR, Yang J, Ameer GA. Biodegradable polyester elastomers in tissue engineering. Expert Opin Biol Th. 2004;4:801-12.
[42] Shimada Y, Nwe TM, Hasebe-Kishi F, Suzuki H. Dynamics of Contractile Proteins Constituting Myofibrils in Living Muscle Cells. In: Dube DK, editor. Myofibrillogenesis. Boston, MA: Birkhäuser Boston; 2002. p. 21-39.
[43] Wang Z, Qin W, Shao Y, Ma S, Borg TK, Gao BZ. Pulse splitter-based nonlinear microscopy for live-cardiomyocyte imaging. Proceedings of SPIE--the International Society for Optical Engineering. 2014;8948.
[44] Legato MJ. Ultrastructure of the atrial, ventricular, and Purkinje cell, with special reference to the genesis of arrhythmias. Circulation. 1973;47:178-89.
[45] Paradis AN, Gay MS, Zhang L. Binucleation of cardiomyocytes: the transition from a proliferative to a terminally differentiated state. Drug discovery today. 2014;19:602-9.
[46] Weber KT. Cardiac interstitium in health and disease: the fibrillar collagen network. Journal of the American College of Cardiology. 1989;13:1637-52.
[47] Ehler E, Gautel M. The Sarcomere and Sarcomerogenesis. Adv Exp Med Biol. 2008;642:1-14.
[48] Lange S, Ehler E, Gautel M. From A to Z and back? Multicompartment proteins in the sarcomere. Trends Cell Biol. 2006;16:11-8.
[49] Frank D, Frey N. Cardiac Z-disc Signaling Network. Journal of Biological Chemistry. 2011;286:9897-904.

[50] Vydyanath A, Gurnett CA, Marston S, Luther PK. Axial distribution of myosin binding protein-C is unaffected by mutations in human cardiac and skeletal muscle. J Muscle Res Cell M. 2012;33:61-74.
[51] Agarkova I, Perriard JC. The M-band: an elastic web that crosslinks thick filaments in the center of the sarcomere. Trends Cell Biol. 2005;15:477-85.
[52] LeWinter MM, Granzier H. Cardiac Titin A Multifunctional Giant. Circulation. 2010;121:2137-45.
[53] Granzier H, Labeit S. Cardiac titin: an adjustable multi-functional spring. J Physiol-London. 2002;541:335-42.
[54] Forbes MS, Sperelakis N. Intercalated discs of mammalian heart: a review of structure and function. Tissue & cell. 1985;17:605-48.
[55] Lyon RC, Zanella F, Omens JH, Sheikh F. Mechanotransduction in cardiac hypertrophy and failure. Circulation research. 2015;116:1462-76.
[56] Russell B, Curtis MW, Koshman YE, Samarel AM. Mechanical stress-induced sarcomere assembly for cardiac muscle growth in length and width. J Mol Cell Cardiol. 2010;48:817-23.
[57] Knoll R, Hoshijima M, Chien K. Cardiac mechanotransduction and implications for heart disease. J Mol Med-Jmm. 2003;81:750-6.
[58] Lammerding J, Kamm RD, Lee RT. Mechanotransduction in cardiac myocytes. Ann Ny Acad Sci. 2004;1015:53-70.
[59] Dabiri GA, Turnacioglu KK, Sanger JM, Sanger JW. Myofibrillogenesis visualized in living embryonic cardiomyocytes. P Natl Acad Sci USA. 1997;94:9493-8.
[60] Rudy DE, Yatskievych TA, Antin PB, Gregorio CC. Assembly of thick, thin, and titin filaments in chick precardiac explants. Dev Dynam. 2001;221:61-71.
[61] Gregorio CC, Antin PB. To the heart of myofibril assembly. Trends Cell Biol. 2000;10:355-62.
[62] Michele DE, Metzger JM. Maintaining the Fully Differentiated Cardiac Sarcomere. In: Dube DK, editor. Myofibrillogenesis. Boston, MA: Birkhäuser Boston; 2002. p. 73-85.
[63] Yin FCP. Ventricular Wall Stress. Circulation research. 1981;49:829-42.
[64] Legato MJ. Sarcomerogenesis in human myocardium. J Mol Cell Cardiol. 1970;1:425-37.
[65] Ferrans V. Growth of the heart in health and disease. Growth of the heart in health and disease. 1984:187-239.
[66] Bishop SP, Cole CR. Ultrastructural changes in the canine myocardium with right ventricular hypertrophy and congestive heart failure. Laboratory investigation; a journal of technical methods and pathology. 1969;20:219-29.
[67] Adomian GE, Laks MM, Morady F, Swan HJ. Significance of the multiple intercalated disc in the hypertrophied canine heart. J Mol Cell Cardiol. 1974;6:105-9.
[68] Bennett PM, Maggs AM, Baines AJ, Pinder JC. The transitional junction: A new functional subcellular domain at the intercalated disc. Mol Biol Cell. 2006;17:2091-100.
[69] Wilson A, Schoenauer R, Ehler E, Agarkova I, Bennett P. Cardiomyocyte growth and sarcomerogenesis at the intercalated disc. Cell Mol Life Sci. 2014;71:165-81.

[70] Yoshida M, Sho E, Nanjo H, Takahashi M, Kobayashi M, Kawamura K, et al. Weaving hypothesis of cardiomyocyte sarcomeres: discovery of periodic broadening and narrowing of intercalated disk during volume-load change. The American journal of pathology. 2010;176:660-78.
[71] Xu F, Beyazoglu T, Hefner E, Gurkan UA, Demirci U. Automated and adaptable quantification of cellular alignment from microscopic images for tissue engineering applications. Tissue engineering Part C, Methods. 2011;17:641-9.
[72] Capulli AK, MacQueen LA, Sheehy SP, Parker KK. Fibrous scaffolds for building hearts and heart parts. Advanced drug delivery reviews. 2016;96:83-102.
[73] Weiss P, Hiscoe HB. Experiments on the mechanism of nerve growth. The Journal of experimental zoology. 1948;107:315-95.
[74] Entcheva E, Bien H. Tension development and nuclear eccentricity in topographically controlled cardiac syncytium. Biomed Microdevices. 2003;5:163-8.
[75] Lucker PB, Javaherian S, Soleas JP, Halverson D, Zandstra PW, McGuigan AP. A Microgroove Patterned Multiwell Cell Culture Plate for High-Throughput Studies of Cell Alignment. Biotechnology and bioengineering. 2014;111:2537-48.
[76] Zhang B, Xiao Y, Hsieh A, Thavandiran N, Radisic M. Micro- and nanotechnology in cardiovascular tissue engineering. Nanotechnology. 2011;22:494003.
[77] Clark P, Connolly P, Curtis AS, Dow JA, Wilkinson CD. Topographical control of cell behaviour: II. Multiple grooved substrata. Development. 1990;108:635-44.
[78] Loesberg WA, te Riet J, van Delft FCMJM, Schon P, Figdor CG, Speller S, et al. The threshold at which substrate nanogroove dimensions may influence fibroblast alignment and adhesion. Biomaterials. 2007;28:3944-51.
[79] Biela SA, Su Y, Spatz JP, Kemkemer R. Different sensitivity of human endothelial cells, smooth muscle cells and fibroblasts to topography in the nano-micro range. Acta biomaterialia. 2009;5:2460-6.
[80] Wang PY, Yu JS, Lin JH, Tsai WB. Modulation of alignment, elongation and contraction of cardiomyocytes through a combination of nanotopography and rigidity of substrates. Acta biomaterialia. 2011;7:3285-93.
[81] Motlagh D, Senyo SE, Desai TA, Russell B. Microtextured substrata alter gene expression, protein localization and the shape of cardiac myocytes. Biomaterials. 2003;24:2463-76.
[82] Kim DH, Lipke EA, Kim P, Cheong R, Thompson S, Delannoy M, et al. Nanoscale cues regulate the structure and function of macroscopic cardiac tissue constructs. P Natl Acad Sci USA. 2010;107:565-70.
[83] Yang JY, Ting YC, Lai JY, Liu HL, Fang HW, Tsai WB. Quantitative analysis of osteoblast-like cells (MG63) morphology on nanogrooved substrata with various groove and ridge dimensions. J Biomed Mater Res A. 2009;90A:629-40.
[84] Chen A, Lieu DK, Freschauf L, Lew V, Sharma H, Wang J, et al. Shrink-film configurable multiscale wrinkles for functional alignment of human embryonic stem cells and their cardiac derivatives. Adv Mater. 2011;23:5785-91.
[85] Bowden N, Brittain S, Evans AG, Hutchinson JW, Whitesides GM. Spontaneous formation of ordered structures in thin films of metals supported on an elastomeric polymer. Nature. 1998;393:146-9.

[86] Yang P, Baker RM, Henderson JH, Mather PT. In vitro wrinkle formation via shape memory dynamically aligns adherent cells. Soft Matter. 2013;9:4705-14.
[87] Jiang XY, Takayama S, Qian XP, Ostuni E, Wu HK, Bowden N, et al. Controlling mammalian cell spreading and cytoskeletal arrangement with conveniently fabricated continuous wavy features on poly(dimethylsiloxane). Langmuir. 2002;18:3273-80.
[88] Greco F, Fujie T, Ricotti L, Taccola S, Mazzolai B, Mattoli V. Microwrinkled Conducting Polymer Interface for Anisotropic Multicellular Alignment. Acs Appl Mater Inter. 2013;5:573-84.
[89] Luna JI, Ciriza J, Garcia-Ojeda ME, Kong M, Herren A, Lieu DK, et al. Multiscale biomimetic topography for the alignment of neonatal and embryonic stem cell-derived heart cells. Tissue engineering Part C, Methods. 2011;17:579-88.
[90] Efimenko K, Rackaitis M, Manias E, Vaziri A, Mahadevan L, Genzer J. Nested self-similar wrinkling patterns in skins. Nat Mater. 2005;4:293-7.
[91] Lim JY, Donahue HJ. Cell sensing and response to micro- and nanostructured surfaces produced by chemical and topographic patterning. Tissue engineering. 2007;13:1879-91.
[92] Khademhosseini A, Eng G, Yeh J, Kucharczyk PA, Langer R, Vunjak-Novakovic G, et al. Microfluidic patterning for fabrication of contractile cardiac organoids. Biomed Microdevices. 2007;9:149-57.
[93] Falconnet D, Koenig A, Assi T, Textor M. A combined photolithographic and molecular-assembly approach to produce functional micropatterns for applications in the biosciences. Adv Funct Mater. 2004;14:749-56.
[94] Ruiz SA, Chen CS. Microcontact printing: A tool to pattern. Soft Matter. 2007;3:168-77.
[95] Akbulut O, Yu AA, Stellacci F. Fabrication of biomolecular devices via supramolecular contact-based approaches. Chem Soc Rev. 2010;39:30-7.
[96] Jang MJ, Nam Y. Aqueous micro-contact printing of cell-adhesive biomolecules for patterning neuronal cell cultures. Biochip J. 2012;6:107-13.
[97] Liu HH, Chen RK, Yang HX, Qin W, Borg TK, Dean D, et al. Enzyme-etching technique to fabricate micropatterns of aligned collagen fibrils. Biotechnol Lett. 2014;36:1245-52.
[98] McDevitt TC, Angello JC, Whitney ML, Reinecke H, Hauschka SD, Murry CE, et al. In vitro generation of differentiated cardiac myofibers on micropatterned laminin surfaces. J Biomed Mater Res. 2002;60:472-9.
[99] Badie N, Bursac N. Novel Micropatterned Cardiac Cell Cultures with Realistic Ventricular Microstructure. Biophys J. 2009;96:3873-85.
[100] Yamane M, Matsuda T, Ito T, Fujio Y, Takahashi K, Azuma J. Rac1 activity is required for cardiac myocyte alignment in response to mechanical stress. Biochem Bioph Res Co. 2007;353:1023-7.
[101] Matsuda T, Takahashi K, Nariai T, Ito T, Takatani T, Fujio Y, et al. N-cadherin-mediated cell adhesion determines the plasticity for cell alignment in response to mechanical stretch in cultured cardiomyocytes. Biochem Bioph Res Co. 2005;326:228-32.

[102] Radisic M, Park H, Shing H, Consi T, Schoen FJ, Langer R, et al. Functional assembly of engineered myocardium by electrical stimulation of cardiac myocytes cultured on scaffolds. P Natl Acad Sci USA. 2004;101:18129-34.
[103] Au HT, Cheng I, Chowdhury MF, Radisic M. Interactive effects of surface topography and pulsatile electrical field stimulation on orientation and elongation of fibroblasts and cardiomyocytes. Biomaterials. 2007;28:4277-93.
[104] Heidi Au HT, Cui B, Chu ZE, Veres T, Radisic M. Cell culture chips for simultaneous application of topographical and electrical cues enhance phenotype of cardiomyocytes. Lab Chip. 2009;9:564-75.
[105] Charest JL, Eliason MT, Garcia AJ, King WP. Combined microscale mechanical topography and chemical patterns on polymer cell culture substrates. Biomaterials. 2006;27:2487-94.
[106] Loesberg WA, Walboomers XF, van Loon JJ, Jansen JA. The effect of combined cyclic mechanical stretching and microgrooved surface topography on the behavior of fibroblasts. J Biomed Mater Res A. 2005;75:723-32.
[107] Vernon RB, Gooden MD, Lara SL, Wight TN. Microgrooved fibrillar collagen membranes as scaffolds for cell support and alignment. Biomaterials. 2005;26:3131-40.
[108] Schoenebeck JJ, Yelon D. Illuminating cardiac development: Advances in imaging add new dimensions to the utility of zebrafish genetics. Semin Cell Dev Biol. 2007;18:27-35.
[109] Weigert R, Porat-Shliom N, Amornphimoltham P. Imaging cell biology in live animals: ready for prime time. The Journal of cell biology. 2013;201:969-79.
[110] Meijering E, Smal I, Dzyubachyk O, Olivo-Marin JC. Time-Lapse Imaging. Microscope Image Processing. 2008:401-40.
[111] Yuste R. Fluorescence microscopy today. Nat Methods. 2005;2:902-4.
[112] Recher G, Rouede D, Richard P, Simon A, Bellanger JJ, Tiaho F. Three distinct sarcomeric patterns of skeletal muscle revealed by SHG and TPEF Microscopy. Opt Express. 2009;17:19763-77.
[113] Campagnola PJ, Wei MD, Lewis A, Loew LM. High-resolution nonlinear optical imaging of live cells by second harmonic generation. Biophys J. 1999;77:3341-9.
[114] Bub G, Camelliti P, Bollensdorff C, Stuckey DJ, Picton G, Burton RAB, et al. Measurement and analysis of sarcomere length in rat cardiomyocytes in situ and in vitro. Am J Physiol-Heart C. 2010;298:H1616-H25.
[115] Campagnola PJ, Loew LM. Second-harmonic imaging microscopy for visualizing biomolecular arrays in cells, tissues and organisms. Nat Biotechnol. 2003;21:1356-60.
[116] Pappinen S, Pryazhnikov E, Khiroug L, Ericson MB, Yliperttula M, Urtti A. Organotypic cell cultures and two-photon imaging: tools for in vitro and in vivo assessment of percutaneous drug delivery and skin toxicity. Journal of controlled release : official journal of the Controlled Release Society. 2012;161:656-67.
[117] Srikakulam R, Winkelmann DA. Chaperone-mediated folding and assembly of myosin in striated muscle. J Cell Sci. 2004;117:641-52.
[118] Manisastry SM, Zaal KJ, Horowits R. Myofibril assembly visualized by imaging N-RAP, alpha-actinin, and actin in living cardiomyocytes. Experimental cell research. 2009;315:2126-39.

[119] Plotnikov SV, Millard AC, Campagnola PJ, Mohler WA. Characterization of the myosin-based source for second-harmonic generation from muscle sarcomeres. Biophys J. 2006;90:693-703.
[120] Liu HH, Shao YH, Qin W, Runyan RB, Xu MF, Ma Z, et al. Myosin filament assembly onto myofibrils in live neonatal cardiomyocytes observed by TPEF-SHG microscopy. Cardiovasc Res. 2013;97:262-70.
[121] Liu HH, Qin W, Shao YH, Ma Z, Ye T, Borg T, et al. Myofibrillogenesis in live neonatal cardiomyocytes observed with hybrid two-photon excitation fluorescence-second harmonic generation microscopy. J Biomed Opt. 2011;16.
[122] Saytashev I, Arkhipov SN, Winkler N, Zuraski K, Lozovoy VV, Dantus M. Pulse duration and energy dependence of photodamage and lethality induced by femtosecond near infrared laser pulses in Drosophila melanogaster. Journal of photochemistry and photobiology B, Biology. 2012;115:42-50.
[123] Ji N, Magee JC, Betzig E. High-speed, low-photodamage nonlinear imaging using passive pulse splitters. Nat Methods. 2008;5:197-202.
[124] Donnert G, Eggeling C, Hell SW. Major signal increase in fluorescence microscopy through dark-state relaxation. Nat Methods. 2007;4:81-6.
[125] Ji N, Shroff H, Zhong HN, Betzig E. Advances in the speed and resolution of light microscopy. Curr Opin Neurobiol. 2008;18:605-16.
[126] Chu KK, Lim D, Mertz J. Enhanced weak-signal sensitivity in two-photon microscopy by adaptive illumination. Opt Lett. 2007;32:2846-8.
[127] Hoebe RA, Van Oven CH, Gadella TWJ, Dhonukshe PB, Van Noorden CJF, Manders EMM. Controlled light-exposure microscopy reduces photobleaching and phototoxicity in fluorescence live-cell imaging. Nat Biotechnol. 2007;25:249-53.
[128] Bol M, Abilez OJ, Assar AN, Zarins CK, Kuhl E. In Vitro/in Silico Characterization of Active and Passive Stresses in Cardiac Muscle. Int J Multiscale Com. 2012;10:171-88.
[129] Komuro I, Kaida T, Shibazaki Y, Kurabayashi M, Katoh Y, Hoh E, et al. Stretching cardiac myocytes stimulates protooncogene expression. The Journal of biological chemistry. 1990;265:3595-8.
[130] Aikawa R, Komuro I, Yamazaki T, Zou Y, Kudoh S, Zhu W, et al. Rho family small G proteins play critical roles in mechanical stress-induced hypertrophic responses in cardiac myocytes. Circulation research. 1999;84:458-66.
[131] Sadoshima J, Izumo S. Mechanical stretch rapidly activates multiple signal transduction pathways in cardiac myocytes: potential involvement of an autocrine/paracrine mechanism. The EMBO journal. 1993;12:1681-92.
[132] Mansour H, de Tombe PP, Samarel AM, Russell B. Restoration of resting sarcomere length after uniaxial static strain is regulated by protein kinase Cepsilon and focal adhesion kinase. Circulation research. 2004;94:642-9.
[133] Zhang WY, Ferguson GS, Tatic-Lucic S. Elastomer-supported cold welding for room temperature wafer-level bonding. Proc Ieee Micr Elect. 2004:741-4.
[134] Pirlo RK, Sweeney AJ, Ringeisen BR, Kindy M, Gao BZ. Biochiplaser cell deposition system to assess polarized axonal growth from single neurons and neuronglia

pairs in microchannels with novel asymmetrical geometries. Biomicrofluidics. 2011;5:13408.
[135] Vickers JA, Caulum MM, Henry CS. Generation of hydrophilic poly(dimethylsiloxane) for high-performance microchip electrophoresis. Anal Chem. 2006;78:7446-52.
[136] Desai SP, Freeman DM, Voldman J. Plastic masters-rigid templates for soft lithography. Lab Chip. 2009;9:1631-7.
[137] Perl A, Reinhoudt DN, Huskens J. Microcontact Printing: Limitations and Achievements. Advanced Materials. 2009;21:2257-68.
[138] Pasqualin C, Gannier F, Yu A, Malecot CO, Bredeloux P, Maupoil V. SarConfoCal: simultaneous sarcomere length and cytoplasmic calcium measurements for laser scanning confocal microscopy images. Bioinformatics. 2016.
[139] McCain ML, Lee H, Aratyn-Schaus Y, Kleber AG, Parker KK. Cooperative coupling of cell-matrix and cell-cell adhesions in cardiac muscle. Proceedings of the National Academy of Sciences of the United States of America. 2012;109:9881-6.
[140] Borg TK, Caulfield JB. The collagen matrix of the heart. Federation proceedings. 1981;40:2037-41.
[141] Pope AJ, Sands GB, Smaill BH, LeGrice IJ. Three-dimensional transmural organization of perimysial collagen in the heart. American journal of physiology Heart and circulatory physiology. 2008;295:H1243-H52.
[142] Vreeker A, van Stuijvenberg L, Hund TJ, Mohler PJ, Nikkels PGJ, van Veen TAB. Assembly of the Cardiac Intercalated Disk during Pre- and Postnatal Development of the Human Heart. PloS one. 2014;9.
[143] Zhou J, Shu Y, Lu SH, Li JJ, Sun HY, Tang RY, et al. The Spatiotemporal Development of Intercalated Disk in Three-Dimensional Engineered Heart Tissues Based on Collagen/Matrigel Matrix. PloS one. 2013;8.
[144] McCain ML, Desplantez T, Kleber AG. Engineering Cardiac Cell Junctions In Vitro to Study the Intercalated Disc. Cell Commun Adhes. 2014;21:181-91.
[145] Liu ZJ, Tan JL, Cohen DM, Yang MT, Sniadecki NJ, Ruiz SA, et al. Mechanical tugging force regulates the size of cell-cell junctions. Proceedings of the National Academy of Sciences of the United States of America. 2010;107:9944-9.
[146] Maruthamuthu V, Sabass B, Schwarz US, Gardel ML. Cell-ECM traction force modulates endogenous tension at cell-cell contacts. Proceedings of the National Academy of Sciences of the United States of America. 2011;108:4708-13.
[147] Guo WH, Frey MT, Burnham NA, Wang YL. Substrate rigidity regulates the formation and maintenance of tissues. Biophysical Journal. 2006;90:2213-20.
[148] Palchesko RN, Zhang L, Sun Y, Feinberg AW. Development of polydimethylsiloxane substrates with tunable elastic modulus to study cell mechanobiology in muscle and nerve. PloS one. 2012;7:e51499.
[149] Pologruto TA, Sabatini BL, Svoboda K. ScanImage: flexible software for operating laser scanning microscopes. Biomedical engineering online. 2003;2:13.
[150] Soares CP, Midlej V, de Oliveira MEW, Benchimol M, Costa ML, Mermelstein C. 2D and 3D-Organized Cardiac Cells Shows Differences in Cellular Morphology, Adhesion Junctions, Presence of Myofibrils and Protein Expression. PloS one. 2012;7.

[151] Frank D, Kuhn C, Katus HA, Frey N. The sarcomeric Z-disc: a nodal point in signalling and disease. J Mol Med-Jmm. 2006;84:446-68.
[152] Dlugosz AA, Antin PB, Nachmias VT, Holtzer H. The Relationship between Stress Fiber-Like Structures and Nascent Myofibrils in Cultured Cardiac Myocytes. The Journal of cell biology. 1984;99:2268-78.
[153] Boateng SY, Hartman TJ, Ahluwalia N, Vidula H, Desai TA, Russell B. Inhibition of fibroblast proliferation in cardiac myocyte cultures by surface microtopography. American journal of physiology Cell physiology. 2003;285:C171-82.
[154] Ciapetti G, Cenni E, Pratelli L, Pizzoferrato A. In vitro evaluation of cell/biomaterial interaction by MTT assay. Biomaterials. 1993;14:359-64.
[155] Shao YH, Liu HH, Ye T, Borg T, Qu JL, Peng X, et al. 3D Myofibril Imaging in Live Cardiomyocytes via Hybrid SHG-TPEF Microscopy. Proc Spie. 2011;7903.
[156] Ojima K, Ichimura E, Yasukawa Y, Wakamatsu J, Nishimura T. Dynamics of myosin replacement in skeletal muscle cells. American journal of physiology Cell physiology. 2015;309:C669-79.